SURVEY ON MODERN RADAR SIGNAL PROCESSING

Joao Paulo Goncalves Barcia

THESIS

SURVEY ON MODERN RADAR SIGNAL PROCESSING

by

Joao Paulo Goncalves Barcia

December 1975

Thesis Advisor: John Bouldry

Unclassified

SECURITY CLASSIFICATION OF THIS PAGE (When Data Entered)

REPORT DOCUMENTATION PAGE		READ INSTRUCTIONS BEFORE COMPLETING FORM
1. REPORT NUMBER	2. GOVT ACCESSION NO.	3. RECIPIENT'S CATALOG NUMBER
4. TITLE (and Subtitle) Survey on Modern Radar Signal Processing		5. TYPE OF REPORT & PERIOD COVERED Master's Thesis; December 1975 6. PERFORMING ORG. REPORT NUMBER
7. AUTHOR(s) Joao Paulo Goncalves Barcia		8. CONTRACT OR GRANT NUMBER(s)
9. PERFORMING ORGANIZATION NAME AND ADDRESS Naval Postgraduate School Monterey, California 93940		10. PROGRAM ELEMENT, PROJECT, TASK AREA & WORK UNIT NUMBERS
11. CONTROLLING OFFICE NAME AND ADDRESS Naval Postgraduate School Monterey, California 93940		12. REPORT DATE December 1975 13. NUMBER OF PAGES
14. MONITORING AGENCY NAME & ADDRESS(if different from Controlling Office) Naval Postgraduate School Monterey, California 93940		15. SECURITY CLASS. (of this report) Unclassified 15a. DECLASSIFICATION/DOWNGRADING SCHEDULE

16. DISTRIBUTION STATEMENT (of this Report)

Approved for public release; distribution unlimited.

17. DISTRIBUTION STATEMENT (of the abstract entered in Block 20, if different from Report)

18. SUPPLEMENTARY NOTES

19. KEY WORDS (Continue on reverse side if necessary and identify by block number)

Radar
Digital
Signal processing

20. ABSTRACT (Continue on reverse side if necessary and identify by block number)

The purpose of this thesis is to investigate the state of the art of radar signal design as well as radar signal processors and determine the actual trends in modern radar design. The use of a digital general purpose radar signal processor is discussed. The concepts of ambiguity and autocorrelation function are investigated in regard to radar resolution capabilities. The concept and analytical development of the DFT/FFT is presented.

DD FORM 1 JAN 73 1473 EDITION OF 1 NOV 65 IS OBSOLETE
S/N 0102-014-6601 |
(Page 1)

Unclassified
SECURITY CLASSIFICATION OF THIS PAGE (When Data Entered)

Quantization noise in a digital MTI processor and its effects in the improvement factor are analyzed. Optimization techniques for the response curve of digital MTI processors using staggered PRF are investigated. The SAR concept and analysis as well as techniques to obtain low correlator rates in SAR digital processors are presented.

Survey on Modern Radar Signal Processing

by

Joao Paulo Goncalves Barcia
First Lieutenant, Portuguese Navy
B.S., Naval Postgraduate School, 1974

Submitted in partial fulfillment of the
requirements for the degree of

MASTER OF SCIENCE IN ELECTRICAL ENGINEERING

from the

NAVAL POSTGRADUATE SCHOOL

ABSTRACT

The purpose of this thesis is to investigate the state of the art of radar signal design as well as radar signal processors and determine the actual trends in modern radar design. The use of a digital general purpose radar signal processor is discussed. The concepts of ambiguity and auto-correlation function are investigated in regard to radar resolution capabilities. The concept and analytical development of the DFT/FFT are presented. Quantization noise in a digital MTI processor and its effects in the improvement factor are analyzed. Optimization techniques for the response curve of digital MTI processors using staggered PRF are investigated. The SAR concept and analysis as well as techniques to obtain low correlator rates in the SAR digital processors are presented.

TABLE OF CONTENTS

ACKNOWLEDGEMENT

The author wishes to acknowledge the support and encouragement provided him by Associate Professor John M. Bouldry. In addition, the author wishes to thank all the Dudley Knox Library staff.

I. INTRODUCTION

The processing of signals has been always a necessity whenever information was to be transmitted through a channel between a source and a destination. It was not until 1948 that Shannon presented the basic theory of information relating the source entropy with channel capacity and the probability of error. Techniques of signal processing were already in use, but the results given by the information theory clarified the limits that could be achieved.

Early analog processors with enough bandwidth and reasonable signal to noise ratio could process data at extremely high data rates, but the components' low stability and high cost, and sometimes low versatility, were responsible for a gradual substitution of analog by digital processors when the price of digital logic went down, and the digital hardware technology suffered a big jump in the last ten years.

In fact, in today's radar signal processing the trend to a substitution of analog by digital processors is inevitable. The theory and boundaries of digital signal processing are continually being improved as well as hardware components. Speed is almost no longer a problem and versatility is immense.

Chapter II is an introduction to radar history. In Chapter III signal processing is related with the radar problem through the radar range equation and a general digital processor for a radar system is presented. In Chapter IV an analysis is

made of the present signal processing techniques in radar with special emphasis into digital approaches. In Chapter V an investigation is made into the recent developments and problems of two major areas of radar digital signal processing. In Chapter V an overall view of the achievements and trends of radar signal processing is explored.

II. RADAR. HISTORY AND APPLICATIONS

The electromagnetism and electromagnetic wave propagation theories of Maxwell, later (1886) experimentally verified by Hertz, contain all the necessary background to understand the principles of radar. The first experiments on detection with radio waves started in 1903. Due to inadequate technology the results were very poor. The obtained ranges were less than those achieved with optical systems and this was enough to discourage any interest in pursuing the experiments. It was only in 1922 at the Naval Research Laboratory that a wooden ship was detected using a CW radar with the transmitter and the receiver as separate units. From then on an increasing interest in radar technology became evident. In 1930 using a bistatic radar, the first aircraft was detected, and by 1932 the detection ranges were already in the 50-mile region. By that time the pulse techniques were not yet explored, so the information was in the presence or absence of a target and not in range information. But in 1935 the British successfully used pulse techniques to measure distance to the targets. In 1936 the detection range was already in the 90-miles region. The basic principles were understood. Its next steps were in technology improvements in order to get stable elements and more power output to increase the range coverage. Higher frequencies were used in order to work with smaller elements and high gain antennas.

The discovery of the magnetron was an important step since powers went up by a factor of 100, and wavelengths of 10 cm were obtained. But the greatest incentive for further developments in the radar field came from the military necessities of World War II. After the War a stagnation of about five years slowed down the rhythm of improvements in the field. But in the fifties the introduction of the high power klystron increased not only the power output but the frequency stability necessary for coherent detection as well as coherent MTI; also very low noise receivers were implemented.

From then on, with more and more perfect technology, more complex systems appeared. The introduction of the computer as a storage and control element was of extreme importance. All ballistic systems and very large coverage systems suffered a big impulse. Digital systems improved the implementation of stereable array antennas, synthetic aperture radar, tracking systems, as well as all digital processing techniques.

With the development of radar, the statistical nature of the detection problem gave rise to an increasing interest in the study of the statistical properties of clutter, radar cross section, rain, etc. So, due to a more precise knowledge (modeling) of the systems environment, the radar systems changed depending on the type of application.

Thus, a design to optimize a given application seldom can be used in others. Today the radar design field is wider. Applications vary from military to civilian to scientific. With improvements in technology and more accurate modeling, research in the field is far from becoming saturated.

III. SIGNAL PROCESSING IN RADAR

A. INTRODUCTION TO THE RADAR RANGE EQUATION

Only the analysis of the equation

$$R = f(n_1, n_2, \ldots n_n) \tag{3-1}$$

where R is the distance from the radar antenna to the target, and $(n_1, n_2, \ldots n_n)$ are the radar and environmental parameters, can give the necessary knowledge to maximize R. If P_t is the peak pulse power radiated and G the gain of the antenna, the transmitted power density is

$$\frac{P_t G}{4 \pi R^2}$$

and the received power density, after reflection in a target of cross section σ_t will be

$$\frac{P_t G \sigma_t}{(4\pi R^2)^2} \tag{3-2}$$

If (3-2) is multiplied by the antenna aperture A_e, the received power will be

$$P_r = \frac{P_t G \sigma_t A_e}{(4\pi R^2)^2} \tag{3-3}$$

If S_{min} is the minimum received signal, then the maximum distance is

$$R_{max}^4 = \frac{P_t G A_e \sigma_t}{(4\pi)^2 S_{min}} \tag{3-4}$$

Since by definition of noise figure (F_n) of a receiver

$$S_i = N_i F_n \left(\frac{S_o}{N_o}\right) \qquad \begin{matrix} i = \text{input} \\ o = \text{output} \end{matrix} \qquad (3\text{-}5)$$

where

$$N_i = kTB_n = \text{input noise} \qquad (3\text{-}6)$$

Then, combining (3-4) with (3-5) and (3-6)

$$R^4_{max} = \frac{P_t G A_e \sigma_t}{(4\pi)^2 kTB_n F_n (S_o/N_o)_{min}}$$

Since in a pulse radar the average power is

$$P_{av} = P_t \tau f_r$$

τ = pulse width

f_r = pulse rejection frequency

and the receiver bandwidth B_n is approximately $1/\tau$

$$R^4_{max} = \frac{P_{av} G A_e \sigma_t}{(4\pi)^2 kTf_r F_n (S_o/N_o)_{min}} \qquad (3\text{-}7)$$

where $(S_o/N_o)_{min}$ is the minimum signal to noise ratio at the output of the linear section of the receiver, necessary for detection. The first important characteristic in equation (3-7) is the fact that some of the variables can be considered deterministic but others must be analyzed as random variables. The random variables are σ_t and S/N. Statistical discriptors for σ_t are already extensively studied [1-2] not only in the general case but also for some specific cases, as for different types of clutter. Since the noise is normally treated as Guassian, all necessary statistical discriptors are available.

The statistical discriptors together with the decision criteria will determine the probability of detection and probability of false alarm.

B. RELATION BETWEEN THE RADAR RANGE EQUATION AND SIGNAL PROCESSING

After the War (1945) most of the effort in increasing range capabilities (eq. # 3-7) was focused on increasing average power (P_{av}), antenna gains (G), and mixers and receivers with lower noise figures (F_n). With the magnetron and the klystron, the peak powers reached the megawatts range. Soon it was verified that since the technology was already in the limits of transmitted peak power, any increase in peak power was questionable from a technical and a financial aspect. Also, since

$$R = k P^{1/4} \quad , \; k = \text{constant}$$

$$\ln R = \ln k + \frac{1}{4} \ln P$$

$$\frac{dR}{R} = \frac{1}{4} \frac{dP}{P}$$

That means, that the percent gain in range is only 1/4 of the percent gain in power. The pulse width could not be increased much more because of the required range resolution. This led to the development of what today is called signal processing techniques. Waveforms were studied in order to increase the average power but maintaining range resolution. The basic techniques will be presented in Chapter IV.

The brute force approach to increase the range of detection (3-7) was used until 1955. The technology then shifted to an improvement of the signal to noise ratio. If the new

signal to noise ratio is

$$(S/N) = D(S_o/N_o),\ D > 1.$$

Since D > 1, there is an increase in the maximum range of detection (3-7).

C. USE OF COMPUTERS AS SIGNAL PROCESSORS IN RADAR

As range and aximuth resolution became finer, as multi-target processing due to digital techniques became more effective, the conventional final processor in the radar system, the man, gradually was substituted by the computer. The total amount of information and the necessary speed for processing, tax the capabilities of man. So, digital techniques are gradually being substituted for not only those processors that used analog devices, but also where human operators were used.

Figure 1 gives an overview of the techniques presently used in digital signal processing. As in the analog theory linear approximation is used. So, using the theory of linear discrete time invariant systems there are two common approaches: digital filtering and spectral analysis. Using the theory of digital filtering, algorithms can be implemented that correspond to finite impulse response filters (FIR) or infinite impulse response filters (IIF). Using spectral analysis, two methods are possible: implementation of Fast Fourier Transform (FFT) algorithms or use of statistical spectrum analysis.

Both digital filters and spectral analysis are affected by quantization noise, which must be taken into account.

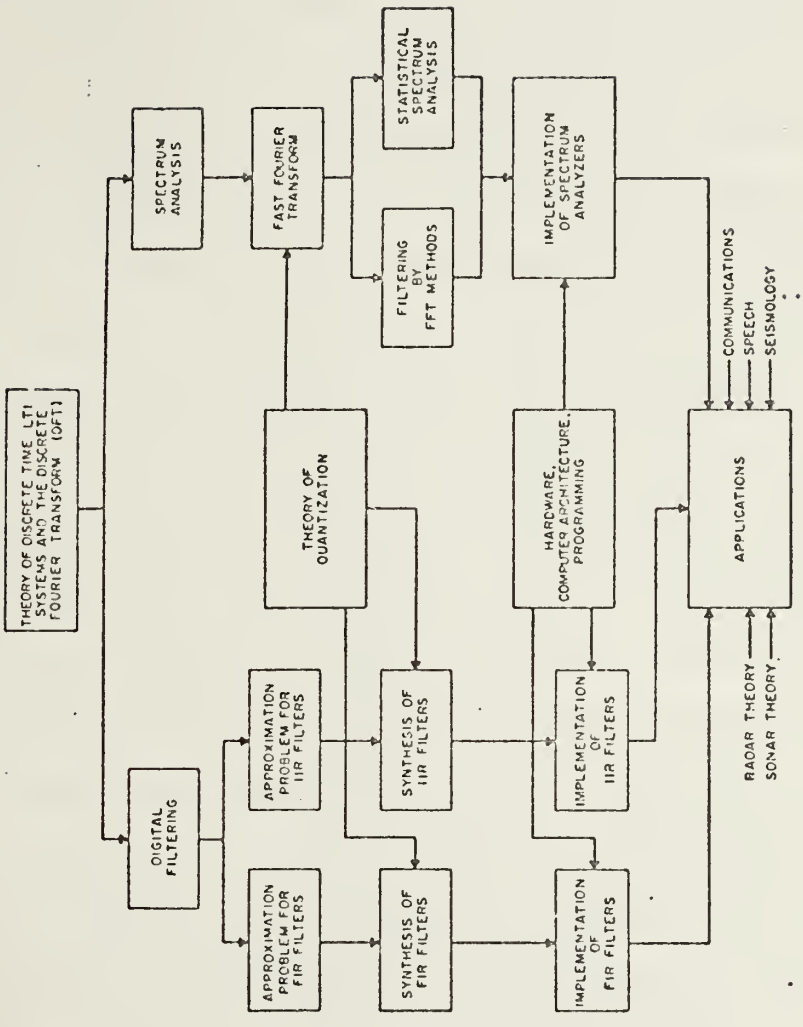
THEORY OF DISCRETE TIME LTI SYSTEMS AND THE DISCRETE FOURIER TRANSFORM (DFT)
DIGITAL FILTERING
SPECTRUM ANALYSIS
APPROXIMATION PROBLEM FOR FIR FILTERS
APPROXIMATION PROBLEM FOR IIR FILTERS
FAST FOURIER TRANSFORM
THEORY OF QUANTIZATION
FILTERING BY FFT METHODS
STATISTICAL SPECTRUM ANALYSIS
SYNTHESIS OF FIR FILTERS
SYNTHESIS OF IIR FILTERS
HARDWARE, COMPUTER ARCHITECTURE, PROGRAMMING
IMPLEMENTATION OF SPECTRUM ANALYZERS
IMPLEMENTATION OF FIR FILTERS
IMPLEMENTATION OF IIR FILTERS
APPLICATIONS
COMMUNICATIONS
SPEECH
SEISMOLOGY
RADAR THEORY
SONAR THEORY

Fig. 1

As seen in Fig. 1, the radar appears as one of the prime applications for digital systems.

It was in the 1960's that the first low data rate digital processors were implemented in radar systems, basically to perform tracking and weapon order computations. The next step was the implementation of the MTI processor. A flexible programmable digital processor was not achieved until very recently. The low cost of semi-conductor memory and the advanced technology in microprogramming, with inherent increase in speed, were the main reasons for this achievement. Now a typical general purpose signal processor for radar will be described. Figure 2 shows a block diagram of a digital signal processing system for a radar. The main processing unit is the arithmetic pipeline, which is a general purpose signal processor (GPSP). This consists of five sections selected in a way that the most frequently necessary operations can be performed; Fast Fourier Transform (FFT), recursive and nonrecursive digital filtering such as MTI, threshold generation, peak detection noncoherent video integration and range and angle estimation. The first block in the pipeline, the matrix switch, selects data from data memories, also from the receiver through a track buffer, or from anoth er GPSP via a wrap-around connection. The second block, data scaling, connects the data for floating point arithmetic. The complex multiplication block does the equivalent for four real multiplications and two real additions, which corresponds to a complex multiplication. Since some operations, like integration,

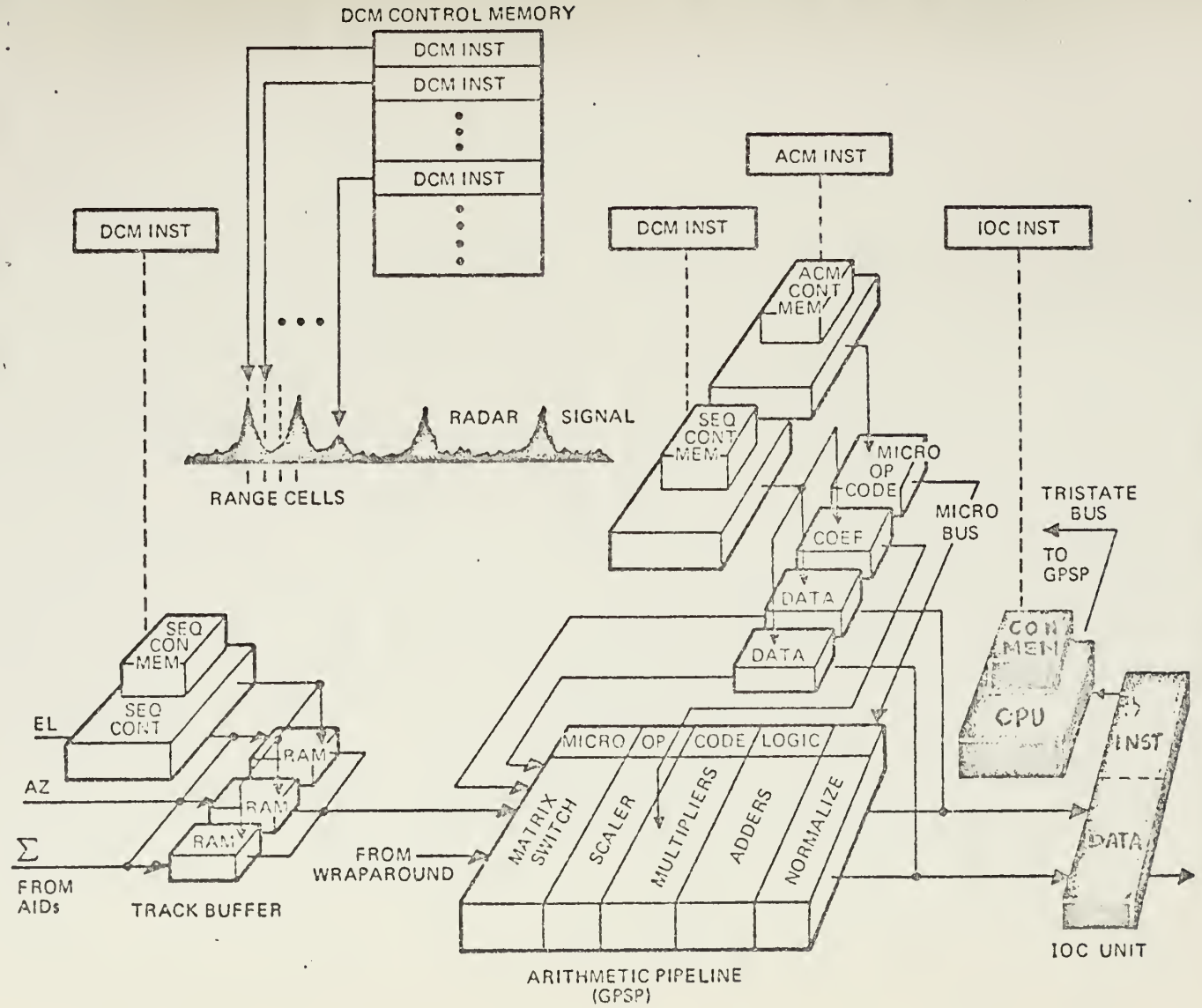
DCM CONTROL MEMORY
DCM INST
DCM INST
DCM INST
DCM INST
ACM INST
DCM INST
IOC INST
ACM CONT MEM
SEQ CONT MEM
MICRO OP CODE
COEF
DATA
DATA
MICRO BUS
TRISTATE BUS
TO GPSP
RADAR SIGNAL
RANGE CELLS
SEQ CON MEM
SEQ CONT
EL
AZ
Σ
FROM AIDs
RAM
RAM
RAM
TRACK BUFFER
FROM WRAPAROUND
MICRO OP CODE LOGIC
MATRIX SWITCH
SCALER
MULTIPLIERS
ADDERS
NORMALIZE
ARITHMETIC PIPELINE (GPSP)
CON MEM
CPU
INST
DATA
IOC UNIT

Fig. 2

The re-normalization block is sometimes needed. Connected to the arithmetic pipeline is a memory section and a control section. The output of the arithmetic pipeline is relayed to an input/output control unit (IOC) which is a buffer for the radar data as well as a macro control for the processing functions of the GPSP. The advantages of this processing system are that: once the data is started the process is continuous, and does not follow the normal sequence of fetch, operate, and store, characteristic of general purpose computers; the processor has a horizontal structure as opposed to the normal vertical structure of computers; this means that an instruction, after execution, causes all operations specified to be executed in a clock cycle; there is a hardware separation of instructions and data in the memory, which simplifies the job of the programmer; the control memory is made of RAM's which implies a much greater flexibility in subroutine changes; and the execution of instructions is within the same time frame that corresponds to a range or doppler cell.

Four memories interact with the arithmetic pipeline. Two of them store and recirculate data, the third stores weighting coefficients for such filters as MTI, FFT or pulse compression, the fourth stores micro opcodes. Data sequences and arithmetic operations are both controlled through software, by two control units. The program that resides in the sequence control memory (SEQ-CONTMEM), informs the machine of range and doppler dimensions of the problem. The program in the Arithmetic Control Memory, ACM, informs the machine of the particular algorithm to be used.

IV. VARIOUS ASPECTS OF THE THEORY OF RADAR SIGNAL PROCESSING

A. SIGNAL PROCESSING

The desire to transmit information is closely related to the processing of signals. Since normally the information to be transmitted cannot flow through the available channels, it is necessary that it be processed to use the chosen channel. Looking at Fig. 3, the inverse process has to be accomplished in order to get the information in an understandable form at the receiving end. The process is not so simple, since in general the processors themselves and the channel introduce noise that may or may not eliminate or change the understanding of the message. So there is a need to interpret the results with some decision criteria. Here decision theory plays an important role. Even for the same type of application, for instance, radar, decision criteria are not the same. The criteria may be of constant false alarm rate, or may be of fixed probability of detection. Basically every application or system must have its decision criteria.

There are two main approaches to the processing of signals, the time domain approach and the frequency domain approach. Besides the fact that they use completely different hardware, in the pure mathematical way, they are duals of each other through the Fourier transform pair. So the only reason for one type of approach is due to more perfect reliable type of hardware.

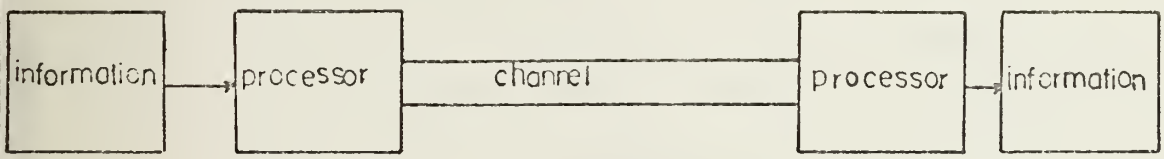

Fig. 3

With the advance of computer techniques, both approaches are split between digital and analog signal processing.

It was only after World War II that electronic engineers became interested in the applicability of digital hardware techniques in signal processing areas. But it was not before the late sixties that digital techniques suffered a big jump replacing some of the analog techniques. The foundations of digital signal processing can be related to the Laplace's Z-transform theory; but only in the mid sixties was the theory presented in a formal way. Various papers appeared at that time related to this subject, but only in 1969 was the first attempt made for a comprehensive theory of digital signal processing [21]. Most recently (1975), two very comprehensive books by Oppenheim [3] and Rabiner [4] can be considered as giving an excellent treatment of the subject, not only through its mathematical structure but with very good applications. Today's trend is definitely towards the substitution of analog processing by digital processing. The speed achieved in today's digital processors, the very fast algorithms used to implement the FFT, the gradual substitution of infinite impulse response methods to finite impulse methods due to a better knowledge of theory and higher efficiency of calculations are the major factors responsible for the increasing shift to digital techniques. There are yet some type of applications where the speeds are so high, or the digital hardware is so complicated that analog techniques are still used.

B. AMBIGUITY FUNCTION AND AUTOCORRELATION

1. Concept

Considering only non-accelerating targets, the two kinds of imformation of interest are the position of the target and its velocity. Given two targets, the capacity to differentiate between their positions and velocities is vital for most radar applications.

The capacity to differentiate in range is called range resolution, and in velocity, velocity resolution.

As far as range resolution is concerned, it is obvious the shorter the pulse the better is the differentiation between the two targets, that is, the higher is the range resolution. With the measurement of velocity, since it is directly related to the phase difference between signals, the longer the pulse the greater the number of cycles that can be compared and consequently the better the doppler and the velocity resolution. So, at first glance it looks like to optimize one of the resolutions the other will have to be sacrificed. The other solution is to try to get an optimum solution for both cases at the same time. There is a quantitative way to express these conditions in a precise way. That was the reason for the appearance of the mathematical concept of ambiguity function.

2. Range Ambiguity Function

Let the transmitted signal be represented by $S(t) = \mathrm{Re}[\psi(t)]$, $\psi(t) = u(t) \exp. j\omega_o t$. Then, with no doppler present the received signals from two different targets are

$\Psi(t)$ and $\psi(t-\tau)$

τ = equivalent time difference between the two targets.

If it is chosen, as a measure of the resolution, the mean square of the difference between the two received signals, then

$$\varepsilon^2(t) = \int_{-\infty}^{+\infty} |\psi(t) - \psi(t-\tau)|^2 dt$$

$$= \int_{-\infty}^{+\infty} |\psi(t)|^2 dt + \int_{-\infty}^{+\infty} |\psi(t-\tau)|^2 dt$$

$$- \int_{-\infty}^{+\infty} [\psi(t)\psi^*(t-\tau) + \psi^*(t)\psi(t-\tau)] dt$$

$$= 2\int_{-\infty}^{+\infty} |u(t)|^2 dt - 2\mathrm{Re}[\exp -j\omega_o\tau[\int u^*(t)u(t-\tau)dt]]$$

Since the first part of the result is proportional to the total energy of the signal and has a constant value, only the second term is going to make $\varepsilon^2(t)$ vary. Therefore

$$c(\tau) = \int_{-\infty}^{+\infty} u^*(t)u(t-\tau)dt, \qquad * = \text{complex conjugate}$$

is defined as the range ambiguity function; only $c(\tau)$ varies the value of $\varepsilon^2(t)$. As can be seen, there is a perfect identity between $c(\tau)$ and the autocorrelation of the signal. The ideal case would be to have the ambiguity function with a spike at the origin and zero anywhere else. That would mean that the only situation where it was impossible to differentiate the two signals was when they were on top of each other.

As an example. Fig. 4(a) shows the autocorrelation function of a pulse of duration T, Fig. 4(b) its uncertainty function $|c(\tau)|^2$. In part (c) there is a rectangle with the same height of $c^2(o)$ and with the same area under $|c(\tau)|^2$,

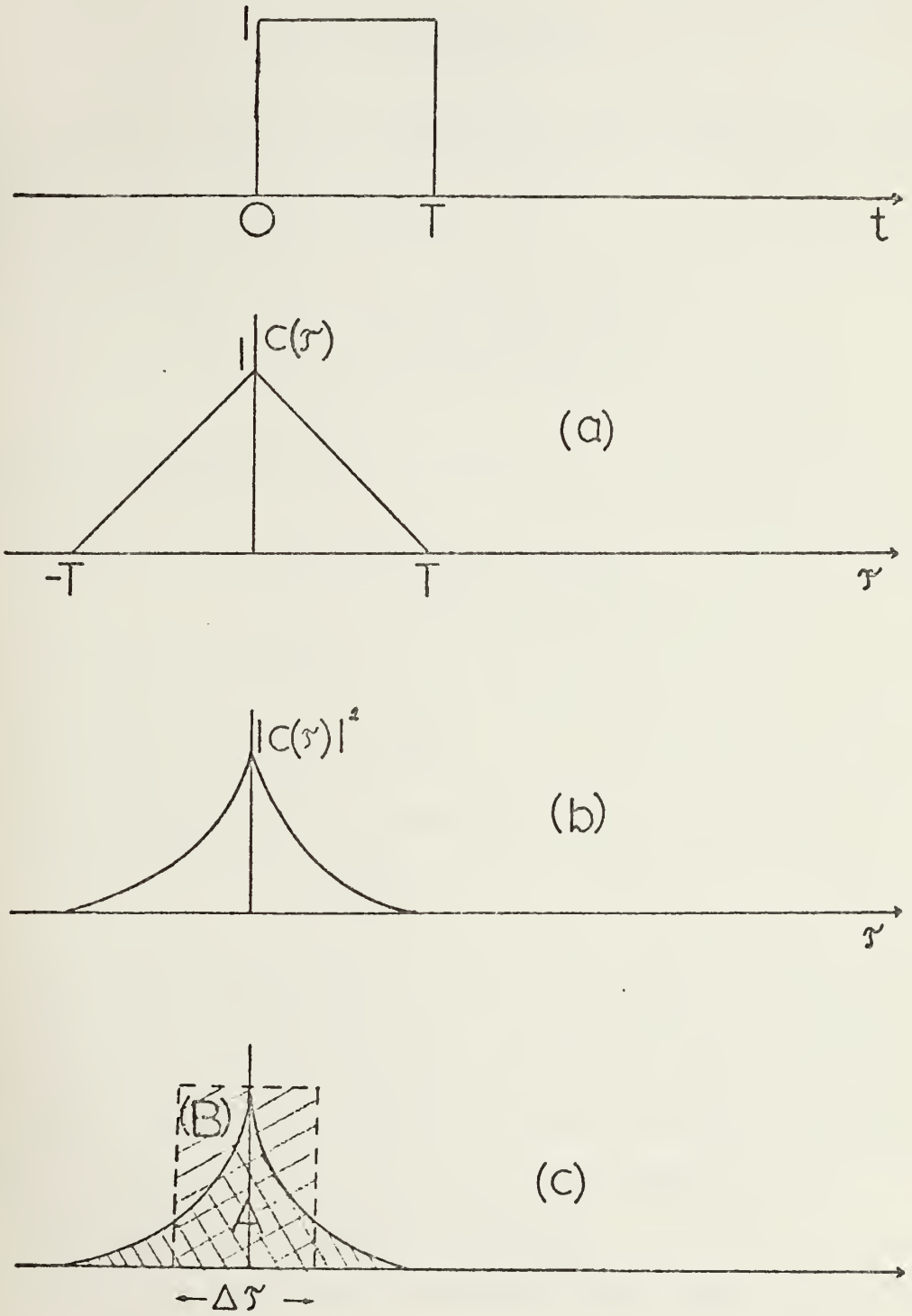

Fig. 4

that is, A = B. As it can be seen, the base of that rectangle is a measure of the spread of the curve and is called the delay resolution constant; so

$$\Delta\tau = \frac{\int_{-\infty}^{+\infty} |c(\tau)|^2 d\tau}{c^2(o)}$$

sometimes is more practical to define $\Delta\tau$ as a function of the bandwidth. Let $u(\omega) = F[u(t)] = \int_{-\infty}^{+\infty} u(t) \exp - j\omega t$.

since by Parsevall's Theorem $F[c(\tau)] = |u(\omega)|^2$

$$\Delta\tau = \frac{2\pi \int_{-\infty}^{+\infty} |u(\omega)|^4 d\omega}{[\int_{-\infty}^{+\infty} |u(\omega)|^2 d\omega]^2}$$

if the effective bandwidth is defined as

$$W_e = \frac{[\int_{-\infty}^{+\infty} |u(\omega)|^2 d\omega]^2}{4\pi \int_{-\infty}^{+\infty} |u(\omega)|^4 d\omega}$$

$$\Delta\tau = \frac{1}{2 W_e}$$

and the range resolution becomes

$$\Delta R = \frac{c\Delta\tau}{2}$$

All these definitions make sense since as pointed out before, with a short pulse there is a higher range resolution, but to have a short pulse there is need of a wider bandwidth, so there is equivalence in the two expressions for $\Delta\tau$.

3. The Velocity Ambiguity Function

Using the same type of mathematical logic and defining

$$\psi(f) = F[\phi(t)]$$

a complex correlation function is determined [5] to be

$$K(f_d) = \int u^*(2\pi f)u(2\pi f - 2\pi f_d)df$$

$$= \int |u(\tau)|^2 \exp j2\pi f_d t\, dt$$

and the doppler resolution constant [5]

$$\Delta f_d = \frac{\int |K(f_d)|^2 df_d}{k^2(o)} = \frac{\int |u(t)|^4 dt}{[\int |u(t)|^2 dt]^2} \equiv \frac{1}{T_e}$$

where T_e is the effective duration.

Since $f_d = \frac{2vfo}{c}$

$$df_d = \frac{2dv\, fo}{c}$$

which infers $\Delta f_d = \frac{2\, fo}{c} \Delta v$

the velocity resolution constant is

$$\Delta v = \frac{c}{2\, fo\, Te}$$

The graphical interpretation for T_e is similar to the graphical interpretation given for $\Delta\tau$ in Fig. 4 but instead of using the function $|c(\tau)|^2$, $|K(f_d)|^2$ is used. But as seen earlier, the optimization of one resolution implies the minimization of the other. This implies the need to study a two dimensional correlation function in order to see the mutual effects between the two resolution parameters.

So if the transmitted signal is

$$\psi(t) = u(t) \exp j2\pi fot$$

the received signal with doppler and delay will be

$$\psi(t-\tau) = u(t-\tau) \exp j2\pi(f_o - f_d)(t-\tau)$$

The mean square of the difference

$$\varepsilon^2 = \int |\psi(t) - \psi(t-\tau)|^2 dt$$

will yield a two dimensional correlation function of the form

$$X(\tau, f_d) = \int u(t)\, u^*(t-\tau) \exp j2\pi f_d t\, dt$$

Easily it can be seen that

$$X(\tau, 0) = c(\tau)$$

$$X(0, f_d) = k(f_d)$$

If the volume under $|X(\tau, f_d)|^2$ is determined and divided by $|X(0,0)|^2$, an equivalent resolution parameter called the effective area of ambiguity is obtained.

$$\Delta(T, f_d) = \frac{\int\int |X(\tau, f_d)|^2 d\tau\, df_d}{|X(0,0)|^2}$$

It is easy to prove [6] that

$$\int\int |X(\tau, f_d)|^2 d\tau\, df_d = |X(0,0)|^2$$

$$\Delta(\tau, f_d) = 1$$

So if an effort is made to improve one dimension, the other will never get better. But given one acceptable resolution in one dimension, there are ways to find the optimal solution for the other dimension if $X(\tau, f_d)$ is known. Fig. 5 is an ambiguity surface for a monochromatic pulse with a smooth envelope. It would be a reasonable temptation to try to design the waveform from a desired ambiguity function. That turns out to be impractical. First, a criteria to design the ambiguity function would be difficult to build. Secondly, and

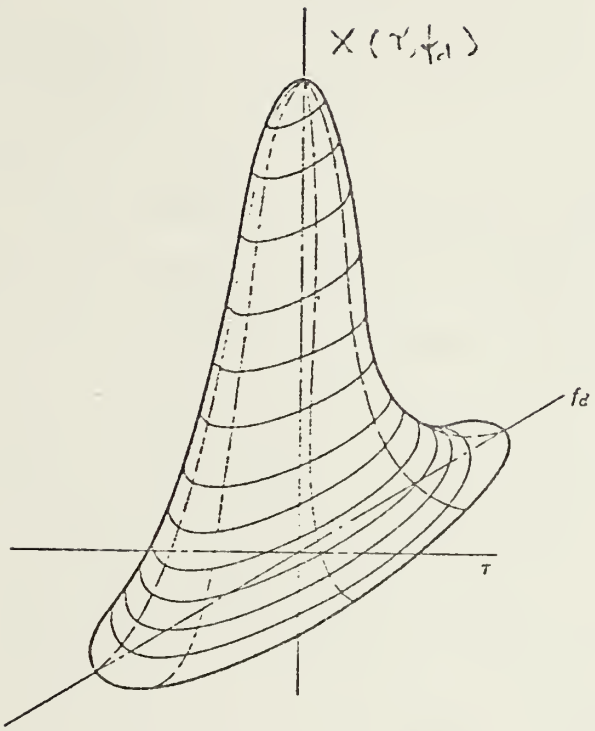

Fig. 5

most importantly, when designing a radar system normally there are other more important factors, from economic to space and weight constraints as well as technical, that dictate the boundaries for the waveform that we have to pick. Also, there is an important relation between the chosen waveform and the type of clutter model, and the approximation of the clutter model. Normally some flexibility in the digital processing is desirable.

C. PULSE COMPRESSION

1. Concept

Soon it was found that trying to increase the maximum range by increasing power, keeping the same pulse width, was the difficult way. Isolation problems were difficult to handle as well as reliable components. The only way to increase the energy of the signal was by increasing the pulse width. But an increase in pulse width would reduce the range resolution. Since the real problem was to increase the time of transmission but at the same time do not decrease the bandwidth (effective) of the waveform some different types of waveforms were studied, using the ambiguity function concept. The processing of the signal should be such that the transmitted waveform with high time of transmission and small effective bandwidth (W_e) should be converted to a high energy pulse with pulse width approximately $1/W_e$. This is called pulse compression. There are two basic ways of implementing pulse compression techniques. The active way, which is a time domain approach which basically uses correlators in the

detection and active elements to produce the waveform in the transmission. The passive way, which is a frequency domain approach, uses passive filters to generate the waveform and matched filters in the receiver. Each of the two has some variations, and it is even possible to build a system as a combination of the two processes. Table I gives a relative performance of various types of pulse compression techniques.

2. Linear FM (Chirp) Pulses Compression

First, the passive generation of linear FM signals will be analyzed. An IF pulse generator feeds a dispersive delay filter with a frequency versus time characteristic as in Fig. 6(c). The signal is then up converted and only one of the bands is transmitted. At the receiver the signal is down converted to IF and then passed through a dispersive filter with the opposite slope (Fig. 6 c). Using at reception a mixer sideband inverter, the same type of dispersive filter can be used because as it can be seen, f_2 and f_3 (Fig. 6 b) have opposite frequency versus time characteristics. In fact, with this technique the same dispersive filter for both transmission and reception can be used.

The analysis approach to this type of processing is the following:

Let the received signal be of the form

$$f(t) = \exp j[(\omega_o + \omega_d)t + \tfrac{1}{2}\mu t^2], \quad |t| < T/2$$

$$= 0, \quad |t| > T/2$$

where $\mu = \frac{\Delta\omega}{T}$ = frequency slope of the dispersive filter.

	Linear FM		Nonlinear FM		Phase-coded	
	Active	Passive	Active	Passive	Active	Passive
Range coverage	Limited range coverage per active correlation circuit.	Provides full range coverage.	Limited to one range cell per active correlation circuit.	Provides full range coverage.	Limited to one range cell per active correlation circuit.	Provides full range coverage.
Doppler coverage	Covers any doppler up to $\pm B/10$ but a range error is introduced. SNR and time-sidelobe performance poor for larger doppler.		Multiple doppler channels required, spaced by $(1/T)$ Hz.			
Range sidelobe level	Requires weighting to reduce the range sidelobes below $(\sin x)/x$ falloff.		Good range sidelobes possible with no weighting. Sidelobes determined by waveform design.		Good range sidelobes. $N^{-1/2}$ for an N-element code.	
Waveform flexibility	Bandwidth and pulse width can be varied.	Limited to one bandwidth and pulse width per compression network.	Bandwidth and pulse width can be varied.	Limited to one bandwidth and pulse width per compression network.	Bandwidth, pulse width, and code can be varied.	
Interference rejection	Poor clutter rejection.		Fair clutter rejection.		Fair clutter rejection.	
SNR	Reduced by weighting and by ripple loss vs. range.	Reduced by weighting.	Reduced by ripple loss vs. range.	No SNR loss.	Reduced by ripple loss vs. range.	No SNR loss.
Comments	1. Limited use. 2. Waveform simple to generate.	1. Widely used. 2. Well-developed technology.	1. Limited use. 2. Waveform difficult to generate.	1. Limited use. 2. Extremely limited development.	1. Widely used. 2. Waveform very easy to generate	1. Limited use. 2. Waveform moderately difficult to generate.

Table 1

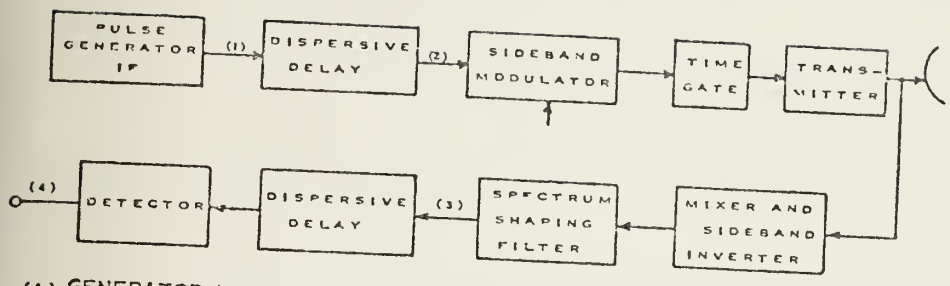

(A) GENERATOR AND DECODER

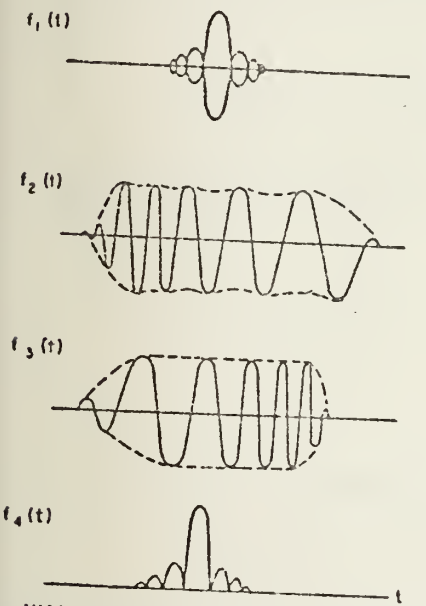

(B) WAVEFORMS (ARBITRARY TIME SCALE)

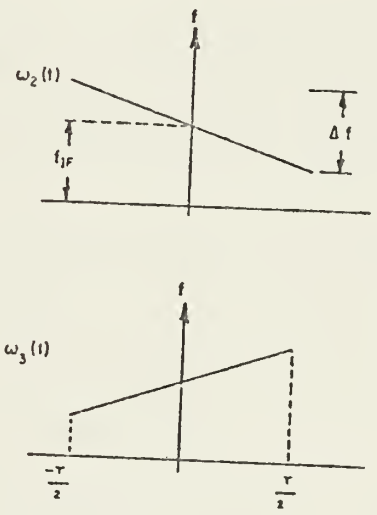

(C) FREQUENCY VS TIME

Fig. 6

T = duration of the transmit pulse envelope

ω_d = doppler shift.

The pulse spectrum is

$$F(\omega) = \int_{-\infty}^{+\infty} f(t) \exp -j\omega t \, dt$$

$$= \int_{-\infty}^{+\infty} \exp j[(\omega_o + \omega_d - \omega)t + \tfrac{1}{2}\mu t^2] \, dt$$

The filter transfer function is

$$H(\omega) = \exp j[(\omega_o - \omega)^2/2\mu]$$

which implies $G(\omega) = H(\omega)F(\omega) = \exp j[(\omega_o - \omega)^2/2\mu]$

$$\int_{-T/2}^{T/2} \exp j[(\omega_o + \omega_d - \omega)t + \tfrac{1}{2}\mu t^2] \, dt$$

which implies the time function at the output of the filter is

$$g(t) = F^{-1}[G(\omega)] = \frac{1}{2\pi} \int_{\infty}^{\infty} G(\omega) \exp j\omega t \, d\omega$$

which implies $g(t) = \frac{1}{2\pi} \int_{-\infty}^{+\infty} \exp j(\omega_o - \omega)^2/2\mu$

$$\int_{-T/2}^{T/2} \exp j[(\omega_o + \omega_d - \omega)\tau + \tfrac{1}{2}\mu\tau^2]$$

$$d\tau \exp j\omega t \, d\omega$$

Inverting the order of integration:

$$g(t) = \int_{-T/2}^{T/2} \int_{-\infty}^{+\infty} \exp j[(\omega_o + \omega_d - \omega)\tau + \tfrac{1}{2}\mu\tau^2 + \frac{(\omega_o - \omega)^2}{2\mu} + \omega t]$$

$$d\omega d\tau$$

$$= \int_{-T/2}^{T/2} \exp j[\omega_o\tau + \omega_d\tau + \tfrac{1}{2}\mu\tau^2 + \frac{\omega_o^2}{2\mu}] \times$$

$$\int_{-\infty}^{+\infty} \exp j[-\omega\tau + \frac{\omega^2}{2\mu} + \omega t - \frac{\omega_o}{\mu}\omega] \, d\omega \, d\tau$$

Call $v = \dfrac{(\omega_o + \mu\tau - \mu t)}{\sqrt{2\mu}}$

$$v^2 = \frac{\omega_o^2}{2\mu} + \frac{1}{2}\mu\tau^2 + \omega_o\tau + \frac{1}{2}\mu t^2 - \mu\tau t - \omega_o t$$

Multiplying $g(t)$ by $\exp -v^2$ and $\exp v^2$

$$g(t) = \frac{1}{2\pi}\int_{-T/2}^{T/2} \exp j[\omega_o\tau + \omega_d\tau + \frac{1}{2}\mu\tau^2 - v^2] \; x$$

$$x \int_{-\infty}^{+\infty} \exp j[\omega - \sqrt{2\mu}\, v]^2/2\mu \, d\omega d\tau$$

Since, $\dfrac{[\omega - \sqrt{2\mu}\, v]^2}{2\mu} = \dfrac{\omega^2}{2\mu} + v^2 - \dfrac{2\sqrt{2\mu}\, v\, \omega}{2\mu}$

$$= \frac{\omega^2}{2\mu} + v^2 - \frac{1}{\mu}\omega\,[\omega_o + \mu\tau - \mu t]$$

$$= v^2 - \omega\tau + \frac{\omega^2}{2\mu} + \omega t - \frac{\omega_o}{\mu}\omega$$

If $u = \dfrac{\omega - \sqrt{2\mu}\, v}{\sqrt{2\mu}}$, the second integral will be of the form

$$\sqrt{2\mu} \int_{-\infty}^{+\infty} \exp j u^2 \, du = \sqrt{2\mu}\,\sqrt{\pi} \exp j\pi/4$$

which implies $g(t) = \sqrt{\left(\dfrac{\mu}{2\pi}\right)} \exp j\left(\omega_o t - \dfrac{1}{2}\mu t^2 + \dfrac{\pi}{4}\right)$

$$\int_{-T/2}^{T/2} \exp j\tau(\omega_d + \mu t)\, d\tau$$

Since $\omega_o\tau + \omega_d\tau + \dfrac{1}{2}\mu\tau^2 - v^2 = \omega_d\tau + \mu\tau t - \dfrac{1}{2}\mu t^2 + \omega_o t$

which implies $g(t) = \sqrt{\left(\dfrac{2\mu}{\pi}\right)} \cos\left(\omega_o t - \dfrac{1}{2}\mu t^2\right) \dfrac{\sin (\omega_d + \mu t)T/2}{(\omega_d + \mu t)/2}$

which implies $g(t) = \sqrt{\left(\dfrac{2\mu T^2}{\pi}\right)} \cos\left(\omega_o t - \dfrac{1}{2}\mu t^2\right) \dfrac{\sin x}{x}$

where $x = (\omega_d + \mu t)T/2$

$$x = \frac{\omega_d T}{2} + \frac{\Delta\omega}{2} t$$

From these results it can be seen that if $\omega_d = 0$, a $\frac{\sin x}{x}$ type of envelope is obtained with a peak at the origin of magnitude $\sqrt{\left(\frac{2\Delta\omega T}{\pi}\right)}$. So the higher $\Delta\omega T$ the better the output signal. If $\omega_d \neq 0$ there is a shift in the sin x/x curve which implies a range error for doppler frequencies greater than zero.

3. Matched-Filter Approach

The matched-filter approach is another passive method. The analysis of the former will give us a basis for comparison. Let the received signal be

$$f(t) = \cos\left[(\omega_o t + \omega_d)t + \frac{1}{2}\mu t^2\right], \quad |t| < T/2, 0 \text{ elsewhere.}$$

The output of the matched filter will be of the form

$$g(\tau) = \int_{-\infty}^{+\infty} f(t)\, h(\tau - t)\, dt$$

where $h(t) = Kf(-t)$ and $F[h(t)] = H(\omega)$ is the filter transfer function. K is a constant factor to give a unity gain. In this case, $K = \sqrt{\left(\frac{2\mu}{\pi}\right)}$. So

$$g(\tau,\omega_d) = \sqrt{\left(\frac{2\mu}{\pi}\right)} \int_{-\infty}^{+\infty} \cos\left[(\omega_o + \omega_d)t + \frac{1}{2}\mu t^2\right] \cos\left[\omega_o(\tau - t) - \frac{1}{2}\mu(\tau - T)^2\right] dt$$

after some steps [7]

$$g(\tau,\omega_d) = \sqrt{\left(\frac{2\mu}{\pi}\right)} \cos\left[(\omega_o + \frac{\omega_d}{2})\tau\right] \frac{\sin\left(\frac{\omega_d + \mu\tau}{2}(T - |\tau|)\right)}{\omega_d + \mu\tau}$$

$$\text{for} \quad |\tau| \leq T$$

$$\text{or,} \quad g(\tau,\omega_d) = \frac{1}{2}(T - |\tau|)\sqrt{\left(\frac{2\mu}{\pi}\right)} \cos\left[(\omega_o + \frac{\omega_d}{2})\tau\right] \frac{\sin x}{x}, \quad |\tau| \leq T$$

where $x = \frac{\omega_d + \mu\tau}{2}(T - |\tau|)$

Since x is not a linear function of τ, the shape of the curve, unlike in the previous case, is not a sin x/x type of curve. Also, since $\omega_d\tau$ does not represent a linear shift in the axis due to the non-linearity of τ with respect to x, if $\omega_d \neq 0$ the curves become distorted and not symetric with respect to the vertical axis as in the previous case (Fig. 7). The advantage is of course the maximization of the signal to noise ratio.

4. Use of Discrete Frequency Sequences in Pulse Compression

The use of a sequence of frequencies each with a pulse duration of τ in order to get a good autocorrelation function is a very common method.

Various combinations, from linear stepped frequency to randomly chosen frequencies, are used in order to increase the main lobe with respect to the side lobes in the ambiguity function. The basic format is that of Fig. 8

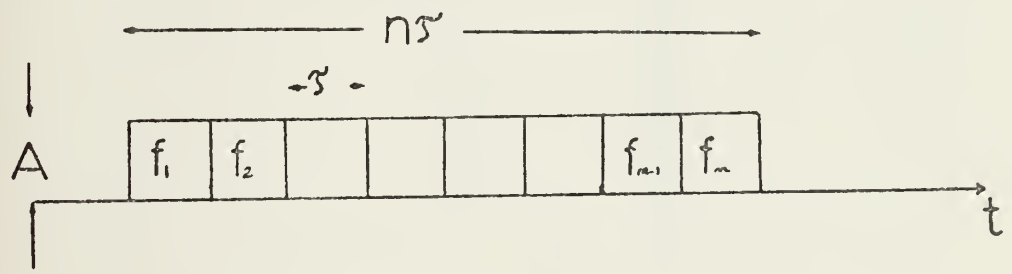

Fig. 8

where the waveform of the nth segment can be expressed as

$$v_n(t) = A \exp j\ 2\pi(f_n t + \phi_n)$$

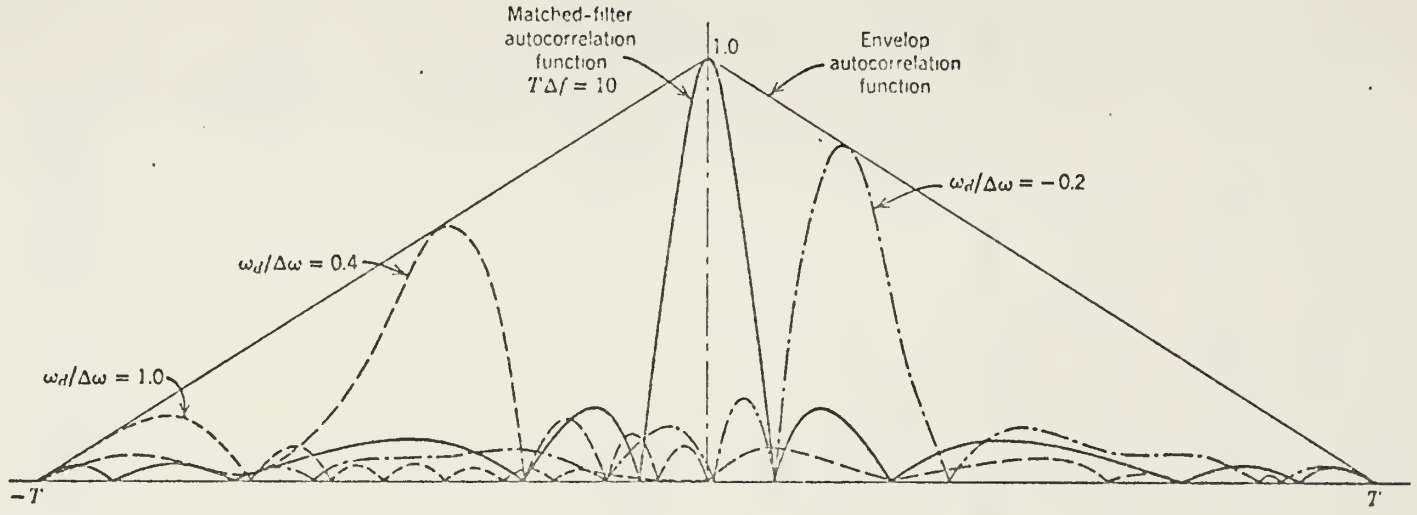
Matched-filter
autocorrelation
function
$T\Delta f = 10$
1.0
Envelop
autocorrelation
function
$\omega_d/\Delta\omega = -0.2$
$\omega_d/\Delta\omega = 0.4$
$\omega_d/\Delta\omega = 1.0$
$-T$
T

Fig. 7

The mathematical analysis for the general case is quite difficult and of little interest. Since only a few cases are of interest, consider the linear stepped frequency, that is, a time function of the form,

$$v(t) = \sum_{n=0}^{N-1} [u(t - n\tau) - u(t-(n+1)\tau)] \cos(\omega_o + n\Delta\omega)t$$

where ω_o = lowest frequency to be transmitted

$\Delta\omega$ = frequency spacing

N = number of frequencies in transmission.

Assuming that there is coherency between all frequencies, that is, $\phi_n = 0$, which could be obtained using a frequency synthesizer with a master oscillator, the matched filter would be of the form indicated in Fig. 9.

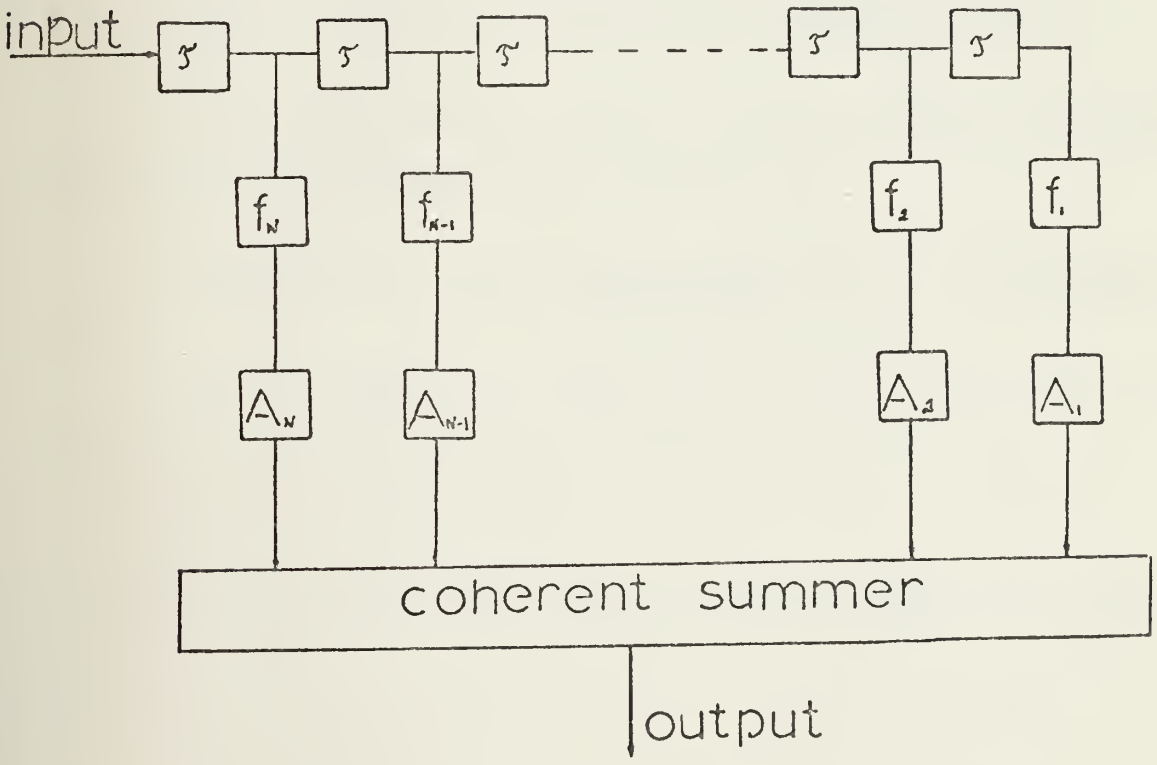

Fig. 9

If $\tau\Delta f > 1$, there will be significant range ambiguities. Also, if $\tau\Delta f < 1$ the subpulse filters f_n of Fig. 9 will overlap. That is the reason why in most cases $\tau\Delta f$ is made equal to unity, that is, $\tau = \frac{1}{\Delta f}$. With that assumption, the convolution of the impulse response of the matched filter $h(t) = v(-t)$ will yield an output

$$e_o(t) = \sum_{n=0}^{N-1} A_n^2 \exp j\ (\omega_o + n\Delta\omega)t$$

where $(N-1)\tau < t < N\tau$.

If $A_n = 1$, for all n, then

$$e_o(t) = \exp j\ \omega_o t \sum_{n=0}^{N-1} (\exp j\ \Delta\omega t)^n$$

Since $|\exp j\ \Delta\omega t| < 1$, then

$$e_o(t) = [\exp j[\omega_o + \frac{(N-1)\Delta\omega}{2}]t] \times \frac{\sin N\ (\Delta\omega/2)t}{\sin\ (\Delta\omega/2)t}$$

Accounting for the autocorrelation of the rectangular pulse, the final output time function is

$$e_o(t) = (1 - |\tau|\Delta f)\ \frac{\sin N(\Delta\omega/2)t}{\sin\ (\Delta\omega/2)t} \cos\ [\omega_o + \frac{(N-1)\Delta\omega}{2}]t$$

Fig. 10 shows the effects of $\tau\Delta f \neq 1$. The nules of the output waveform occur at $\sin N\Delta\omega/2t = 0$.
Which implies $N\ \frac{\Delta\omega}{2}\ t = \pm\ m\pi$

For $N > 50$, the first side lobe is 13.46db below the main lobe.

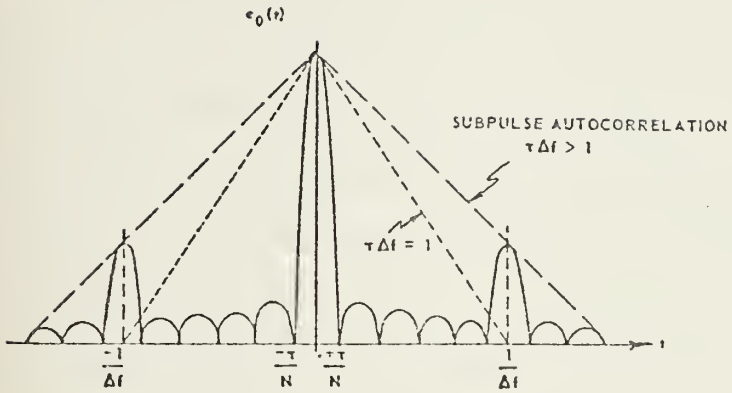
$e_0(t)$
SUBPULSE AUTOCORRELATION
$\tau\Delta f > 1$
$\tau\Delta f = 1$
$\frac{-1}{\Delta f}$
$\frac{-\tau}{N}$
$\frac{+\tau}{N}$
$\frac{1}{\Delta f}$
t

Fig. 10

A very important quantitative factor in all these waveforms with sharp autocorrelation function is the pulse compression ratio. It is defined as the ratio of peak power after compression to peak power before compression. Table II gives some data including compression ratios for some typical linear pre-pulse generation and compression circuits.

Another important quantitative factor is the side lobe reduction factor which is defined as the power ratio of the main lobe with reference to any side lobe.

Depending on the specific application, it is sometimes preferable to sacrifice the main lobe peak power or even width (3 db point), but get a higher side lobe reduction. In the radar problem those side lobes may be identified with targets, the need to suppress them if wanting to use a larger dynamic range is obvious.

There are various types of weighting functions. The weighting is applied in the amplitude response of the matched filter in order to deliberately produce a mismatch.

The frequency response of the matched filter is such that the signal to noise ratio is maximized. So any mismatch will lower that signal to noise ratio.

The loss in signal to noise ratio due to weighting is called the loss factor L_s. It is defined as

$$L_S = \frac{(S/N)\ \text{weighted}}{(S/N)\ \text{matched}} = \frac{[\int_T \omega(t)\, dt]^2}{T\int_T \omega^2(t)\, dt}$$

$\omega(t)$ = weighting function

T = processing time interval or the length of the transmitted waveform.

Technique	Compression ratio, $T\Delta F$	Center frequency, MHz	Compressed pulse width, μsec	Peak sidelobe, dB below peak
(1) Lumped constant	50	13.5	0.10	35
dispersive lines	~130	13.5	0.077	31
(2) Dispersive strip	~110 (80)	60	~0.18 (.25)	30
delay lines	118 (72)	30	~0.36 (.56)	40
F(steel) 5-45 MHz	(64)	15	0.8	28
F(aluminum) 1-5 MHz	35	5	0.8	
L~10-40 dB	~500	2.0	~1.3	
(3) Diffraction dispersive	64	30	0.18-(.25)	36
delay lines perpendicular	400 (250)	45	0.05-(.08)	35
$T_{max} \approx 225\mu$sec	400	60	0.07+	
F = 20 to 60 MHz	1,000	100	0.025	
L = 15 to 60 dB				
(4) Diffraction dispersive	64	30	~0.02	28
delay lines-wedges	250	500	~0.004	
$T_{max} \approx 65\mu$sec		(Sapphire)		
(5) Discrete frequency	1,000	15	1.0	~23
	1,024	30	0.012	~30
(6) Waveguide near cut off	~120	2,775	~0.009	12-18
(7) YIG	125	2,880	0.014	>13

Table II

In the case of discrete frequency amplitude weighting, the loss factor is

$$L_s = \frac{[\sum_1^N A_n]^2}{N[\sum_1^N A_n^2]} \qquad [8]$$

The problem of weighting is in effect a way of producing a pulse compressed spectrum that yields the wanted waveform.

In the continuous linear FM case, the spectrum of the match filter is of course a pulse in the frequency domain. Since the inverse transform of a pulse is a sin x/x type of function, that is why for the linear FM waveform a sin x/x type of output is obtained. From the Fourier transform pair it is known that a wide pulse in one domain corresponds to a sharp pulse in the opposite domain. So the amplitude weighting functions that will lower the side lobes will have a bell or tapered shape characteristic in the frequency domain. That is why the time output of a matched filter with a pulse in the frequency domain as transfer function, is

$$e_o(t) = \frac{1}{2\pi} \int_{-W}^{W} a(\omega) \exp j\,\omega t \, d\omega$$

where $a(\omega)$ is the weighting function; the most commonly used weighting functions are:

The cosine function where

$$a(\omega) = \cos \frac{\pi\omega}{2W}$$ where $a(\omega) = 1$ at the center of the spectrum.

So, $$e_o(t) = \frac{1}{2\pi} \int_{-W}^{W} \cos \frac{\pi\omega}{2W} \exp j\,\omega t \, d\omega = \frac{2W}{\pi^2 - 4tW^2} \cos \omega t.$$

The main lobe will be between nules. The nules will occur at cos Wt = 0

which implies $wt = (2n + 1)\frac{\pi}{2}$, n = 0, ±1, ±2,...

or $t = \frac{(2n + 1)\pi}{2w}$

Considering the lobes between nules the side lobe reduction is 23.5 db.

Another class of tapers are the Hamming functions which have the general form

$$G(\omega) = a + (1 - a) \cos \left(\frac{\pi\omega}{W}\right) \quad 0 < a < 1$$

where the center of the spectrum is assumed to be at $\omega = 0$.

In this case the output will be

$$e_o(t) = \frac{a}{2} \frac{\sin Wt}{Wt} + \frac{1-a}{2w(1-t^2)}$$

for a = .54 the side lobe reduction is 42.8 db which represents a much larger dynamic range. Table III gives data on side lobe suppression on frequency coded waveforms.

D. MOVING TARGET INDICATOR (MTI)

The MTI is basically a processor that separates moving targets from clutter. Since the clutter spectrum is a very low frequency spectrum, the MTI processor must be a high pass filter. In the early MTI processors the main technical problems were in the processor itself due to instability of some elements. Today the main problems result due to the existence of a variety of types of clutter which make the design difficult. If only the elimination of one type of

Weighting function	a	Time mismatch, %	Main-lobe broadening		Processing loss, dB	Highest sidelobe, –dB	Sidelobe decay function*
			Theor.	Exp.**			
Unweighted		0	1.00	1.00	0	13.2	$1/t$
Cosine		0	1.56		1.0	23.6	$1/t$
Hamming	0.54	0	1.47	1.46	1.34	42.8	$1/t$
		5	1.52		1.42	36.6	$1/t$
		10	1.55		1.47	32.2	$1/t$
(Cosine-squared)	0.50	0	1.59	1.70	1.76	31.4	$1/t^3$
Hamming	0.52	0	1.55		1.54	36.1	$1/t$
Hamming	0.56	0	1.45		1.16	37.7	$1/t$
Hamming	0.58	0	1.41		1.01	34.2	$1/t$
Dolph-Chebyshev		0	1.20	1.40	0.80	30.0	1
Dolph-Chebyshev		0	1.35		1.20	40.0	1
Cosine-cubed		0	1.88		2.38	39.1	$1/t^4$
Taylor $\bar{n} = 5$		0	1.34	1.44	1.1	34.0	$1/t$
$\bar{n} = 6$		0	1.41	1.7	1.23	40.0	$1/t$
$\bar{n} = 6$		10	--		—	28.0	$1/t$
$\bar{n} = 8$		0	~1.50		1.46	47.5	$1/t$
$\bar{n} = 8$		10	--		1.66	34.5	$1/t$

*Decay function far from compressed-pulse location.
**Compression ratio = 50:1 (experimental).

Table III

clutter is required, then the efficiency of the MTI is good, but if various types of clutter must be handled at the same time by the same processor, the efficiency drops.

Depending on the parameter used, the MTI processors are basically divided into three types: those that use the phase information of the returned signal, those that use the amplitude, and those that use both phase and amplitude. The basic configuration of the phase processing or coherent MTI is that of Fig. 11. The use of two oscillators, the stalo and coho, is for up and down converting the waveforms in order to get a perfect phase comparison, since at low frequencies the phase accuracy measurement increases. Coherency is also obtained.

Consider two signal returns from the same moving target with a separation in time by $T = 1/f_R$ where f_R = pulse rejection frequency. The signals presented to the summer are

$$E_1 = E \sin (\omega_d t + \phi_1)$$

$$E_2 = E \sin [\omega_d (t + T) + \phi_2]$$

$$\phi_1 = \phi_2 = 4\pi R_o/\lambda = \phi$$

The output of the canceller will be

$$E_r = E_1 - E_2 = 2E \sin(\frac{\pi f d}{f_R}) \cos[\omega_d (t + \frac{T}{2}) + \phi]$$

where it is seen that the cosine waveform is modulated by a $\sin \frac{\pi f d}{f_R}$. So, independently of t, there are some doppler frequencies where the power out will be zero. These are the frequencies where $\frac{\pi f d}{f_R} = n\pi$. That is, $f_d = nf_R$ (multiples of the pulse repetition frequency).

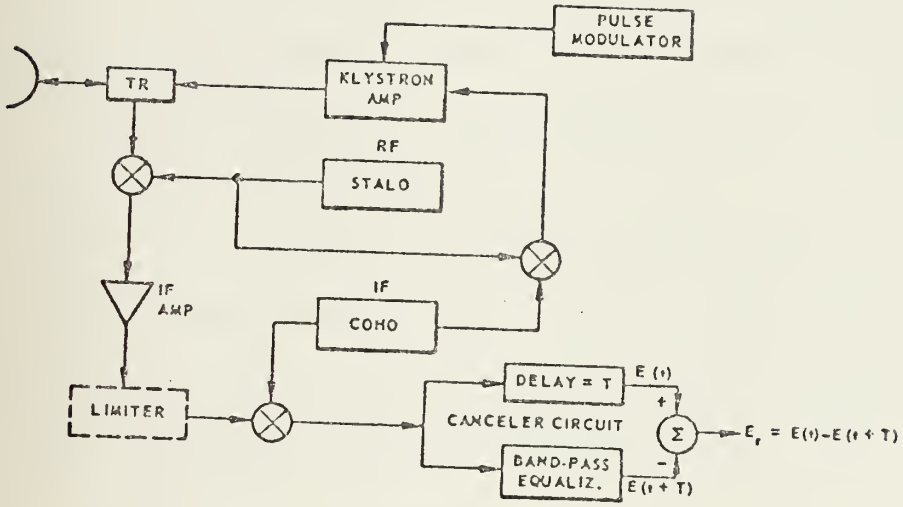
PULSE MODULATOR
TR
KLYSTRON AMP
RF
STALO
IF AMP
IF
COHO
LIMITER
DELAY = T
E (t)
CANCELER CIRCUIT
BAND-PASS EQUALIZ.
E (t + T)
+
-
Σ
E, = E(t)-E(t + T)

Fig. 11

Since the doppler frequency is a function of the radial velocity V_R, $f_d = \frac{2V_R}{\lambda}$, there are also blind speeds that correspond to the blind frequencies $(f_d = nf_R)$

$$V_{blind} = n(\frac{\lambda f_R}{2}) \text{ , n is an integer.}$$

Fig. 12 shows the power response for a single delay line MTI processor. As it is seen, the multiples of the PRF are at nules but the other frequencies are not processed in the same way. That is very far away from the ideal case.

The clutter spectrum beating with the pulse repetition frequency is translated to every multiple of the PRF. So if the clutter spectrum is, after translated, of the form indicated in Fig. 13 (a) the ideal MTI processor should have a response as in Fig. 13 (b).

As it is known the single delay line processor response is far away from that of Fig. 13 (b). One way to improve the MTI processor is by using multiple canceller filters.

For an n-stage cascaded canceller (Fig. 14)

$$(\frac{S_o}{S_i})_n = 2^{2n}\sin^{2n}(\frac{\pi f_d}{f_R}) \qquad [9]$$

where S_o and S_i are the peak output power and peak input power. The problem is that if many cascaded blocks are used, the $(\sin \frac{\pi f_d}{f_R})^{2n}$ function may cut some low velocities of interest.

The transmitted waveform has a spectrum as in Fig. 15. The fact that there is more than one line in the spectrum is of no importance to the MTI processor since all the lines are at blind frequencies.

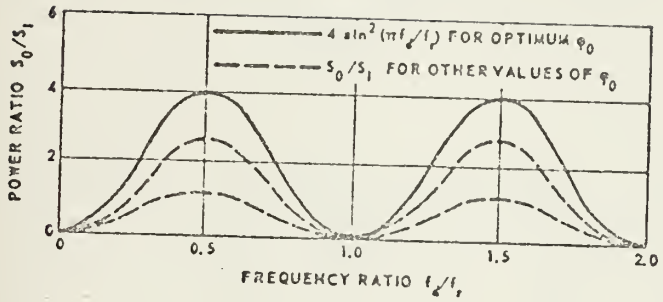
$4 \sin^2(\pi f_d/f_r)$ FOR OPTIMUM φ_0
S_0/S_1 FOR OTHER VALUES OF φ_0
POWER RATIO S_0/S_1
FREQUENCY RATIO f_d/f_r
0
2
4
6
0.5
1.0
1.5
2.0

Fig. 12

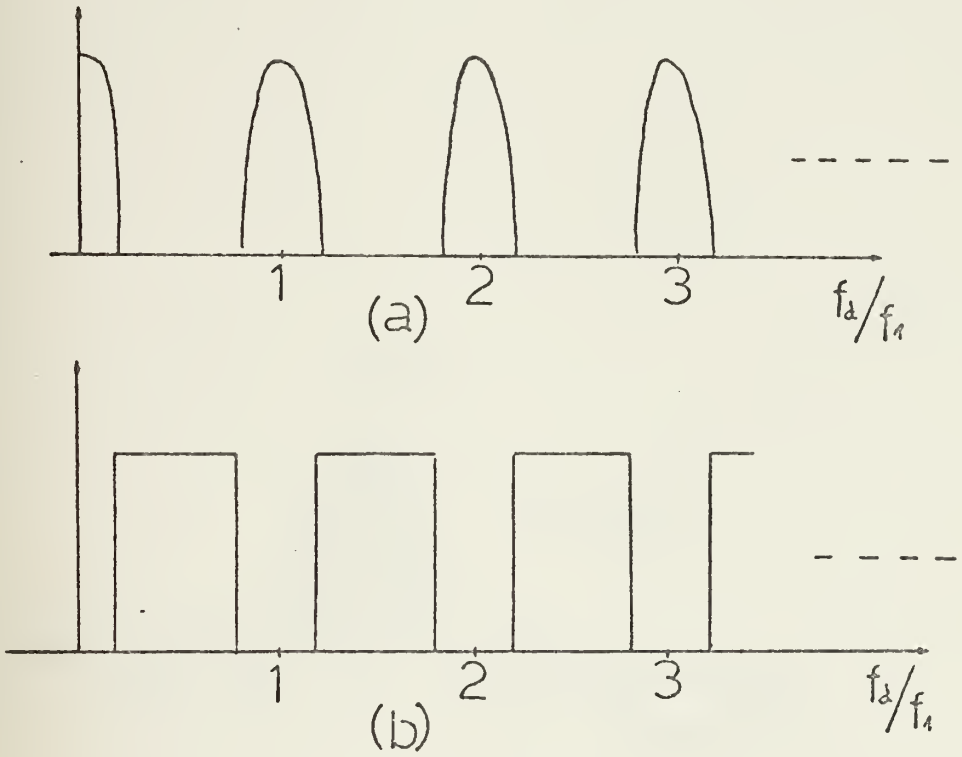

Fig. 13

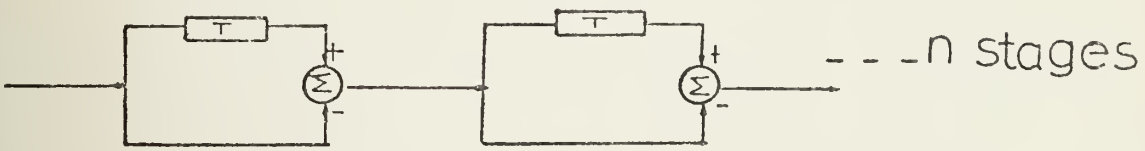

Fig. 14

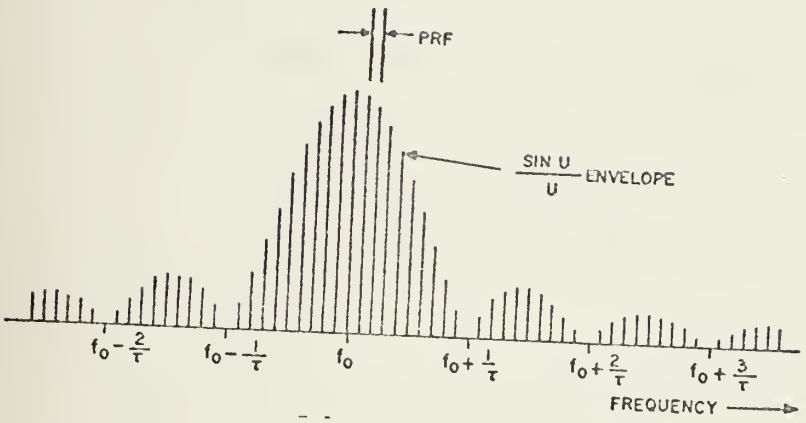
PRF
SIN U / U ENVELOPE
$f_0 - \frac{2}{\tau}$
$f_0 - \frac{1}{\tau}$
f_0
$f_0 + \frac{1}{\tau}$
$f_0 + \frac{2}{\tau}$
$f_0 + \frac{3}{\tau}$
FREQUENCY

Fig. 15

The amplitude processor, also called noncoherent processor, has a block diagram as in Fig. 16. The advantage of this processor is due to the fact that stability problems almost disappear since there is no coherency. Since most high power transmitters are not very stable, this is a real advantage. The big disadvantage is that it needs a permanent existence of a strong clutter return since without it, it won't work. Fig. 17 represents the phasor diagram that explains how the noncoherent processor works. Since the clutter is of the form, E_c = dc value, in a phasor diagram is represented by a stationary vector.

Let $E_s(t)$ be the return of a moving target.

Then $$E_s(t) = |E_s(t)| \cos \omega_d t$$

$$E_s(t + T) = |E_s(t)| \cos [\omega_d (t + T)]$$

Let $$\omega_d t = \phi - \Delta\phi/2$$

$$\omega_d (t + T) = \phi + \Delta\phi/2 = \phi - \Delta\phi/2 + \omega_d T$$

which implies $\omega_d T = \Delta\phi$

Let the total signal at time t (Fig. 17 b) be

$$\vec{E}_1(t) = \vec{E}_c + \vec{E}_s(t)$$

and the total signal at time (t + T) (Fig. 17 c) be

$$\vec{E}_2(t) = \vec{E}_1(t + T) = \vec{E}_c + \vec{E}_s(t + T).$$

From Fig. 17 (d) it can be seen that due to E_c there exists an amplitude difference between $|E_1(t)|$ and $|E_2(t)|$. This difference in amplitude is going to be used to identify the

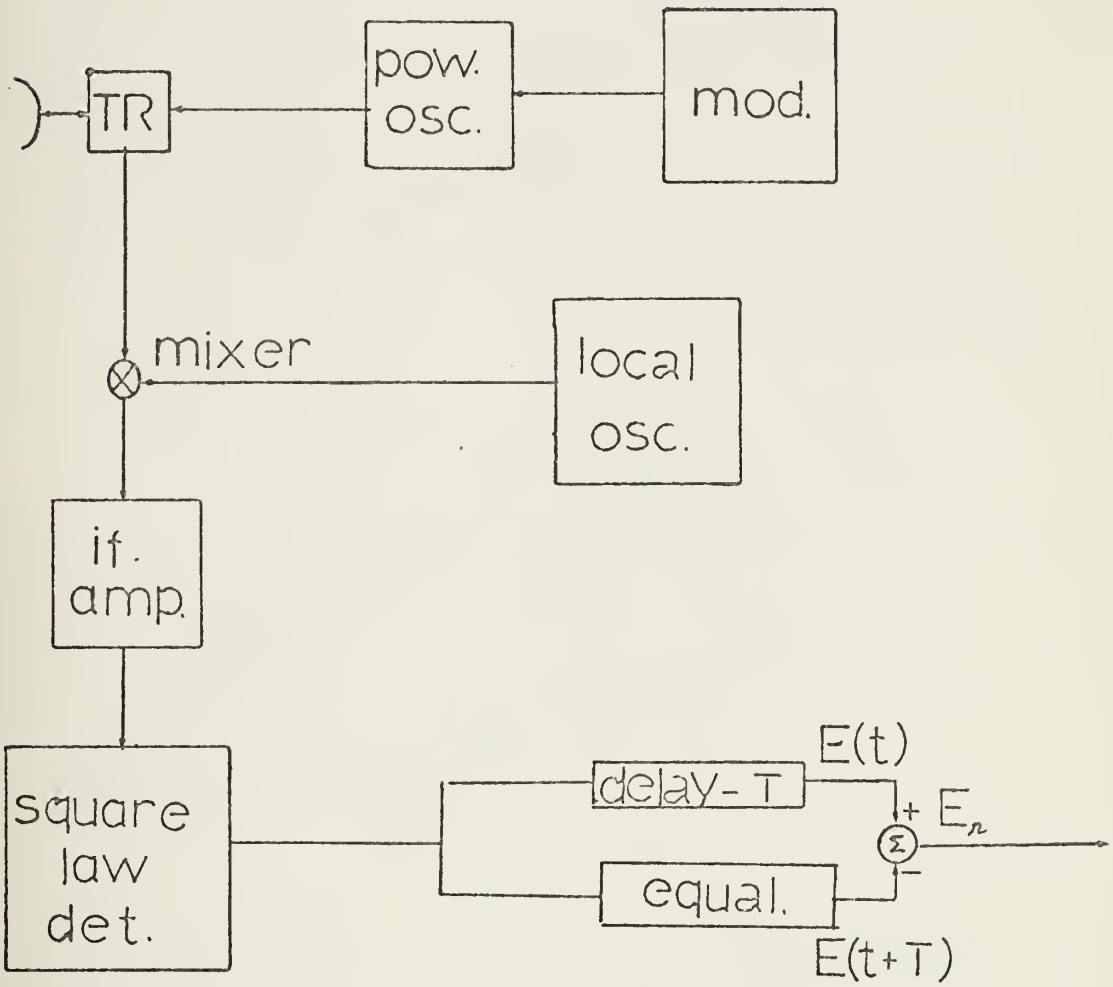
TR
pow.
osc.
mod.
mixer
local
osc.
if.
amp.
square
law
det.
E(t)
delay - T
+
E_n
Σ
−
equal.
E(t+T)

Fig. 16

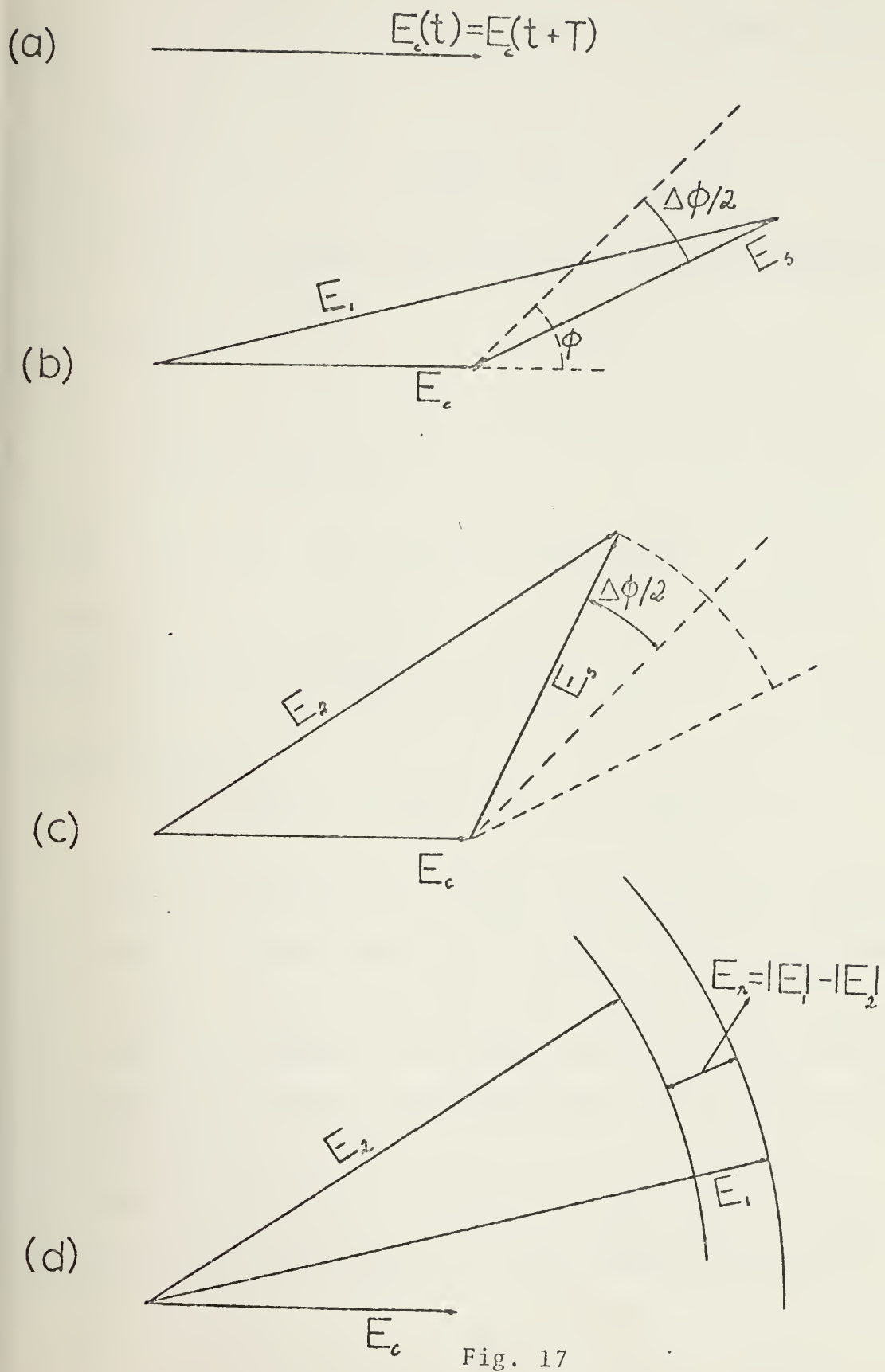
(a)
$E_c(t)=E_c(t+T)$
(b)
$\Delta\phi/2$
E_3
E_1
ϕ
E_c
(c)
$\Delta\phi/2$
E_3
E_2
E_c
(d)
$E_R=|E_1|-|E_2|$
E_2
E_1
E_c

Fig. 17

moving target. In order to get better results, instead of the difference in amplitude, the difference of the square of the amplitudes will be used. That is the reason for a square law detector in Fig. 16.

From Fig. 17 (b):

$$E_1^2 = E_c^2 + E_s^2 - 2E_c^2E_s^2 \cos(\phi - \Delta\phi/2)$$

(the equation relates only the absolute values of the vectors)

From Fig. 17 (c):

$$E_2^2 = E_c^2 - E_s^2 - 2E_cE_s \cos(\phi + \Delta\phi/2)$$

(only amplitude relations)

Then $E_r^2 = E_1^2 - E_2^2 = 4E_cE_s \sin\phi \sin\frac{\Delta\phi}{2}$

since $\phi = \omega_d t + \Delta\phi/2$

and $\Delta\phi = \omega_d T = \frac{2\pi f_d}{f_R}$, $T = \frac{1}{f_R}$

which implies

$$E_r^2 = 4E_cE_s \sin\frac{\pi f_d}{f_R} \sin(\omega t + \Delta\phi/2)$$

So, the blind speeds are the same as in the coherent processor, and the transfer function must have the same shape. But if $E_c = 0$, that implies $E_r = 0$. That is the reason why an amplitude processor must have a clutter return, and the stronger the clutter return the better since E_r increases linearly with E_c.

Clutter cancellation can also be made at IF frequencies instead of at the video part of the receiver (Fig. 18).

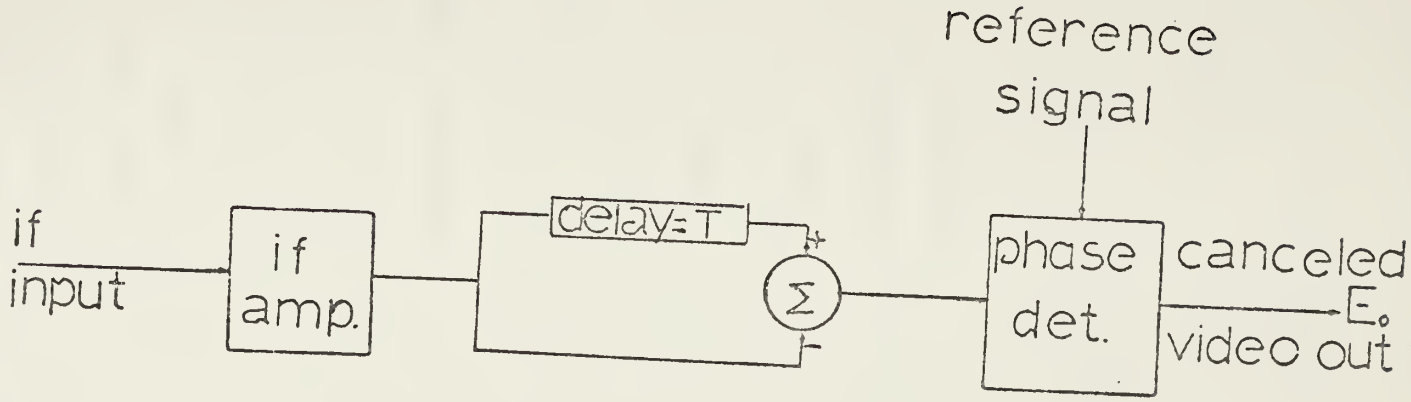
reference
signal
if
input
if
amp.
delay=T
+
Σ
-
phase
det.
canceled
video out
E₀

Fig. 18

Let the two IF signals separated by $T = \frac{1}{f_R}$ be

$$E_1 = E \sin [2\pi(f_{IF} \pm f_d)t - \phi_o]$$

$$E_2 = E \sin [2\pi(f_{IF} \pm f_d)(t + T) - \phi_o]$$

where $\phi_o = \frac{4\pi f_{IF} R_o}{c}$

$$E_r = E_1 - E_2 = 2E \sin [\pi(f_{IF} \pm f_d)T] \cos$$
$$[2\pi(f_{IF} \pm f_d)(t + \tfrac{T}{2}) - \phi_o]$$

is the output of the summer.

The output of the phase detector would be

$$E_o = E \sin [\pi(f_{IF} \pm f_d)T] \cos \{2\pi[f_d t + (f_{IF} \pm f_d)\ \tfrac{T}{2}] - \phi_o\}$$

where the video envelope is of the form $E \sin [\pi(f_{IF} \pm f_d)T]$. Since in an MTI processor if $f_d = 0$ the output must be zero that means that $\pi f_{IF} T = n\pi$ is a necessary condition. That is, $f_{IF} = \frac{n}{T} = n f_R$, the IF frequency must be a multiple of the pulse repetition frequency.

The existence of blind speeds can constitute a problem since every velocity is not processed in the same way. One of the most often used methods to improve that situation is with the use of staggered PRF systems. There are some quantitative factors that describe the efficiency of an MTI processor. Since they are the descriptors of the MTI processor, it is worthwhile to state their proper definitions.

Improvement factor is defined as $I = r_o/r_i$, where r_o is the output target to clutter ratio and r_i the input target

to clutter ratio. This definition reflects the gain as well as the clutter rejection of the processor.

Subclutter visibility is defined as the capacity of a radar to detect moving targets in a clutter environment. A radar with x db of SCV is one that is able to detect a target over a clutter that has a signal x db stronger than the moving target. The SCV cannot be used as a parameter for comparison between radars since the target to clutter ratio is a function of the size of the radar resolution cell.

The two main problems with MTI processors design are: first, a correct modeling of the expected type of clutter, and second, the correct shaping of the transfer function depending on the type of clutter. In [2] there is an extensive description of the different types of clutter and modeling processes.

When the platform of the radar is moving, the stationary targets will have a doppler return different from zero. This is the typical case of the Airborne MTI processors. Various techniques of clutter looking and automatic tracking must be used. The techniques get much more complicated and the processor becomes much more dependent for specific application.

E. DIGITAL SIGNAL PROCESSING, DFT AND FFT

Due to high speed, low cost, versatility and almost independence of external condition of recent digital computers, the processing of radar signals in digital form covers now a wide spectrum of the radar signal processing.

The two basic methods of approach are represented in block diagram in Fig. 19. In the first case (Fig. 19 a) the signal is first sampled and quantized in such a way that the signal is converted into a sequence of numbers. The numbers are then stored and the processor, using arithmatic and logical operations, manipulates the numbers according to an algorithm which is a function of the type of filter we want. The resultant numbers are then dequantized and passed through a low pass filter (D/A). The second method (Fig. 19 b) is basically a frequency domain approach of the problem. The signal is quantized and a discrete Fourier transform algorithm is applied to the quantized signal. The spectrum of the signal is then weighted as a function of the type of filtering required. Then, the inverse operations take place. Due to recent improvements in faster algorithms to implement the DFT this second method is becoming widely used. The theory behind the first method is based on the Z transform theory [10]. The variable Z represents a delay and is defined through its Laplace transform by

$$Z = \exp ST$$

where 1/T is the sampling frequency. Given an analog function f(t), the transform of f(t) will be

$$F(Z) = \sum_{n=0}^{\infty} f(nT)Z^{-n}$$

The two basic configurations are recursive and nonrecursive filters. In the nonrecursive case the output is of the form

$$E_o = B_i[1 + A_1Z^{-1} + \ldots A_nZ^{-n} \ldots],$$

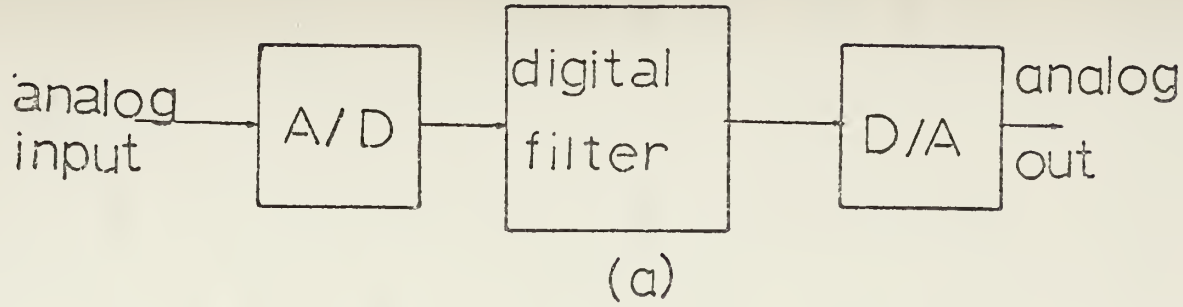
analog input
A/D
digital filter
D/A
analog out

(a)

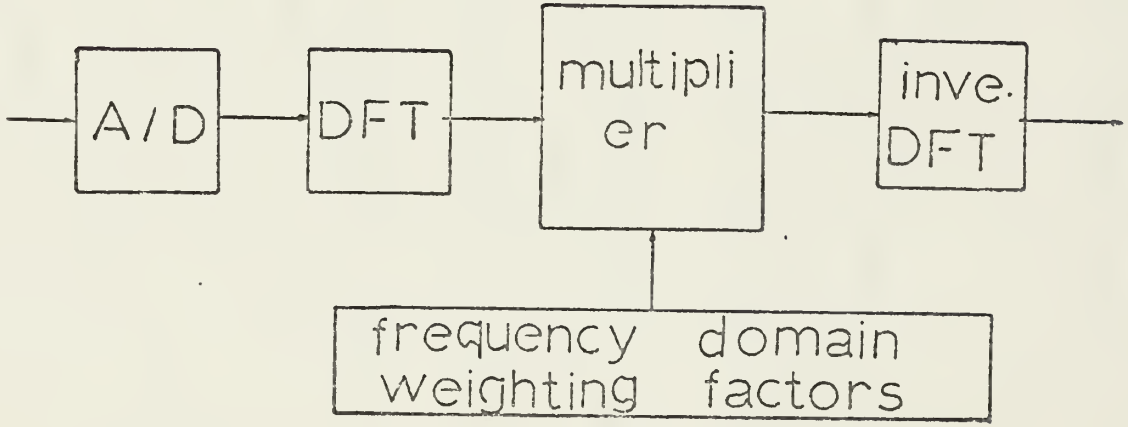
A/D
DFT
multipli er
inve. DFT
frequency domain weighting factors

(b)

Fig. 19

where the coefficients A_i are obtained from the coefficients of a Fourier series expansion of the frequency domain function of the desired filter.

The feedback or recursive filters are normally obtained using the analog transfer function of the required filter and substituting S by a chosen relation between S and Z. Usually the bilinear transformation

$$[11] \qquad S = \frac{2}{T} \frac{1 - Z^{-1}}{1 + Z^{-1}}$$

is used since with the correct sampling frequency it is very accurate and easy to implement. Figure 20 shows the basic configurations for the nonrecursive (Fig. 20 a) and recursive (Fig. 20 b) filters.

In many radar applications the discrete Fourier transform is being used especially as a bank of filters for obtaining doppler outputs. The understanding of what it is and its limitations are thus fundamental.

In order to get a Fourier transform with a digital processor not only the input waveform must be in digital form but also the values of the Fourier transform must be represented by discrete values. Figure 21 gives us the graphical derivation of the discrete Fourier transform pair. The input waveform h(t) (Fig. 21 a) must be sampled in order to be manipulated by a digital processor. The sampling operation is the same as multiplying h(t) by a string of delta functions (Fig. 21 b). Since multiplication in time is the same as convolution in the frequency domain, the resulting spectrum is that of Fig. 21 c). Here it is seen that if the samples

$$H(z) = \frac{E_o(z)}{E_i(z)} = 1 + A_1 z^{-1} + \cdots + A_m z^{-m}$$

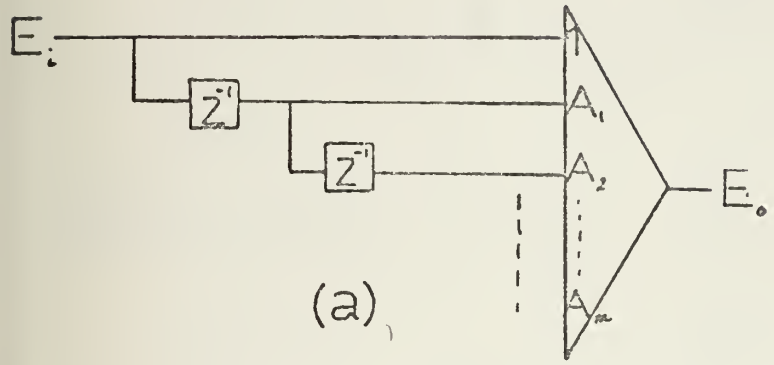

(a)

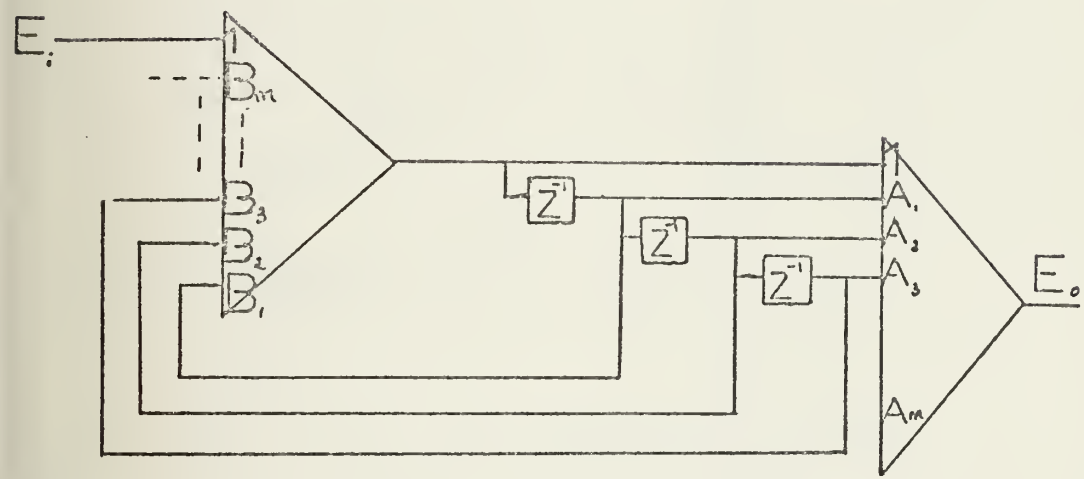

$$\left)= \frac{E_o(z)}{E_i(z)} = \frac{z^m + A_1 z^{m-1} + \cdots + A_m}{z^m - B_1 z^{m-1} - \cdots - B_m}\right.$$

(b)

Fig. 20

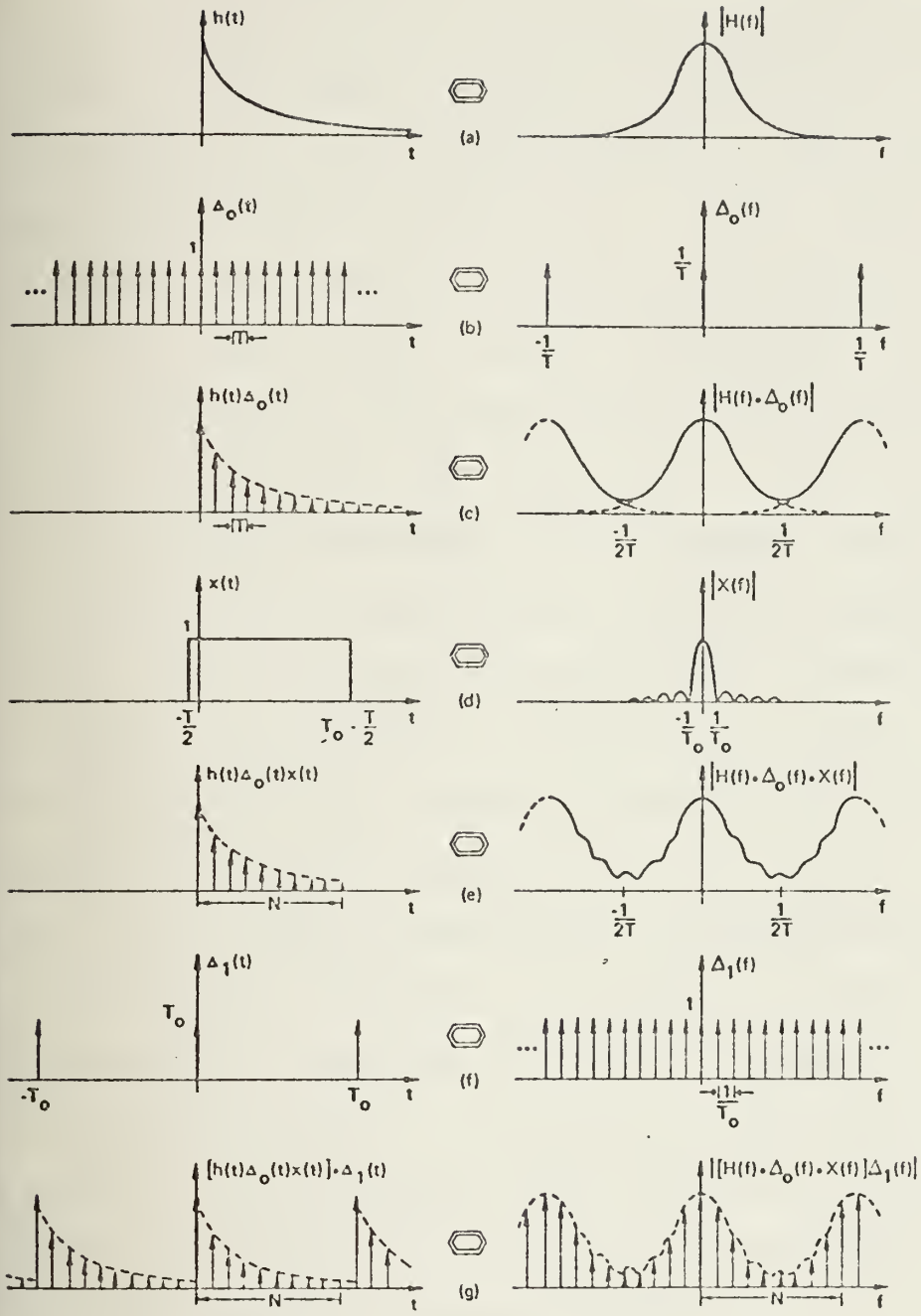
h(t)
t
(a)
|H(f)|
f
Δ0(t)
1
T
t
(b)
Δ0(f)
1/T
-1/T
1/T
f
h(t)Δ0(t)
T
t
(c)
|H(f)•Δ0(f)|
-1/2T
1/2T
f
x(t)
1
-T/2
T0 - T/2
t
(d)
|X(f)|
-1/T0
1/T0
f
h(t)Δ0(t)x(t)
N
t
(e)
|H(f)•Δ0(f)•X(f)|
-1/2T
1/2T
f
Δ1(t)
T0
-T0
T0
t
(f)
Δ1(f)
1
1/T0
f
[h(t)Δ0(t)x(t)]•Δ1(t)
N
t
(g)
|[H(f)•Δ0(f)•X(f)]Δ1(f)|
N
f

Fig. 21

are not at a frequency higher than the Nyquist rate there will be an aliasing effect that will distort the waveform. But since in most systems, and especially in any real time radar system, the waveform must be processed in a finite time, there are for computation only a finite set of samples. This is equivalent to multiplying $h(t)\Delta_o(t)$ (Fig. 21 c) by a rectangular function (Fig. 21 d). Again, the previous spectrum must be convolved with the spectrum of the rectangle to get the result in Fig. 21 (e). As expected, the larger the T_o, the smaller is the distortion in the spectrum. But as stated before, the output must be in a digital format. So it is necessary to multiply in the frequency domain $|H(f) * \Delta_o(f) * x(f)|$, by a string of delta functions, separated by $1/T_o$. That is equivalent to the convolution in time of a string of impulses separated by T_o with $h(t)\Delta_o(t)$ $x(t)$. The final result is in Fig. 17 (g). As can be seen, the output of the DFT processor is not a sampled replica of $|H(f)|$. Aliasing effects and finite time of processing are responsible for the amount of distortion introduced. In order to get the mathematical expression for the DFT, it is only necessary to make a parallel derivation to that of the graphical derivation already discussed. The time domain expression for the output (Fig. 17 g) will be obtained; then the Fourier coefficients of that periodic function represent the DFT.

Let h(t) be the input function. The operation of sampling h(t) is equivalent to a multiplication by

$$\Delta_o(t) = \sum_{K=-\infty}^{+\infty} \delta(t - KT)$$

so $h(t)\Delta_o(t) = \sum_{K=-\infty}^{+\infty} h(KT)\,\delta(t - KT)$

Since $x(t) = \begin{cases} 1 & -\frac{T}{2} < t < T_o - T/2 \\ 0 & \text{otherwise} \end{cases}$

is to be multiplied by $h(t)\Delta_o(t)$

$$h(t)\Delta_o(t)x(t) = \sum_{K=0}^{N-1} h(KT)\,\delta(t - KT)$$

where $NT = T_o$

then we have to sample the Fourier transform of $h(t)\Delta_o(t)x(t)$ by a string of impulses in the frequency domain

$$\Delta_1(f) = \sum_{-\infty}^{+\infty} \delta(f - 1/T_o)$$

which infers $\Delta_1(t) = F^{-1}[\Delta_1(f)] = T_o \sum_{r=-\infty}^{+\infty} \delta(t - r\,T_o)$

must be convolved with $h(t)\Delta_o(t)x(t)$ to obtain the time domain answer.

$$h_D(t) = [h(t)\Delta_o(t)x(t)] * \Delta_1(t) =$$

$$= \left[\sum_{K=0}^{N-1} h(KT)\delta(t - KT)\right] * \left[T_o \sum_{r=-\infty}^{+\infty} \delta(t - rT_o)\right]$$

$$= T_o \sum_{r=-\infty}^{+\infty} \left[\sum_{K=0}^{N-1} h(KT)\delta(t - KT - rT_o)\right]$$

Since $h_D(t)$ is a periodic function with a period NT, in order to avoid time aliasing $x(t)$ is chosen in such a way that the end points of $x(t)$ don't coincide with sampling points.

If they did coincide, it would generate an additive effect at the boundary. But NT is still equal to T_o. Also, the Fourier transform of a periodic function is given by the Fourier coefficients of a series expansion. So

$$H_D(nf_o) = H_D(\frac{n}{T_o}) = \sum_{-\infty}^{+\infty} c_n \, \delta(f - nf_o)$$

where $$c_n = \frac{1}{T_o} \int_{-T/2}^{T_o - T/2} h_D(t) \exp -j \frac{2\pi nt}{T_o} \, dt, \quad n = 0, \quad 1, ..$$

So, $$c_n = \frac{1}{T_o} \int_{-T/2}^{T_o - T/2} T_o \left[\sum_{r=-\infty}^{\infty} \sum_{K=0}^{N-1} h(KT) \delta(t - KT - rT_o) \exp -j \frac{2\pi nt}{T_o} \right] dt$$

Since the integration is only over one period T_o

$$c_n = \int_{-T/2}^{T_o - T/2} \left[\sum_{K=0}^{N-1} \delta(t - KT) \exp -j \frac{2\pi nt}{T_o} \right] dt$$

$$c_n = \sum_{K=0}^{N-1} h(KT) \int_{-T/2}^{T_o - T/2} \exp -j \frac{2\pi nt}{T_o} \, \delta(t - KT) \, dt$$

$$= \sum_{K=0}^{N-1} h(KT) \exp -j \frac{2\pi KnT}{T_o}$$

Since $T_o = NT$

$$c_n = \sum_{K=0}^{N-1} h(KT) \exp -j \frac{2\pi Kn}{N}, \quad n = 0, \quad 1, \quad 2, ..$$

and the Fourier transform of $h_D(t)$ is

$$H_D\left(\frac{n}{NT}\right) = \sum_{n=-\infty}^{+\infty} \sum_{K=0}^{N-1} h(KT) \exp -j \frac{2\Pi nK}{N} \, \delta\left(f - \frac{n}{NT}\right)$$

To see that $H_D\left(\frac{n}{NT}\right)$ is also periodic, it is necessary to show that c_n is periodic with a period NT.

Let $n = r + N$

since $\exp -j \frac{2\pi K(r+N)}{N} = \exp -j \frac{2\pi Kr}{N}$

which implies $c_n (r+N) = c_n(r)$

which implies $H_D\left(\frac{r+N}{NT}\right) = H_D\left(\frac{r}{NT}\right)$

so there are only N distinct values that can be evaluated. Normally the function

$$H\left(\frac{n}{NT}\right) = \sum_{K=0}^{N-1} h\,(KT) \exp -j\, 2\pi nK/N\,,\ n = 0,\ 1 \ldots\ N-1$$

is called the discrete Fourier transform (DFT) which relates N samples in the time domain to N samples in the frequency domain. The inverse discrete Fourier transform, is, as expected

$$h\,(KT) = \frac{1}{N} \sum_{K=0}^{N-1} H\left(\frac{n}{NT}\right) \exp j \frac{2\pi nK}{N}\ ,\ K = 0,\ 1 \ldots\ N-1$$

So it is seen that with very simple complex multiplications and additions there is conversion from one domain to the other.

The Fast Fourier transform is an algorithm to implement the discrete Fourier transform which, by reducing the number of multiplications reduces the processor time to perform the algorithm. For a better understanding of the FFT, it must be reduced to a matrix form.

Consider the DFT

$$x(n) = \sum_{K=0}^{N-1} x_o(K) \exp -j \frac{2\pi nK}{N}\ ,\ n = 0,\ 1 \ldots\ N-1$$

if $W = \exp -j\, 2\pi/N$, then in a compact form

$$x(n) = W^{nK}\, x_o(K)$$

where $x(n) = \begin{bmatrix} x(o) \\ \vdots \\ x(N-1) \end{bmatrix}$, $x_o(K) = \begin{bmatrix} x_o(o) \\ \vdots \\ x_o(N-1) \end{bmatrix}$

$$W^{nK} = \begin{bmatrix} W^o & \cdots & W^o \\ \vdots & & \vdots \\ W^o & \cdots & W^{(N-1)(N-1)} \end{bmatrix}$$

the examination of the matrix equation shows that there will be N^2 possible complex multiplications and $N(N-1)$ complex additions. If $N = 2^\gamma$, and the FFT algorithm [12] is used, the number of multiplications will be reduced to $N\gamma/2$ and the number of additions to $N\gamma$. Figure 22 gives a comparison between the FFT algorithm and the direct computation with respect to the number of required multiplications.

As it was shown, complex notation is greatly used in the mathematical structure of signal processing. So the need to represent signals in complex notation becomes a necessity even in their implementation. It will be seen how a sine wave type of function is converted in order to be represented by a complex number.

In Fig. 23, let the input signal be

$$S(t) = A \sin [(\omega_{IF} \pm \omega_d)t + \phi_o]$$

where ω_{IF} and ω_d can be thought as the intermediate frequency and doppler frequency in a radar receiver. If the local

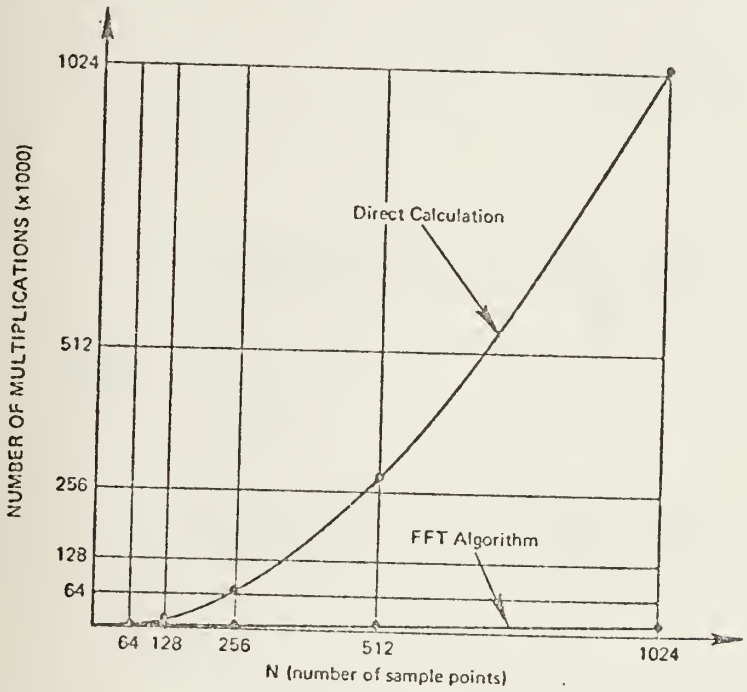
NUMBER OF MULTIPLICATIONS (x1000)
1024
512
256
128
64
Direct Calculation
FFT Algorithm
64
128
256
512
1024
N (number of sample points)

Fig. 22

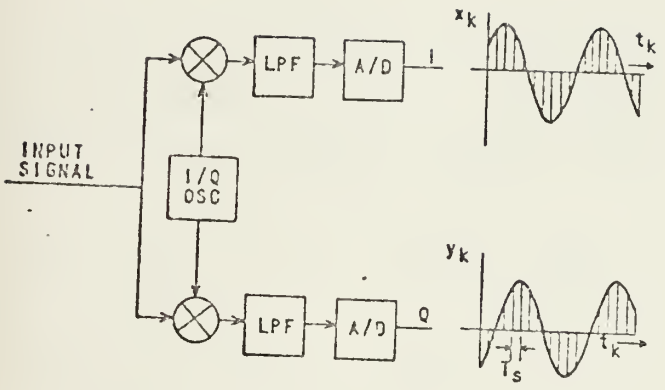

Fig. 23

oscillator (I/Q) generates 2 cos ω_{IF} and -2 sin $\omega_{IF}t$ which can be obtained with a 90° phase shifter, the in phase channel (I) and the out of phase channel (Q) outputs are of the form

$$I = A \cos (\omega_d t + \phi_o)$$

$$Q = A \sin (\omega_d t + \phi_o)$$

Since the low pass filter retains only the difference frequency. The I and Q signals can then be thought as the real and imaginary part of the complex signal

$$Z = I + j\ Q$$

If the I and the Q channels are sampled and converted to sequences of numbers x_K and y_K, the resultant sampled pair can be considered a complex digital word.

$$A_K = x_K + j\ y_K = |A_K| \exp j\ \phi_K$$

where $x_K = A \cos (\omega_d K T + \phi_o)$

$$y_n = A \cos (\omega_d K T + \phi_o)$$

$$|A_K| = A,\ \phi_K = \omega_d K T + \phi_o$$

assuming a sampling frequency $f = \frac{1}{T}$. Since ϕ_K varies linearly with K, the complex digitized signal can be interjected as a vector of amplitude A that shifts at every sampling time KT, by $\omega_d K \Delta T$.

F. SYNTHETIC APERTURE RADAR

Using the pulse compression techniques already mentioned, it is possible to achieve very small values of range resolution. In many radar applications such as aerial photography not only a very small range resolution is necessary but also an equivalent small aximuth resulution is desired. The conventional method of reducing azimuth resolution by very small beamwidths will always require big antennas which, especially in airborne radars, is a problem since space is a limiting factor. Also, the fact that azimuth resulution is an increasing function with distance makes it many orders of magnitude higher than the range resolution even for small distances.

Consider a radar without a pulse compression processor. Then the range resolution δR is

$$\delta R \simeq \frac{c}{2\ B_W}$$

c = speed of propagation

B_W = bandwidth

If the antenna has an aperture D, the beamwidth is $\theta_B = \frac{\lambda}{D}$, So the azimuth resolution δ_{AZ} is

$$\delta_{AZ} = R\theta_B = \frac{R\lambda}{D}$$

R = distance to the target

if B_W = 10 MHZ, f = 5000 MHZ, D = 10 yds and R = 100 mi, then

δR = 16.4 yds

δ_{AZ} = 1300 yds

Synthetic aperture radar is a way of processing radar signals in order to get an equivalent antenna aperture much bigger than the real antenna to reduce δA_Z. In the synthetic

aperture case a single antenna is translated along a line. The received signals are then stored, and processed after the radiating element has travelled a fixed distance. The synthetic aperture concept can be viewed through two different aspects. From a doppler viewpoint or from a linear array viewpoint, the basic principle of the doppler effect viewpoint is that there exists a one to one correspondence between the long track coordinates of a reflecting object and the instantaneous doppler shift.

Consider Fig. 24 in which an airplane flies at an altitude h_o with a constant speed v and with a radar antenna that illuminates the area A. The radar antenna does not rotate but simply moves with the airplane.

If there is no pulse compression and the width of the transmitted pulse is τ, it is known that the slant resolution constant is

$$\delta_R \simeq \frac{c\tau}{2} \simeq \frac{c}{2\,B_w}$$

so the corresponding ground resolution constant is

$$\rho_R = \delta_R \sec \psi = \frac{c\tau}{2} \sec \psi$$

Also, from Fig. 24 it is seen that $L = \beta R$ where β is the beamwidth of the transmitting antenna and L_{eff} is the the along track resolution ρ_x.

Since $$\beta = \frac{\lambda}{D}$$

then $$\rho_x = L_{eff} = \frac{\lambda}{D} R$$

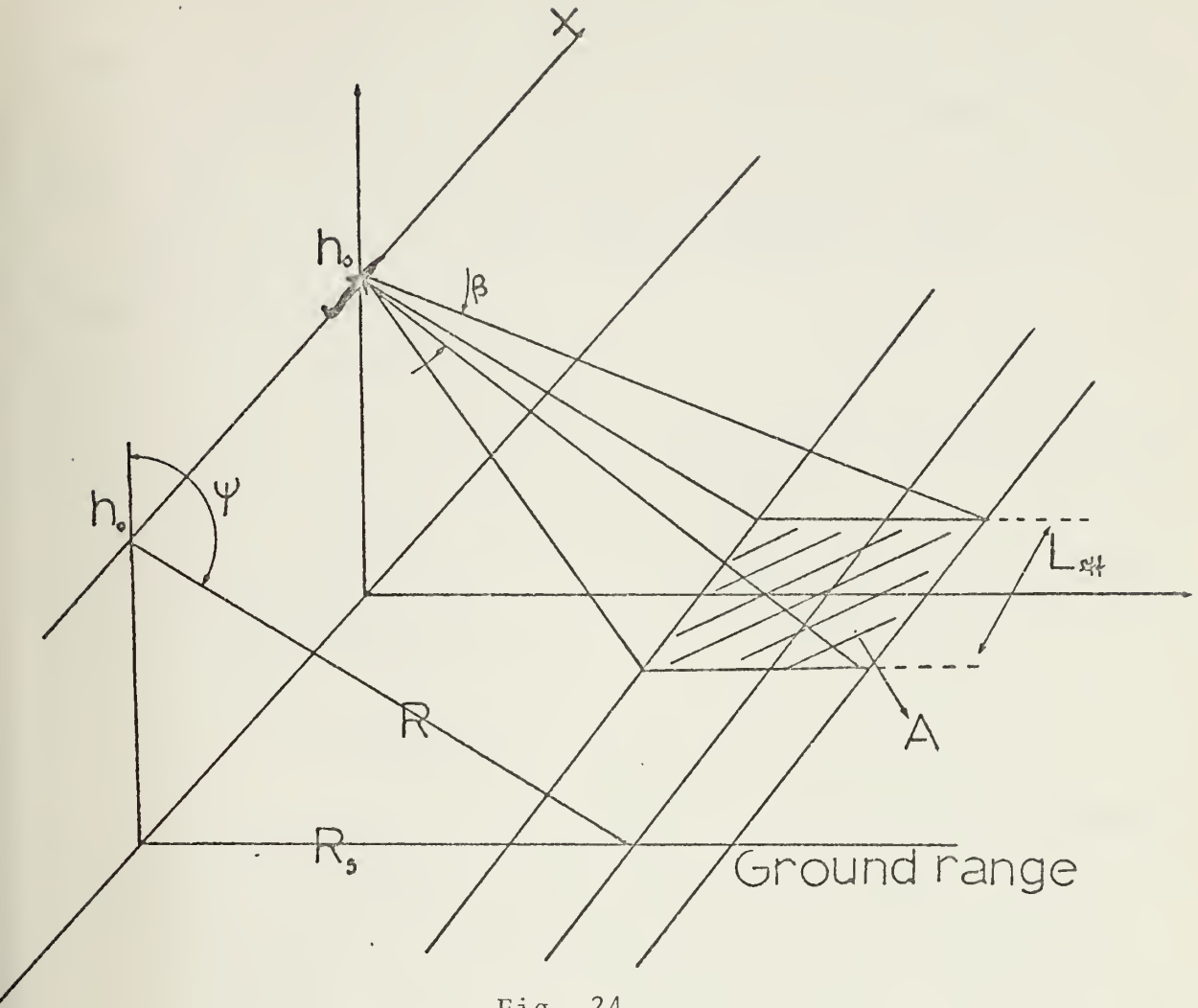
X
h_o
β
h_o
ψ
L_{sl}
R
A
R_s
Ground range

Fig. 24

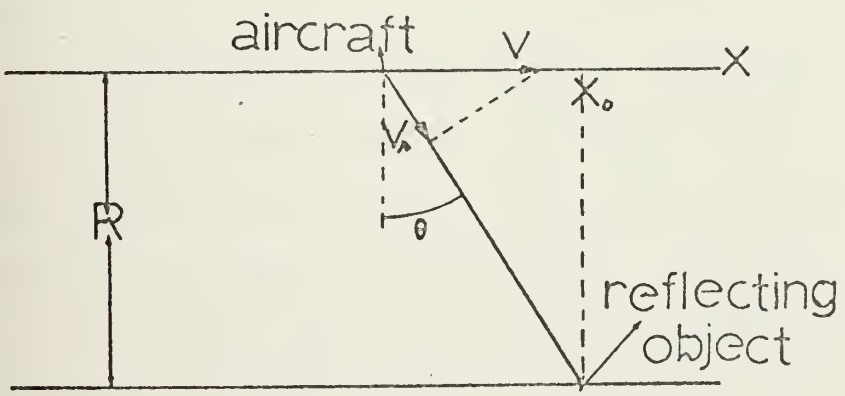
aircraft
V
X
X_o
V_s
R
θ
reflecting
object

Fig. 25

and as pointed out, it is impossible to increase D beyond certain limits in order to decrease ρ_x. But if a relation is found between doppler frequency and the position x of the radar, then it is possible to make an azimuth discrimination.

From Fig. 25 it is seen that the radial velocity with respect to the target is

$$v_r = v \sin \theta$$

So the doppler shift will be $f_d = \frac{2v}{c} f_o \sin \theta$ where f_o is the transmitted frequency. But if θ is small, which is the normal physical situation since the total illuminated area is small and R is big, then $\sin \theta \simeq \theta = x_o - x$, which makes

$$f_d = \frac{2v}{\lambda R} (x_o - x)$$

So it is seen that with a frequency analysis of the received signal, it is possible to get an azimuth resolution that is only a function of discriminating between the closeness of two frequencies. The basic principle for the explanation of synthetic aperture radar using the linear array theory is the following:

In a linear array various elements are fed at the same time and the received echo is also received at the same time, but due to path differences a receiving pattern is generated. In the synthetic aperture case there is only one transmitting element that moves with constant speed along a line. So a long antenna will be formed not by physical means but by signal processing. After the radiating element has travelled a distance L_{eff} corresponding to the illumination time of the real

beam, the stored signals after weighting and phase shifting resemble the signals received by a big linear array.

Two cases are important to differentiate: the unfocused synthetic aperture and the focused synthetic aperture.

In the focused synthetic aperture radar if $\theta = 0$ (Fig. 26 a), by signal processing (for $R \neq \infty$) or by real situation ($R = \infty$) the signals all arrive with the same phase. In a real linear array the angle selectivity is provided only during the reception of the signals. But in the synthetic case, since only one element is radiating and is moving, it is necessary to account for the phase shift due to the transmitted and received path. So, due to the fact that all the round-trip phase counts for the formation of the receiving pattern, as opposed to the real case in which only the received path is responsible for the receiving pattern, the effective beamwidth is

$$\beta_{eff} \simeq \frac{\lambda}{2\, L_{eff}} \qquad \text{instead of } \frac{\lambda}{L_{eff}} \ .$$

Since the length of the synthetic aperture radar is equal to the distance corresponding to the time of illumination, $L_{eff} = \frac{R\lambda}{D}$, where D is the horizontal aperture of the physical antenna and R the distance to the target (Fig. 24), then the azimuth resolution is

$$\delta_{AZ} = \beta_{eff}\, R = \frac{\lambda}{2\, L_{eff}}\, R = \frac{D}{2}$$

The azimuth resolution is independent of λ and R in the focused case which is of course an important result. This means that the smaller the antenna the higher the azimuth resolution.

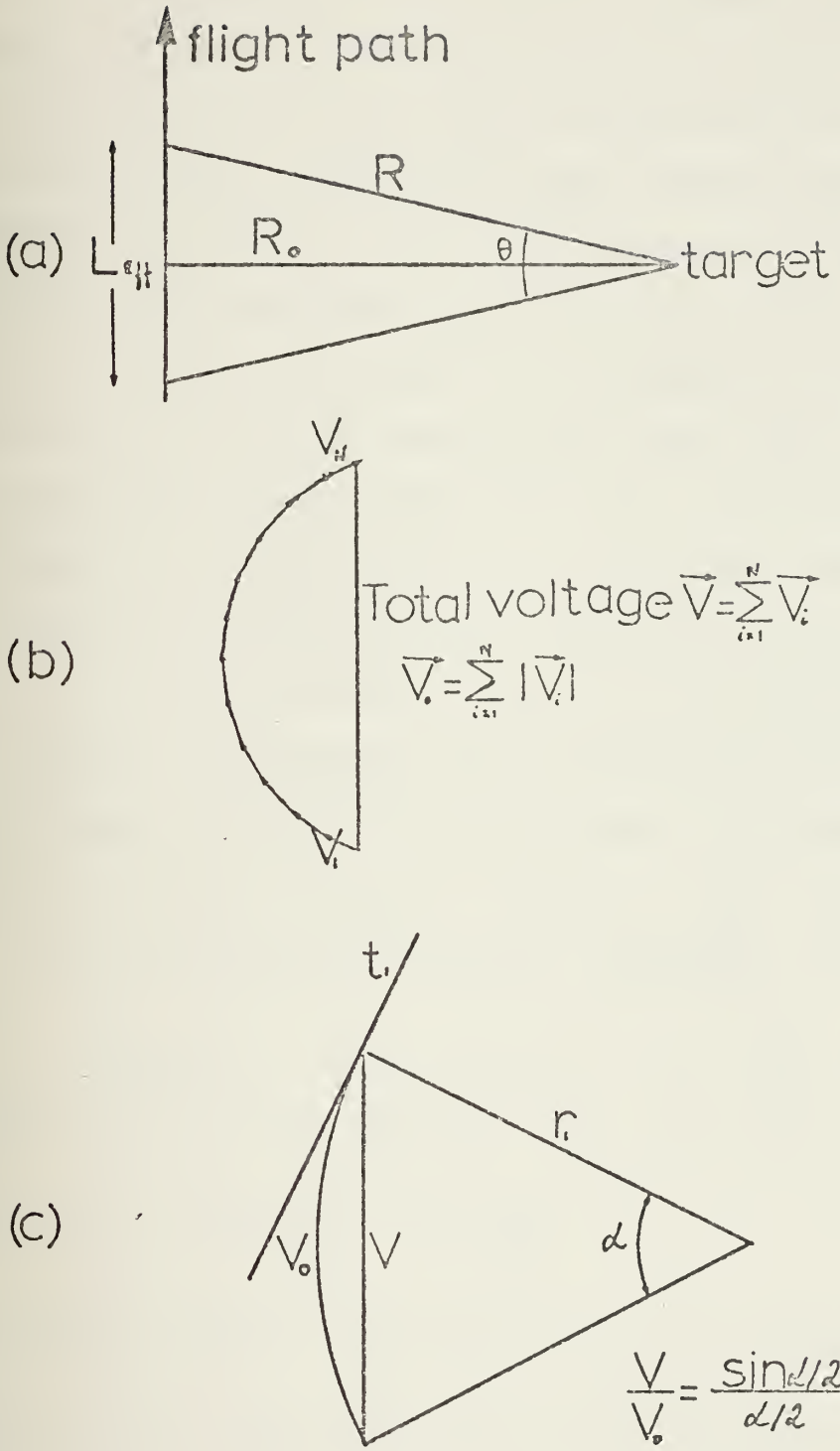
flight path
R
(a)
R_o
θ
target
(b)
Total voltage $\vec{V}=\sum_{i=1}^{N}\vec{V}_i$
$\vec{V}_o=\sum_{i=1}^{N}|\vec{V}_i|$
(c)
r_i
V_o
V
α
$\frac{V}{V_o}=\frac{\sin\alpha/2}{\alpha/2}$

Fig. 26

In the unfocused case it is important to account for the phase difference between the center and the ends of the equivalent linear array. A quantitative interpretation of the unfocused synthetic aperture radar can be explained as follows:

Consider Fig. 26 (a): Due to the fact that $R_o \neq R$, there is a phase shift between the center and the end. The total voltage is the vector sum of small discrete voltages that are received along the path L_{eff} (Fig. 26 b). If the number of discrete voltages is large, it is possible to make the approximation of Fig. 26 (c) and determine the relationship between the resultant voltage V and the linear sum of the discrete voltages V_o. If the 3 db point is defined as the boundary for the drop in voltage, α must be approximately $\pi/2$. But, when $\alpha \simeq \pi/2$, the radius r_1 (Fig. 26 c) is perpendicular to the tangent t_1, implying that the phase difference between the voltage at the end and at the center must approximate 45°. This sets a limit on L_{eff}. So when $R = R_o + \lambda/8$ (round trip $< > \lambda/4$) the conditions are met. Using Fig. 26 (a):

$$(L_{eff}/2)^2 + R^2 = (R + \lambda/8)^2 = R^2 + \frac{R\lambda}{4} + \frac{\lambda^2}{64}$$

if $\frac{\lambda^2}{64}$ is very small compared to the other terms $L_{eff} = \sqrt{R\lambda}$

Since $\theta_{3db} = .455 \frac{\lambda}{L_{eff}} \simeq \frac{1}{2}\sqrt{\frac{\lambda}{R}}$

the azimuth resolution would be $\delta_{AZ} = R\theta = \frac{1}{2}\sqrt{\lambda R}$

Since δ_{AZ} is a function of $R^{1/2}$, this is a solution between the focused case and the conventional case. Figure 27 gives a relation between the three cases.

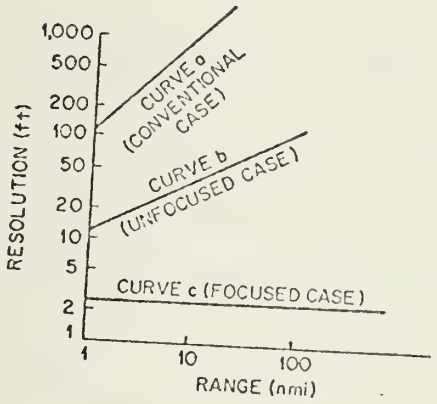
1,000
500
200
100
50
20
10
5
2
1
RESOLUTION (ft)
CURVE a (CONVENTIONAL CASE)
CURVE b (UNFOCUSED CASE)
CURVE c (FOCUSED CASE)
1
10
100
RANGE (nmi)

Fig. 27

The signal processing theory for synthetic aperture radar can be understood through the analysis of the ambiguity function of the received signal. If it is possible to separate the range and azimuth as the two ambiguity factors from the general ambiguity function, then the determination of the azimuth ambiguity function and consequently the azimuth resolution function are immediate.

Consider a transmitted signal f(t). After reflection in the ground or target with reflectivity $\rho(x,y,z)$, the received signal will be

$$S(t) = \iiint \rho(x,y,z)\, f\left(t - \frac{2R}{c}\right) dxdydt \quad [13]$$

where the integration is made over the illuminated region, and R is the distance between (x,y,z) and the radar antenna. The processing of the signals in fact recovers a signal proportional to $\rho(x,y,z)$. Using matched filter techniques, the output will be of the form,

$$e_o(t) = \int f^*\left(t - \frac{2R'}{c}\right) S(t)\, dt$$

$$= \iiint \rho(x,y,z)\, f\left(t - \frac{2R}{c}\right) f^*\left(t - \frac{2R'}{c}\right) dtdxdydz$$

where R' is the distance from the antenna to the point (x',y',z') corresponding to $\rho(x',y',z')$. Let's find the ambiguity function of f(t). By definition it will be

$$\psi(x,y,z,x',y',z') = \int f\left(t - \frac{2R}{c}\right) f^*\left(t - \frac{2R'}{c}\right) dt$$

where * means complex conjugate.

So

$$e_o(t) = \iiiint \psi \rho\,(x,y,z)\; dxdydz,$$

is a weighted average of $\rho(x,y,z)$ where the weighting function is $\psi(x,y,z,x',y',z')$.

Let $f(t) = g(t) \exp j\,\omega_o t$

then

$$\psi = \int g(t - \frac{2R}{c})\, g^*\,(t - \frac{2R'}{c}) \exp j\,\omega_o(\frac{2R}{c} - \frac{2R'}{c})\; dt$$

Assume the energy is transmitted in finite amounts of time. If during those finite lengths of time the exponential does not vary too much, then during a transmission the exponential part can be considered constant although varying between transmissions. So it can be taken out of the integral. The result will be

$$\psi = \Sigma\,[\int g(t - \frac{2R}{c})\, g^*\,(t - \frac{2R'}{c})\; dt] \exp -j\,\omega_o(\frac{2R}{c} - \frac{2R'}{c})$$

If gg^* is constant during a transmission period, it can be moved out of the summation and

$$\psi = [\int gg^* dt]\; \Sigma \exp -j\omega_o[\frac{2R}{c} - \frac{2R'}{c}]$$

It is obvious that the first factor is the range ambiguity function, and the second, the azimuth ambiguity function. So, the azimuth ambiguity function is

$$\psi_{AZ} = \Sigma \exp -j\,\omega_o(\frac{2R}{c} - \frac{2R'}{c})$$

Figure 28 indicates a real situation. From that figure it can be seen that:

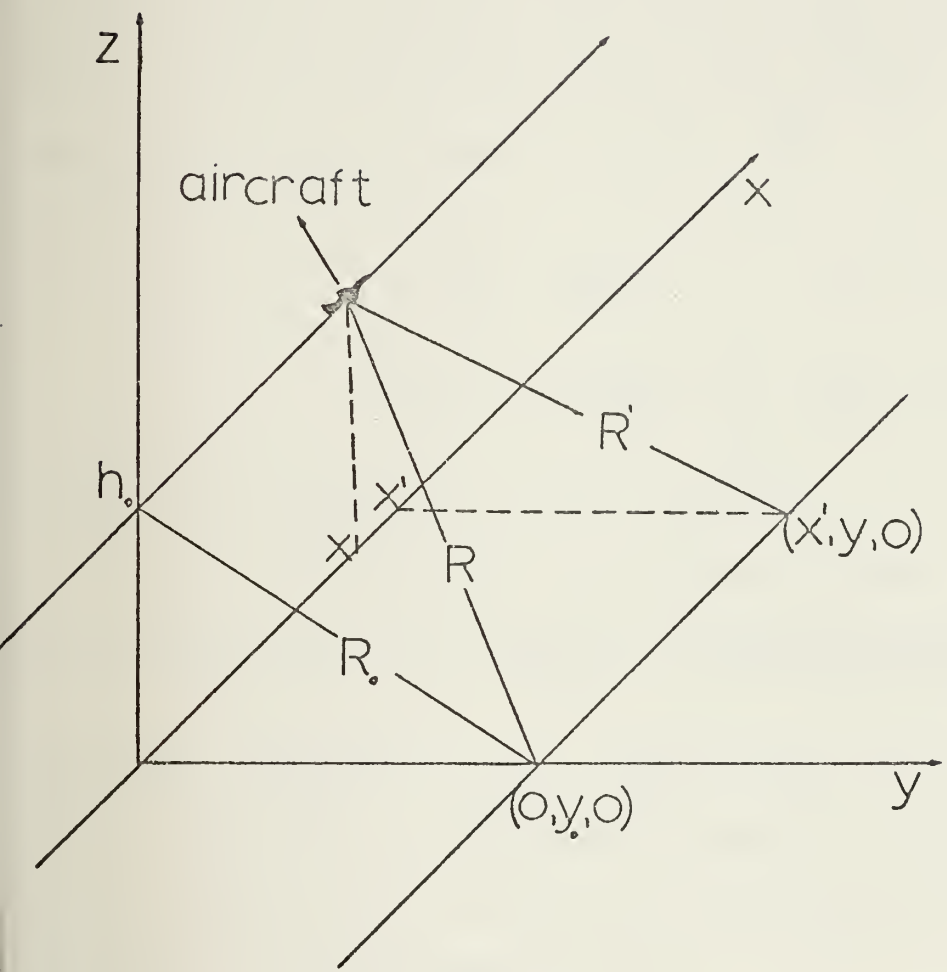

Fig. 28

$$x = vt$$

$$R = \sqrt{R_o^2 + x^2} \simeq R_o + \frac{x^2}{2R_o}$$

$$R' = \sqrt{R_o^2 + (x - x')^2} \simeq R_o + \frac{(x - x')^2}{2R_o}$$

if $x << R_o$ and $(x^2 - x') << R_o$, which is basically the same restriction given to θ in Fig. 25.

If the radar transmits with a PRR of $f_R = 1/T$, then $x = nvT$ are the positions where transmission occurs.

which infers $\psi_{AZ} = \Sigma \exp -j\ \omega_o(\frac{2R}{c} - \frac{2R'}{c})$

$$= \Sigma \exp - \frac{\omega_o}{2R_o c} (2xx' - (x')^2)$$

$$= \exp + j\ \frac{\omega_o (x')^2}{c R_o} \sum_{-N/2}^{N/2} \exp -j\ 4\pi(x'/\lambda R_o)\, nvT$$

where L, the synthetic aperture length is

$$L = N v T\ , \quad v = \text{aircraft speed.}$$

which infers $\psi_{AZ} = \exp j\ \frac{\omega_o (x')^2}{R_o c}\ \frac{\sin (N+1) 4\pi x' vT/2\lambda R_o}{\sin 4\pi x' vT/2\lambda R_o}$

where $\exp j\ \frac{\omega_o (x')^2}{R_o c}$ is only a phase factor. The $\sin (N+1)\alpha / \sin \alpha$ is the amplitude factor of interest. The azimuth resolution is given by the 3 db points separation. If $\frac{N}{N+1} \simeq 1$, the 3 db point is at

$$\frac{2\pi x' L}{\lambda R_o} = 1.4$$

and $$\delta_{AZ} = 2x' = \frac{1.4\, \lambda\, R_o}{\pi L}$$

Since $L = \beta R_o = \frac{\lambda}{D} R_o$

$$\delta_{AZ} = \frac{1.4}{\pi} D \simeq \frac{D}{2}$$

which is a result in agreement with that already derived.

In generating the synthetic aperture radar, in order to reduce the side lobes of ψ_{AZ}, it is sometimes useful to weight the returned signals before combining them. In the case of the focused antenna, phase compensation must also be used. So, if N returns are processed in order to get

$$L = N v T$$

the focused processing will be of the form

$$\Sigma S_n [\exp j \psi_n] W_n$$

and the unfocused processing of the form

$$\Sigma S_n W_n$$

where W_n is the weighting function and S_n are the discrete returns. This is the basic processing technique. Various methods, from optical, electronic, as well as acoustic, are used to generate the synthetic aperture radar.

V. RECENT DEVELOPMENTS IN TWO MAJOR AREAS

A. DIGITAL MTI

The structure of an MTI processor clearly points into the direction of a digital implementation. The increase in digital data rates associated with the cost decay of present digital components led to the implementation of reliable, flexible, low cost digital MTI processors.

Fig. 29 is a typical block diagram of one of the types of MTI digital implementation. I and Q channels are used in order not to lose 3 db on the average due to blind phases. The structure is parallel to the analog MTI processor. The use of A/D's and D/A's, storage devices instead of delay lines, make up the differences with respect to the analog processor. The capacity of the memory depends basically on the number of range cells and on the use of multiple cancellers.

The quantization process introduces a new dimension to the noise problem: that is, the quantization noise. Quantization noise is present along all the dynamic range of the processor, but the errors at the extremes are of particular importance to the MTI processor. At the lower level, clutter cannot be cancelled below one bit of quantization; at the upper level, abrupt clipping distorts the signal creating additional noise. This extra noise affects the improvement factor (I) of the processor. If it is assumed that signal and quantization noise are uncorrelated, then for a single canceller, the improvement factor is [14],

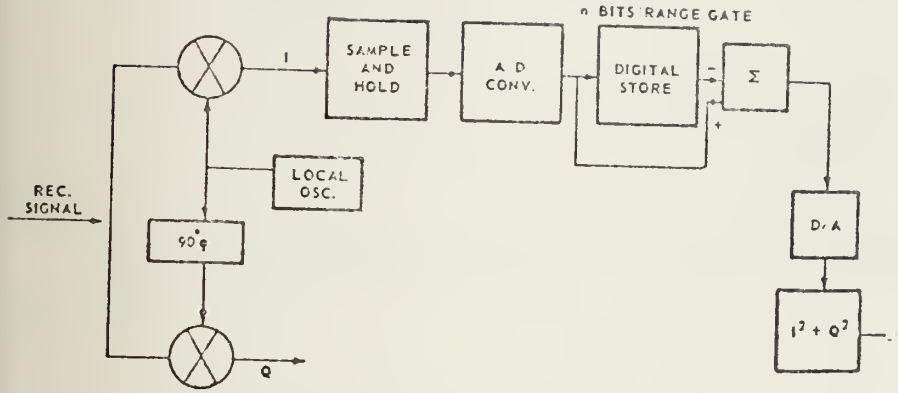
n BITS RANGE GATE
REC. SIGNAL
I
SAMPLE AND HOLD
A D CONV.
DIGITAL STORE
Σ
LOCAL OSC.
90°φ
D/A
I² + Q²
Q

Fig. 29

$$I_1 = \frac{1 + (\sigma_\varepsilon^2/E^2)[\rho_\varepsilon(T) - \rho_{\varepsilon S}(T)}{1 - \rho(T) + (\sigma_\varepsilon^2/P_{ic})[1 - \rho_\varepsilon(T)]}$$, where

ρ_ε = correlation coefficient of quantization error for clutter alone

$\rho_{\varepsilon s}$ = correlation coefficient of quantization error when both clutter and signal are present

σ_ε^2 = noise power

E = signal voltage

P_{ic} = input power clutter

$\rho(T)$ = correlation coefficient of clutter signals.

Since $\sigma_\varepsilon^2/E^2 \simeq 0$ and $\rho_\varepsilon(T) \simeq 0$

$$I_1 \simeq \frac{1}{1 - \rho(T) + \sigma_\varepsilon^2/P_{ic}}$$

which differs from the equivalent analog factor only by the term $\sigma_\varepsilon^2/P_{ic}$.

Also, for a double canceller, the improvement factor I_2 is [14]

$$I_2 = \frac{1}{1 - \frac{4}{3}\rho(T) + \frac{1}{3}\rho(2T) + \sigma_\varepsilon^2/P_{ic}}$$

For the triple and higher order cancellers, the expressions get more complicated but the derivation is the same for all cases. Also in I_2, the only difference from the analog expression is the factor $\sigma_\varepsilon^2/P_{ic}$. Assuming a uniform error distribution

$$\sigma_\varepsilon^2 = \frac{E_m^2}{12(2^{n-1} - 1/2)^2}$$

where E_m = saturation voltage of the digital register

n = number of bits used in the quantization.

$P_{ic}/\sigma_{\varepsilon}^2$ is called the improvement factor limitation. Figure 30 relates the improvement factor limitation with the total number of bits for different values of P_{ic}/E_m^2.

In many applications the fact that the MTI processor has blind speeds at multiples of the PRF is completely undesirable. The method usually used to attenuate this effect makes use of staggered PRF. The scan-to-scan staggered PRF is less efficient but requires less complex hardware than the pulse-to-pulse stagger, but for some applications the first one is inadequate. The staggered PRF technique is based on the use of different spacing between transmitted pulses which, at the receiver, are properly delayed (de-staggered), such that the spacings at the input of the delay line cancellers are all equal. The necessary use of delays makes staggered PRF perfectly matched for digital techniques. Since the concept is completely defined, the recent trend has been focused in the development of optimization techniques in order to improve the performance of the processor. The first difficulty with any optimization problem is, of course, the definition of optimum. Some try to optimize the improvement factor, others to optimize the signal to clutter gain (SCG) within a finite number of frequency slots, or even the optimization of some defined indicator.

An important factor in the optimization process is the statistical model that is chosen for the clutter power distribution. It has been verified that a Gaussian distribution centered at zero doppler frequency is adequate in most cases as a power density function of clutter. Various standard

deviations have been calculated for different types of clutter [2].

Figure 31 is a block diagram of a staggered PRF processor. The pulse staggered sequence is such that the i^{th} pulse is delayed $(i-1)T + \Delta T_i$ seconds with respect to the first pulse. In the processor, after de-staggering, the pulses are weighted (W_i's in Fig. 31). By observation, the impulse response of the processor is

$$h(t) = W_1\,\delta(t - \Delta T_1) + W_2\,\delta[t - (T + \Delta T_2)] + \ldots + W_N\,\delta\{t - [(N-1)T + \Delta T_N]\}$$

which implies a transfer function

$$H(\omega) = \sum_{i=1}^{N} W_i \exp\{-j\omega[(i-1)T + \Delta T_i]\}$$

and a filter power response

$$G(\omega) = H(\omega)\,H^*(\omega), \qquad * \equiv \text{complex conjugate.}$$

With $G(\omega)$ and the power spectral density of the clutter, different optimization criteria can now be devised. One factor is common to all techniques. The Δ_i's, W_i's and the clutter variance, assuming a Gaussian distribution, are the parameters that will optimize the processor, given an optimization procedure. In the analysis, it is always assumed a step scanned array antenna in order that for each position, N pulses are transmitted. Figure 31 is a processor for a given range cell. If there are K large cells, the general block diagram is presented on Fig. 32, where W_i's and the summing network is presented for the K_i cell.

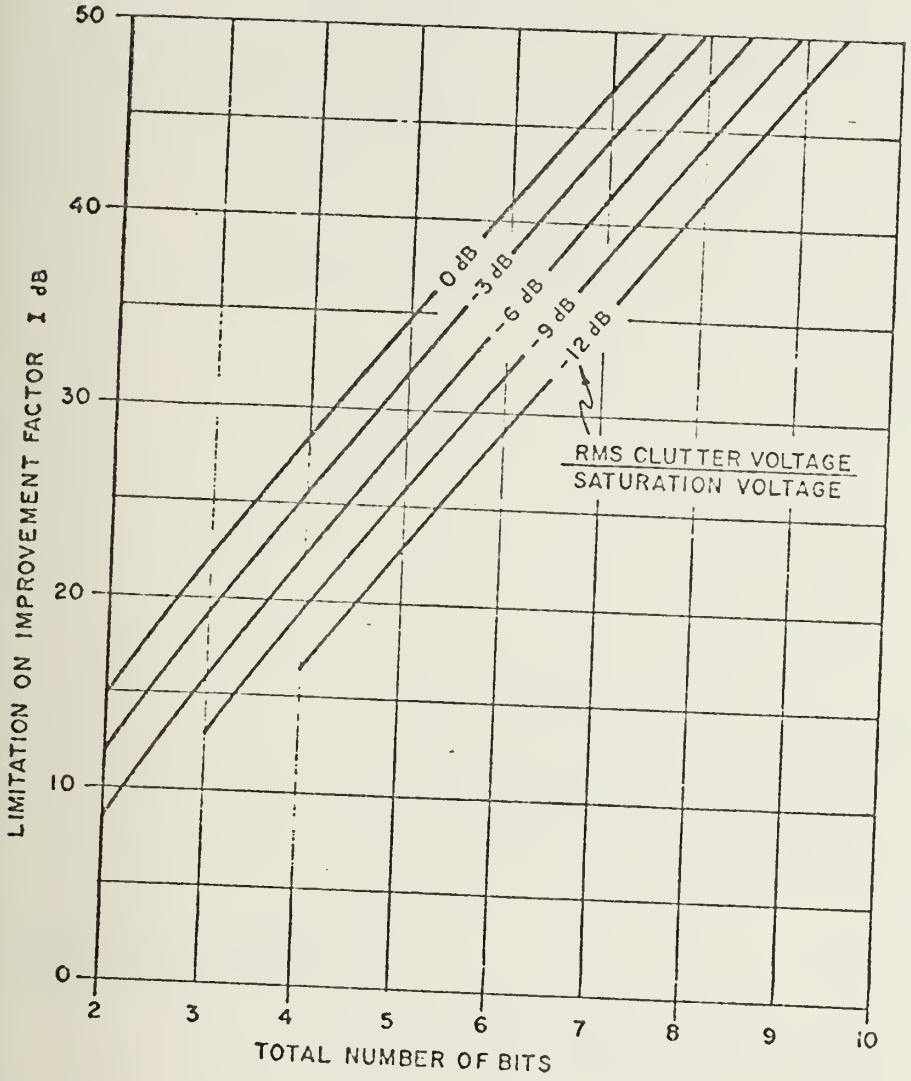
LIMITATION ON IMPROVEMENT FACTOR I dB
50
40
30
20
10
0
0 dB
-3 dB
-6 dB
-9 dB
-12 dB
RMS CLUTTER VOLTAGE
SATURATION VOLTAGE
2
3
4
5
6
7
8
9
10
TOTAL NUMBER OF BITS

Fig. 30

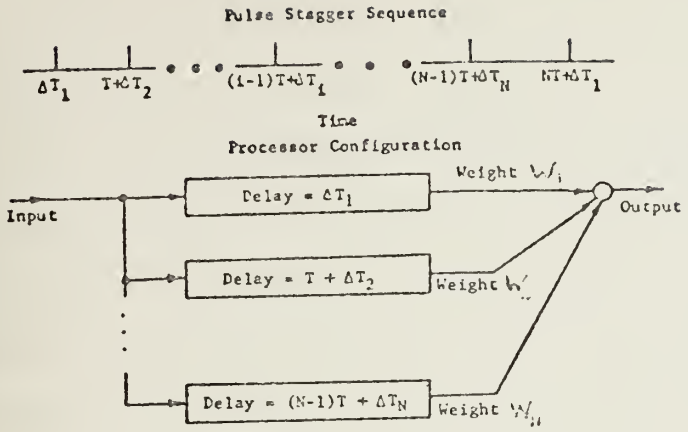
Pulse Stagger Sequence
ΔT1
T+ΔT2
(i-1)T+ΔTi
(N-1)T+ΔTN
NT+ΔT1
Time
Processor Configuration
Input
Delay = ΔT1
Weight W1
Delay = T + ΔT2
Weight W2
Delay = (N-1)T + ΔTN
Weight WN
Output

Fig. 31

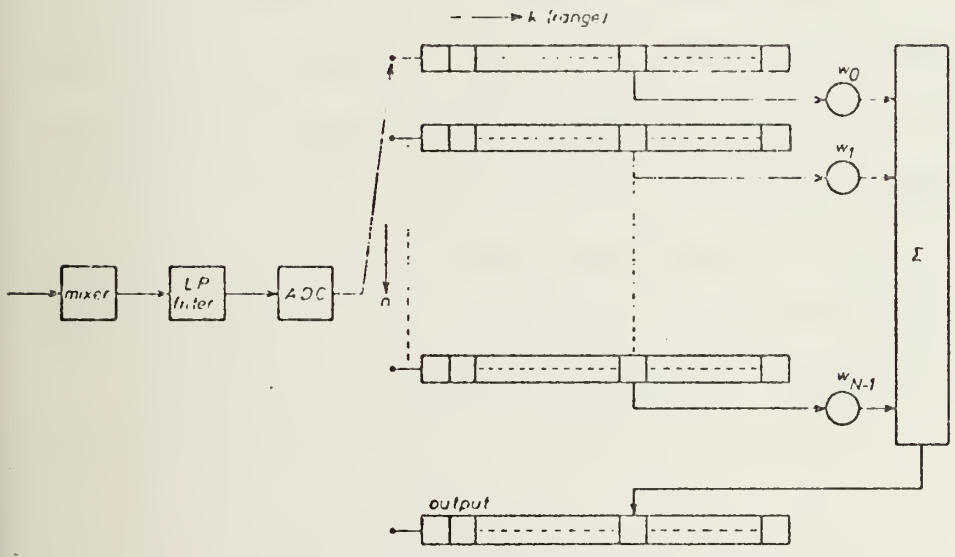
k (range)
mixer
LP filter
ADC
n
w0
w1
wN-1
Σ
output

Fig. 32

The ideal MTI filter is a high-pass filter with rejection from zero frequency to the maximum frequency of the clutter. Rejection may also occur after the maximum desired doppler frequency but it is not absolutely necessary.

For a better understanding of staggered PRF some general concepts should be explored. If a constant PRF is used, not only the dc component of the doppler spectrum but the whole clutter spectrum is translated to multiples of the PRF. It is shown [15] that with staggered PRF the clutter spectrum still is translated to multiples of the average PRF, but the spectrum of the signal is dispersed into N (number of Δ_i's) separate frequency lines. So, if a target produces a doppler frequency that is a multiple of the basic PRF, only one part in the whole signal is distorted by the clutter spectrum where the remaining M-1 parts of the signal may possess enough power to be detected. An MTI filter which notches in a region around dc as well as in multiples of PRF can eliminate the clutter, but if staggered PRF is used only one part in N of the signal is lost, thus increasing the probability of detection of targets with potential blind velocities.

In [16] an optimization process, based on a performance index P defined as

$$P = \int_{B_1}^{B_u} \frac{1}{[S^2(f)]^M} \, df$$

is developed. B_1 and B_u are the lower and upper bounds of the velocity region, $S^2(f)$ is the signal to clutter gain and M is a parameter that reflects the emphasis the criteria puts on

spectral amplitude variations. As M increases, smaller spectral amplitudes have more influence in the final result of the integral.

For an understanding of the significance of P, it should be noted that good clutter attenuation as well as a high improvement factor correspond to a good performance index. Using the optimization procedure described in [16] and using M = 8, practical results (figures 32, 33, 34) for different values of N and $(B_u - B_l)$ were obtained. It can be seen that as N increases, the minimum value for the signal-to-clutter gain in the velocity region increases as well as the improvement factor $I = \overline{SCR(f)}$ (Fig. 32, 33), but with a fixed N and the velocity region increased on the upper bound, the minimum value of SCR(f) in the velocity region decreases (Fig. 33, 34).

As was said earlier, the clutter variance σ is also an important parameter in the optimization process. Fig. 35 relates σ with the improvement factor for the case of N = 5 and $B_u = 10\ B_l$. In the solid line the interpulse periods $T + \Delta_i$ were optimized for the value of $\sigma = 0.02\ B_l$ and the coefficients W_i were optimized in parallel with the variation of σ in the horizontal axis. On the dotted line, both coefficients and interpulses were optimized for $\sigma = 0.02\ B_l$, and the variations of I with σ were recorded. This situation occurs when the real clutter parameters are not those used in the design of the filter. It is apparent that there are not too many differences between the two cases.

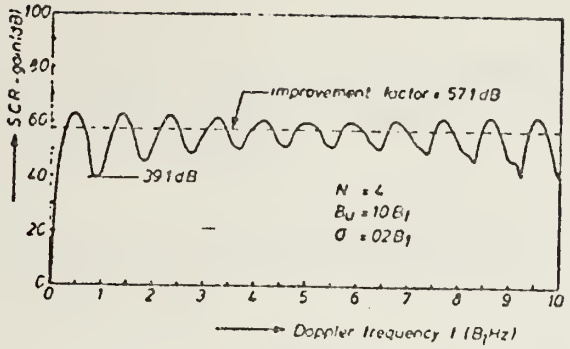

SCR gain as a function of Doppler frequency; $N = 4$, $B_U = 10B_1$, $\sigma = 0.02B_1$. Optimum intervals: 1.100, 1.094, 1.000. Optimum coefficients: 1.000, −3.003, 3.155, −1.152.

Fig. 32

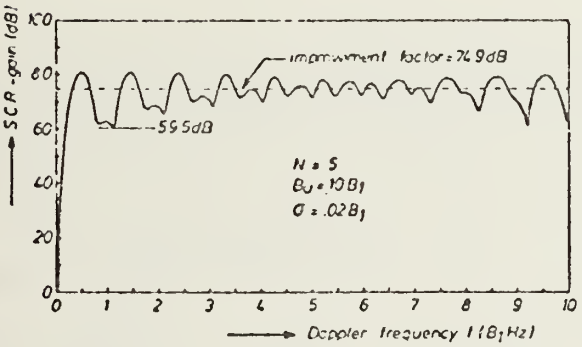

SCR gain as a function of Doppler frequency; $N = 5$, $B_U = 10B_1$, $\sigma = 0.02B_1$. Optimum intervals: 1.111, 1.000, 1.091, 1.058. Optimum coefficients: 1.000, −4.258, 6.242, −4.031, 1.048.

Fig. 33

SCR gain as a function of Doppler frequency: $N = 5$, $B_U = 40B_1$, $\sigma = 0.02B_1$. Optimum intervals: 1.007, 1.021, 1.000, 1.299. Optimum coefficients: 1.000, −3.784, 5.432, −3.273, 0.626.

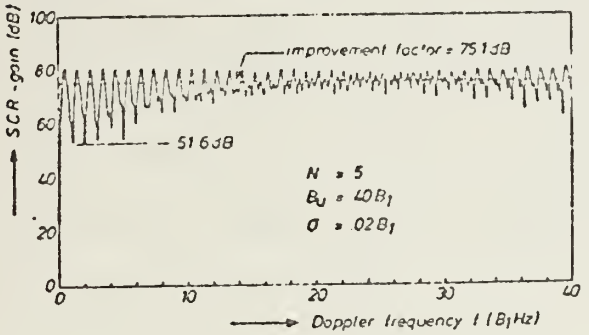

Fig. 34

Improvement factor as a function of clutter spectral width σ; $N = 5$, $B_U = 10B_1$. Coefficients for dotted curve (optimum for $\sigma = 0.02B_1$): 1.000, −4.258, 6.242, −4.031, 1.048. Intervals for both solid and dotted curves (optimum for $\sigma = 0.02B_1$): 1.111, 1.000, 1.091, 1.058 (c.f., Fig. 8).

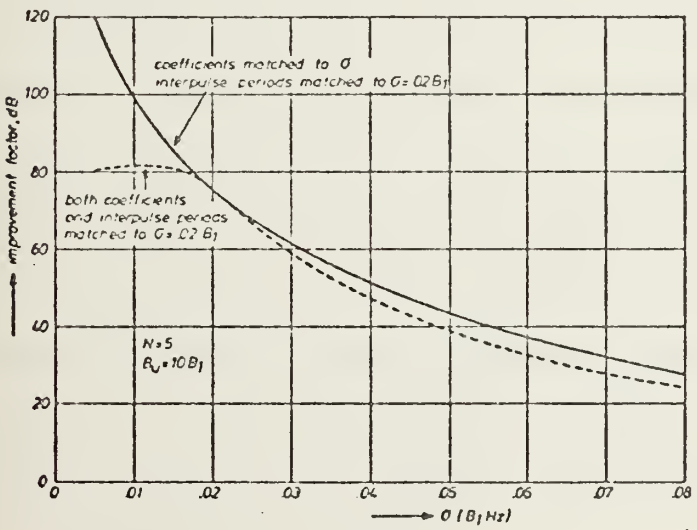

Fig. 35

Another criterion to optimize the staggered PRF processor is developed in [17]. Instead of maximizing the average signal-to-clutter gain over the entire velocity region, the signal-to-clutter gain is maximized in small Δf intervals within the velocity region. The number of intervals is, of course, directly related to the complexity of the processor. Using the optimization algorithm developed in [19], a final block diagram for the processor is reached (Fig. 36, 37). In Fig. 36 the input signal after being split in I and Q channels is weighted with the optimum set of weights A and B for each channel. The results are then combined in order to get an output of positive doppler as well as an output of negative doppler. Fig. 37 represents the implementation of the filter that generates the sets of A and B weights for each of the M frequency sub-intervals in a channel. The T_i's are the interpulse delays and the

$$a_{ij}, b_{ij} \qquad \begin{matrix} 0 < i < N - 1 \\ 0 < j < M - 1 \end{matrix}$$

are the coefficients determined by the optimization process. It should be noted that in this optimization process the interpulse periods are not optimized: only the weights are optimized. Fig. 38 relates the signal-to-clutter gain averaged over the entire velocity region with the signal-to-gain maximized in each of eight frequency sub-intervals. Both $N = 5$ and $N = 10$ are presented. A substantial improvement due to optimization is evident. Another optimization technique is developed in [18].

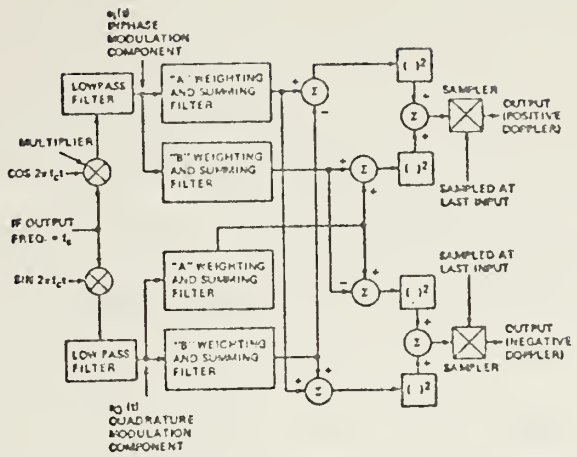
INPHASE MODULATION COMPONENT
LOWPASS FILTER
"A" WEIGHTING AND SUMMING FILTER
"B" WEIGHTING AND SUMMING FILTER
MULTIPLIER
IF OUTPUT FREQ. = f_c
LOW PASS FILTER
SAMPLER
OUTPUT (POSITIVE DOPPLER)
SAMPLED AT LAST INPUT
OUTPUT (NEGATIVE DOPPLER)
QUADRATURE MODULATION COMPONENT

Fig. 36

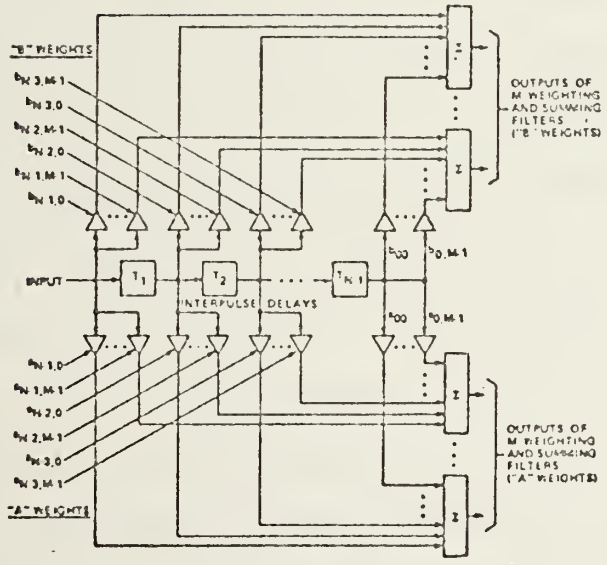
"B" WEIGHTS
INPUT
INTERPULSE DELAYS
OUTPUTS OF M WEIGHTING AND SUMMING FILTERS ("B" WEIGHTS)
OUTPUTS OF M WEIGHTING AND SUMMING FILTERS ("A" WEIGHTS)
"A" WEIGHTS

Fig. 37

The optimized processors are called Constrained Improvement MTI Processors (CIP). Given a specified improvement factor, the number of pulses to be processed and the PRF stagger sequence, the mean square deviation from a constant response in the velocity region is minimized. Two main approaches can be given to the problem. In the first, the PRF stagger sequence is fixed and the weighting coefficients are chosen in order to optimize the processor; in the second, the weighting coefficients are fixed while the stagger sequence is chosen in order to optimize the processor. Defining

$$f' = \frac{F'}{F_r}, \qquad \begin{aligned} F' &= \text{maximum PRF} \\ F_r &= \text{unstaggered PRF} \end{aligned}$$

figures 39, 40 and 41 represent the optimum filter response with a four pulse return, $f' = 8$, $\sigma = 0.01$ and $I = 30$ db, using respectively a linear PRF stagger with $\pm 20\%$ interpulse variation, and a sinosoidal PRF stagger with $\pm 10\%$ (Fig. 40) and $\pm 90\%$ (Fig. 41) interpulse variation. As it can be seen, as the variation increases the response becomes more uniform. Comparing figures 42, 39 and 43, in which the number of pulses are respectively 3, 4 and 6 for a common interpulse variation of 20%, it can also be seen that the response improves with the number of pulses processed.

A comparison between optimization procedures, different from a direct comparison between responses, can be devised using the fraction of frequencies for which a response is less than some specified value as a comparison parameter. If the 0 db scale corresponds to the mean value of the

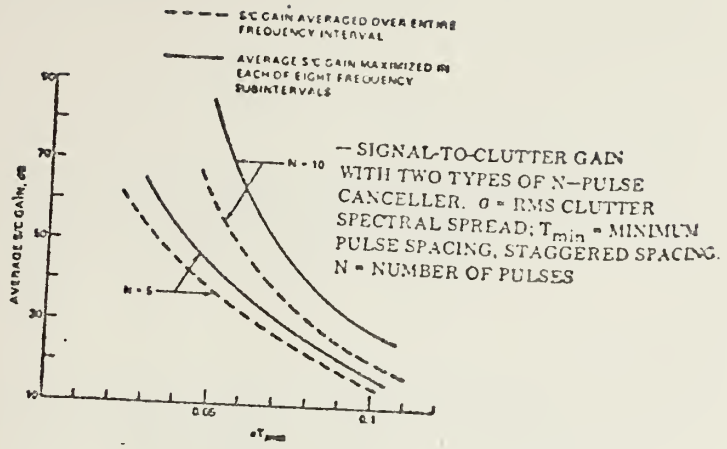

— SIGNAL-TO-CLUTTER GAIN WITH TWO TYPES OF N-PULSE CANCELLER. σ = RMS CLUTTER SPECTRAL SPREAD; T_{min} = MINIMUM PULSE SPACING, STAGGERED SPACING. N = NUMBER OF PULSES

Fig. 38

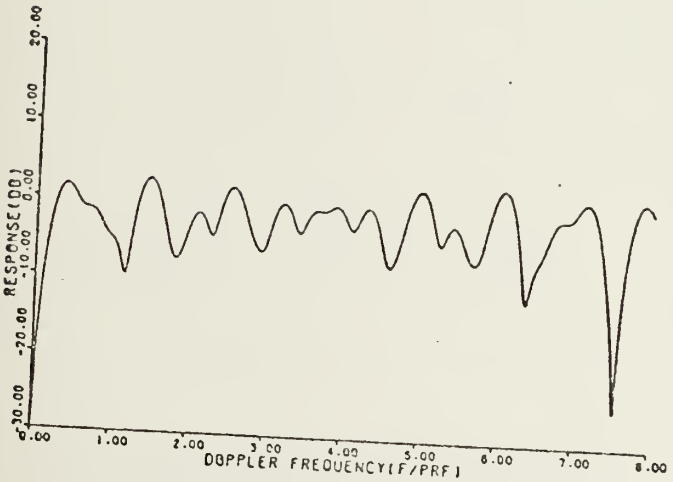

Frequency response of a four-pulse CIP using linear PRF stagger with ± 20 percent interpulse period variation.

Fig. 39

Frequency response of four-pulse CIP using sinusoidal PRF stagger with ± 10 percent interpulse period variation.

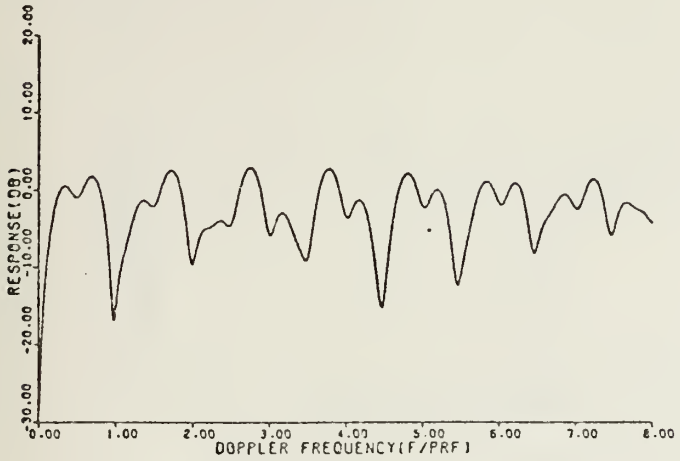

Fig. 40

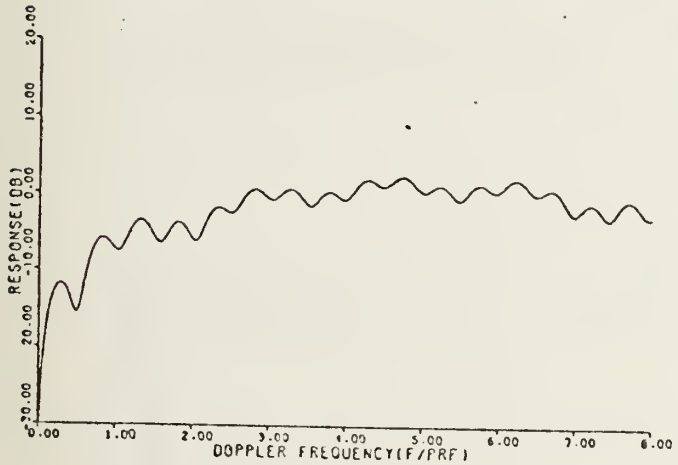

Frequency response of four-pulse CIP using sinusoidal PRF stagger with ± 90 percent interpulse period variation.

Fig. 41

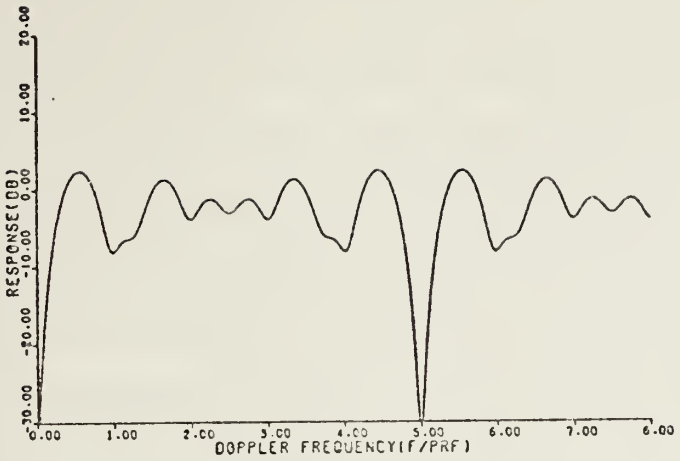

Frequency response of three-pulse CIP with ± 20 percent interpulse period variation.

Fig. 42

Response of six-pulse CIP using sinusoidal PRF stagger with ± 20 percent variation in interpulse period.

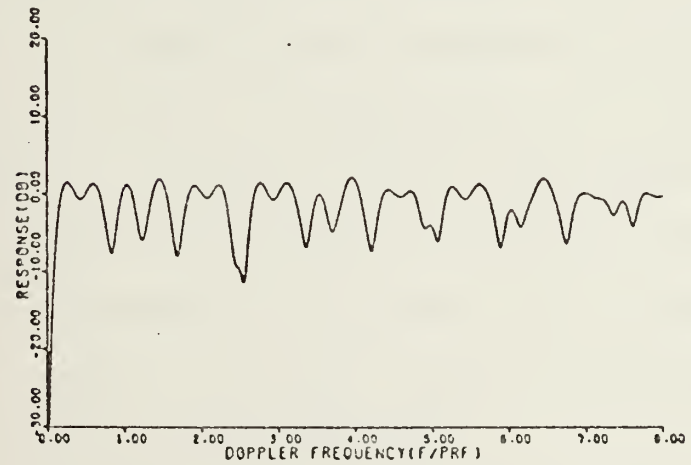

Fig. 43

frequencies of interest, that means that 50% of the frequencies are above as well as below the 0 db level. This leads to a cumulative distribution function in which instead of a fraction of frequencies, the term probability is used. Fig. 44 is a cumulative distribution of the responses of a four pulse CIP and a four pulse processor using the Ref. [16] optimization criteria. This comparison criteria gives a better performance for the CIP processor since its curve is closer to being the ideal step response at 0 db than the other one, but on the average they are similar.

Another type of digital MTI processor is called the matrix MTI. In this case there is no parallel between the analog and the matrix MTI processor. This processor (Fig. 45), in addition to the tremendous flexibility in the modification of the shape of the response curve, has associated with it a very simple clutter locking mechanism that shifts the response curve whenever there is an average velocity associated with clutter. To simplify the explanation of the processor in Fig. 45, only two levels of quantization are used. Basically the processor is a coherent system that compares the phase difference between two successive returns and weights that difference in phase according to the shape it is intended to give to the response curve. Since $d\phi = \omega_d dt$, by weighting $d\phi$ in effect the doppler is being weighted.

The phase angle of a signal return is defined by

$$\phi = \text{the}^{-1} \frac{Q}{I}$$

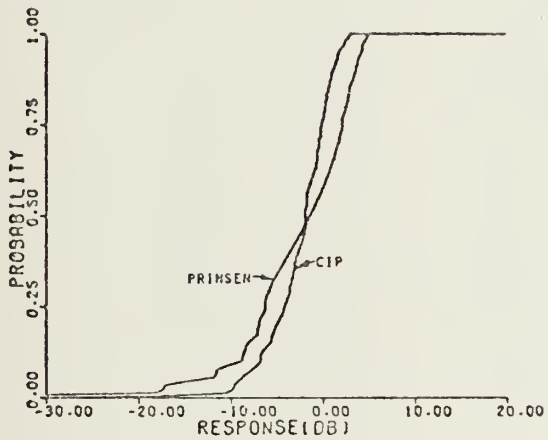
PROBABILITY
1.00
0.75
0.50
0.25
0.00
PRIMSEN
CIP
-30.00
-20.00
-10.00
0.00
10.00
20.00
RESPONSE(DB)

Fig. 44

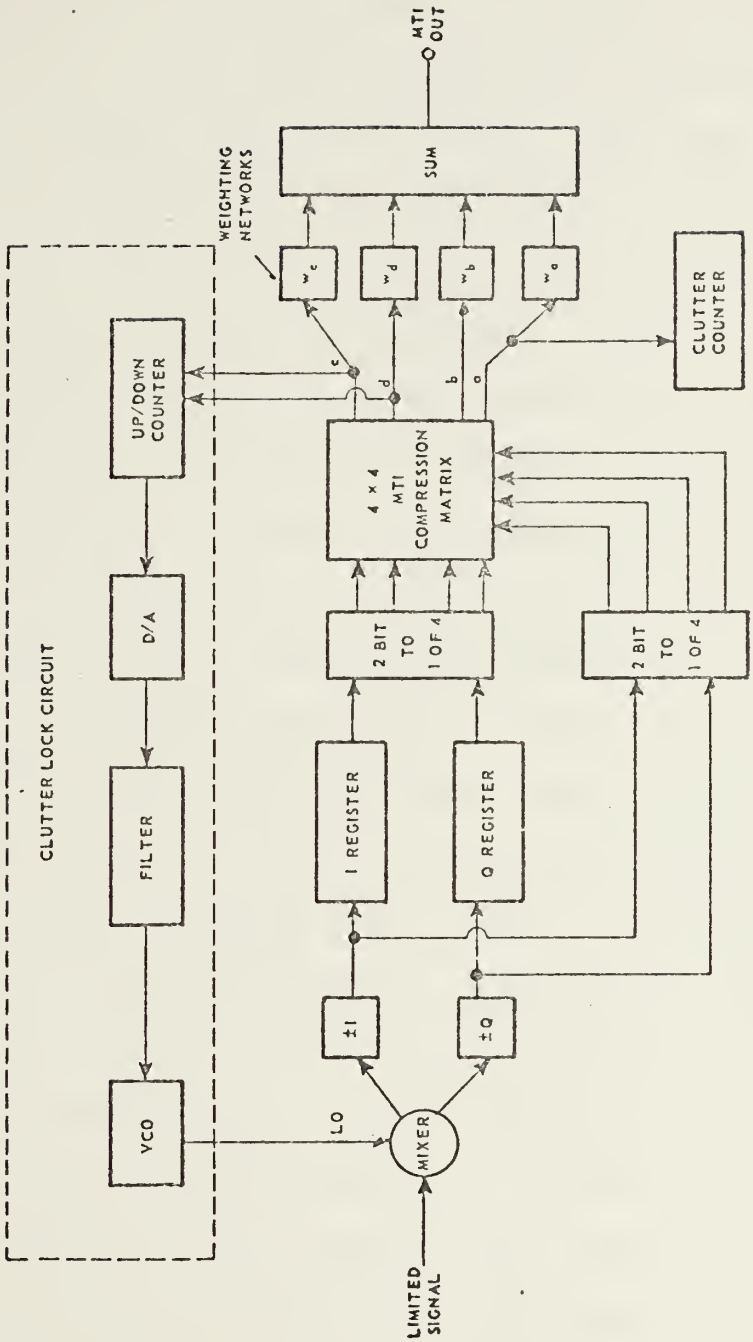
MTI OUT
SUM
WEIGHTING NETWORKS
w_c
w_d
w_b
w_a
CLUTTER COUNTER
UP/DOWN COUNTER
c
d
b
a
4 x 4 MTI COMPRESSION MATRIX
D/A
2 BIT TO 1 OF 4
2 BIT TO 1 OF 4
FILTER
I REGISTER
Q REGISTER
CLUTTER LOCK CIRCUIT
±I
±Q
VCO
LO
MIXER
LIMITED SIGNAL

Fig. 45

and the amplitude by $(I^2 + Q^2)^{1/2}$.} Since in the case of Fig. 45 there is only one quantization level for I and Q, that means that the only possible phases for I are 0° and 180° and for Q, 90° and 270°, assuming a signal to noise ratio much greater than 1. When the average phase difference is 0°, it implies a stationary target, but if $d\phi_T = 180°$ that indicates an optimum velocity target. Since each vector return can be located in all of the four positions $\pm I \pm jQ$, there are 4 x 4 possible combinations for two consecutive returns. So, what the compression matrix block in Fig. 45 does is to generate signals proportional to the phase difference output $d\phi_T$ between two consecutive vector returns, which in this particular case can take the values 0°, 90°, 180° and 270°. Each of the four outputs has a corresponding weighting factor W and the result is summed to generate the MTI output. Fig. 46 indicates the four types with the vector combinations that generated them, as well as the weighting factors used in order to approximate an MTI response curve. The final response curve corresponds to a statistical average of $d\phi_T$ when uniformly random phases are introduced at the input. In order to have a signal proportional to the clutter velocity, it is only necessary to subtract the outputs of the region (d) (Fig. 46) from those of region (c) and divide by the number of range gates, that is, for two quantization levels and a uniformly distributed phase input

$$\overline{d\phi} = \frac{[(d) - (c)](90°)}{N}$$

and

$$\text{VAR } d\phi = \frac{2}{3N}(45°)$$

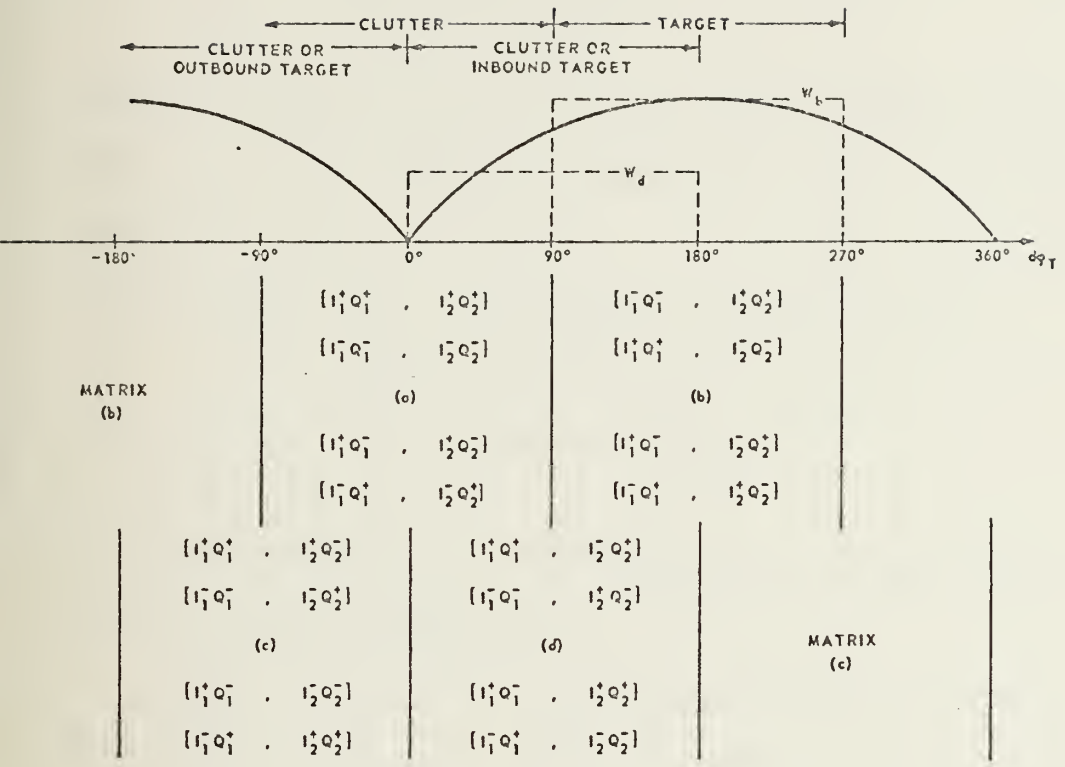
CLUTTER
TARGET
CLUTTER OR OUTBOUND TARGET
CLUTTER OR INBOUND TARGET
W_b
W_d
-180°
-90°
0°
90°
180°
270°
360°
$d\theta_T$
MATRIX (b)
(a)
(b)
(c)
(d)
MATRIX (c)

Fig. 46

So, in a large clutter environment if N is large, $\overline{d\phi}_T$ can smoothly adjust the local oscillator to place the MTI null at the mean value of the clutter doppler.

Consider now an n quantization bit circuit. For each channel there are 2^n possible quantization levels. If only one quadrant of possible phase differences is considered, it can be seen that there are (Fig. 47)

$$\frac{2^n}{2} \times \frac{2^n}{2} - \frac{2^n}{2} + 1$$

possible phases. The $-2^{n-1} + 1$ parcel results from the fact that of all the diagonal combinations (45° zone) only one combination can be counted. As an example, let's use two quantization bits. That means that there are

$$4[2^{2n-2} - 2^{n-1} + 1] \Big|_{n=2} = 12$$

possible phases in all four quadrants, which also implies 12 possible phase differences.

Figure 48 (a) represents the response and figure 48 (b) is the matrix output (phase) for each 12 x 12 possible combination of two consecutive vector returns. Since there is flexibility in modifying the weighting coefficients, it is possible to adapt the filter as a function of the type of expected clutter spectrum. Again, the mean clutter velocity can be determined by subtracting the outputs of the (b) region (Fig. 48) from those of the (m) regions and applying the result to the VCO associated with the local oscillator.

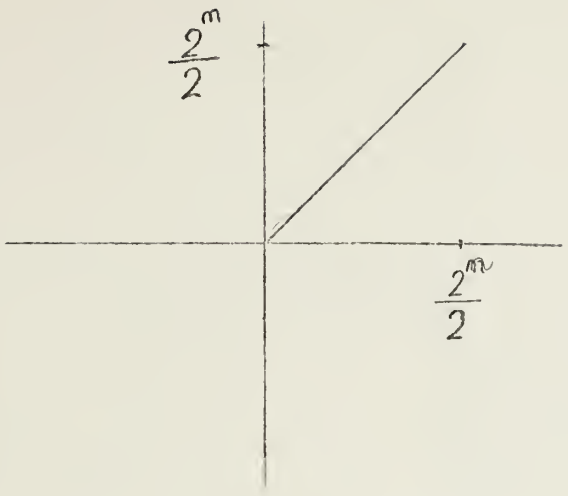

Total number of combinations per quadrant counting the diagonal combinations only as one =

$$2^{n-1} \times 2^{n-1} - 2^{n-1} + 1$$

Total number of combinations for the four quadrants =

$$4[2^{n-1} \cdot 2^{n-1} - 2^{n-1} + 1]$$

$$= 2^{2n} - 2^{n+1} + 4$$

Fig. 47

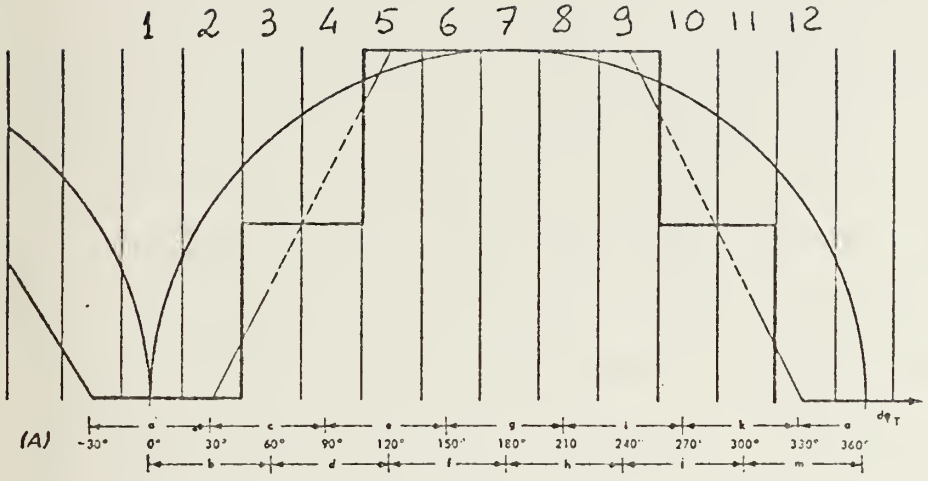
1 2 3 4 5 6 7 8 9 10 11 12
(A)
-30° 0° 30° 60° 90° 120° 150° 180° 210 240° 270° 300° 330° 360°
a b c d e f g h i j k l a
b d f h i m

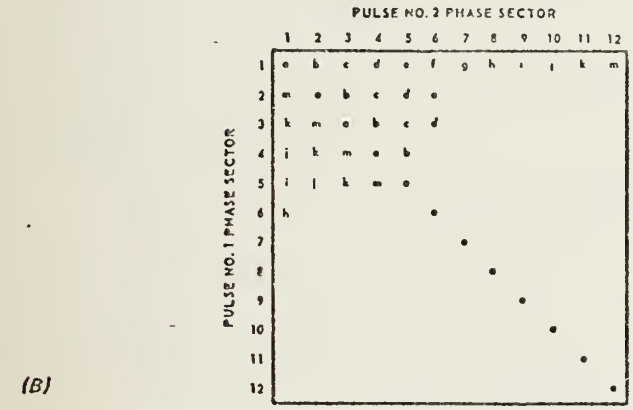
PULSE NO. 2 PHASE SECTOR
1 2 3 4 5 6 7 8 9 10 11 12
PULSE NO. 1 PHASE SECTOR
1 2 3 4 5 6 7 8 9 10 11 12
(B)

Fig. 48

B. DIGITAL SAR

The synthetic aperture radar (SAR) is a typical example of signal processing where digital techniques are being substituted for the former optical processors. With the present technology mini-computers can compensate for the aircraft movement, and, as with a real antenna, the synthetic antenna can be steered and even scanned. The basic problem with SAR processors is the need for high storage capabilities and very fast data rates. The film as an optical storage device became almost impractical since a real time display is impossible. The use of storage tubes is also inadequate due to low efficiency and poor dynamic range and stability. With the present high speed A/D converters (100 MHZ), low cost, and high speed compact digital storage devices, it becomes feasible for real time SAR processors.

Table IV shows a time overview of the late achievements in SAR techniques.

Figure 49 is a block diagram of a digital synthetic aperture radar. Theoretically, the processor must, for each range gate, perform the integral

$$\int_{\Delta T} s(t)\, r(t)\, dt$$

where s(t) is the signal return and r(t) the correlator reference function.

$$r(t) = A_R(t) \exp -j\, \phi_R(t)$$

$A_R(t)$ = weighting function to control the side lobes of the synthetic antenna pattern.

$\phi_R(t)$ = phase reference that tracks the phase of s(t).

Date	Development
1951	Carl-Wiley postulates doppler beam sharpening concept.
1952	University of Illinois demonstrates beam sharpening concept.
1957	First SAR imagery using optical correlator is produced.
Mid 1960's	Analog electronic SAR correlation demonstrated in non real time.
Late 1960's	Digital electronic SAR correlation demonstrated in non real time.
Early 1970's	Real time digital SAR demonstrated with motion compensation.

Table IV

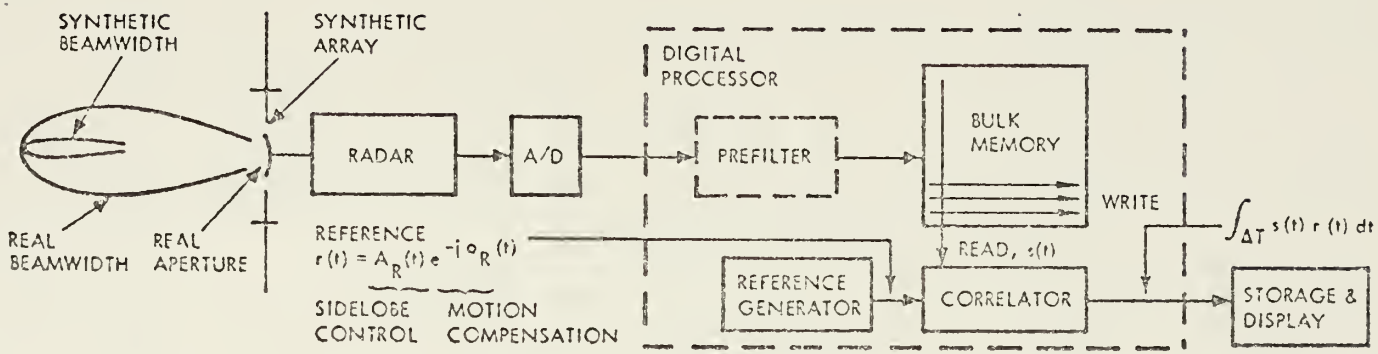
SYNTHETIC BEAMWIDTH
SYNTHETIC ARRAY
REAL BEAMWIDTH
REAL APERTURE
RADAR
A/D
DIGITAL PROCESSOR
PREFILTER
BULK MEMORY
WRITE
READ, s(t)
REFERENCE
$r(t) = A_R(t)\, e^{-i\phi_R(t)}$
SIDELOBE CONTROL
MOTION COMPENSATION
REFERENCE GENERATOR
CORRELATOR
$\int_{\Delta T} s(t)\, r(t)\, dt$
STORAGE & DISPLAY

Fig. 49

Since $\phi_R(t)$ follows the phase of s(t) but with an unknown difference, the signals are processed in an I (in phase) and Q (90° out of phase) channel in order to prevent signal losses. The digital processor operates in the following way: The radar returns pass an A/D converter that samples the signal at a rate, at least higher than the Nyquist rate, and separates the returns in range bins which are approximately equal to the range resolution. The number of bits used per range bin are a function of the desired dynamic range of the processor. The digital data passes through a buffer and prefilter which translates the A/D rate to the rate of the correlator. The bulk memory stores the data corresponding to an integration time, ΔT. The data is then correlated with the reference generator output in order to form an azimuth line with a length corresponding to the number of range gates. After correlation, new data enters the memory and the process repeats itself to produce a new azimuth line.

From Fig. 50 it can be seen that the bulk memory in bits must be equal to the number of cells times the average number of bits per cell, so

$$BM = \text{bulk memory} = 2K_a \; N \; N_R$$

$$N_R = \text{number of range gates} = \frac{\Delta R}{r_r}$$

$$N = \text{number of azimuth data lines} = \frac{\Delta T}{T} = T \; f_r$$

The factor of 2 is because of the use of an I and Q channel. But if, for example, the desired range resolution is 30 m, that corresponds to a bandwidth

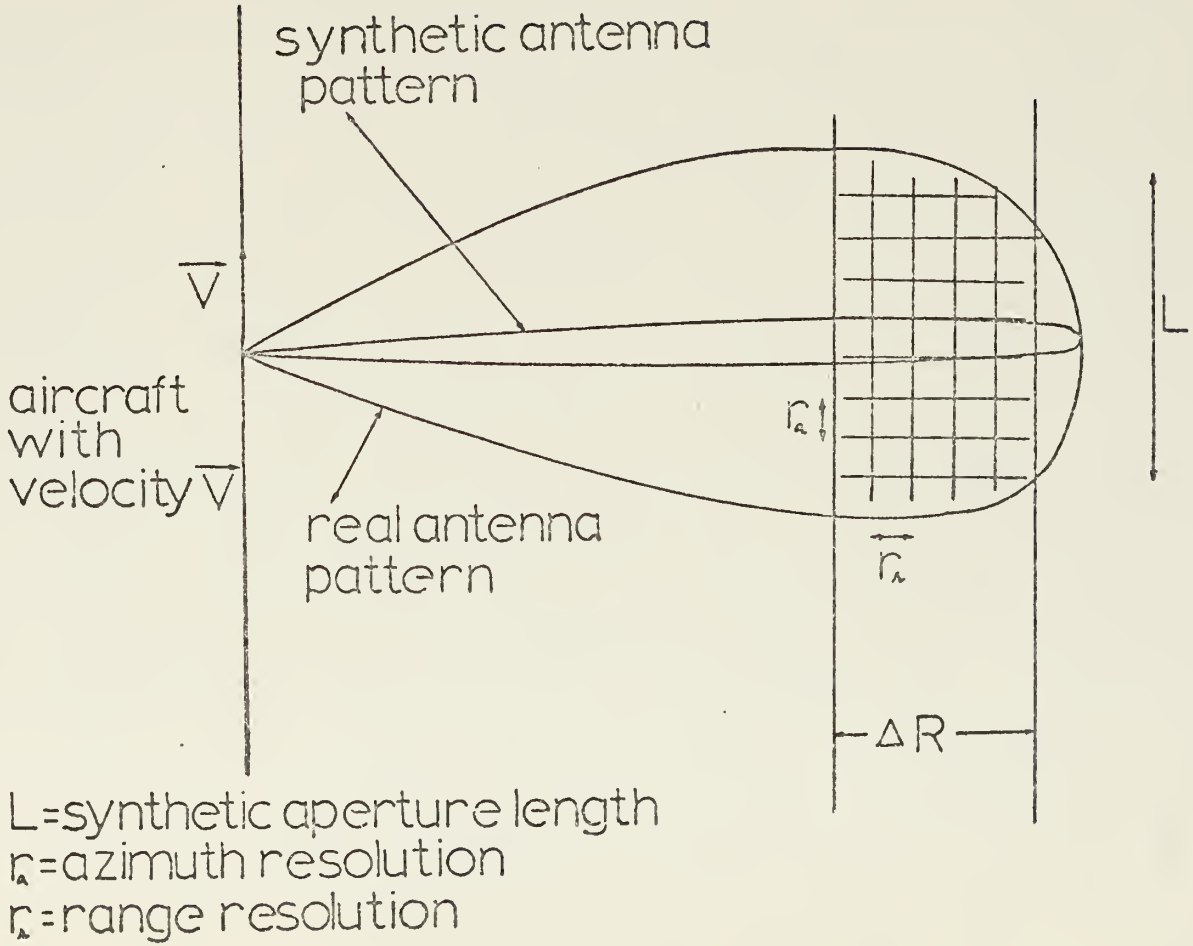
synthetic antenna pattern
$\overrightarrow{V}$
aircraft with velocity $\overrightarrow{V}$
real antenna pattern
r_a
$\overrightarrow{r_r}$
L
ΔR
L=synthetic aperture length
r_a=azimuth resolution
r_r=range resolution

Fig. 50

$$BW = \frac{c}{2r_a} = \frac{3 \times 10^8 \text{ m/sec}}{2 \times 30 \text{ m}} = 5.0 \text{ MHZ} ,$$

which implies an A/D sampling rate per channel of 5.0 MHZ. On the other hand, for a 1 KHZ PRF the unambiguous range is 80 mi, which for a typical ΔR = 10 mi of mapping, means that there is still an equivalent 70 mi excess time to process that data. This results that in fact there is no need for the correlator to work at such high data rates. Using a buffer that accepts the data at a very high data rate during a short period of time but delivers it at a lower rate to the correlator, it is possible to reduce the correlator rates by many orders of magnitude. In fact, analyzing the function of the correlator, it can be seen that it must in ΔT seconds produce a number of outputs equal to the total number of cells, that is, $(L/R_a)N_R$, where L/r_a = CA is the azimuth compression rate. Since the real antenna illuminates $(L/r_a)N_R$ cells and is ready to receive new data after T seconds, the correlator rate (CR) is

$$CR = \frac{(L/r_a)N_R}{T} = CA\ N_R\ f_r$$

defining

$N_F = K_a$ CA = total number of doppler filters

K_e = azimuth over sample factor $\simeq$ 1

Then

$$CR = N_F\ N_R\ f_r$$

if N_R = 500 and f_r = 1 KHZ for one doppler channel CR = .5 MHZ < A/D sampling rate.

On the other hand, if the spacing corresponding to V/T is much finer than the range resolution r_r, that means excessive data is being used. If the PRF cannot be lowered due to power or doppler considerations, then a prefilter can be used to effectively reduce the PRf = f_r, by a factor f_s/f_r where f_r is the prefilter sampling rate. The prefilter will reduce the correlator rate by a factor f_s/f_r. If the required reduction is in order to have V/T of the order of r_a, then $f_s \simeq \frac{V}{r_a} \simeq \frac{L}{r_a} \frac{1}{T} \simeq \frac{N_F}{T}$, which implies a new correlator rate.

$$CR = K_{os} K_s N_F^2 N_R f_r$$

K_{os} = prefilter over sample factor

k_s = synthetic array weighting

These two factors, the bulk memory and the correlator rate, determine the type of design for a SAR processor. The main objective is to reduce both CR and BM. Today's technology is attacking this problem in two ways: devising correlator algorithms which will reduce the bulk memory and arithmetic, at low cost, with fewer power consuming elements. The first approach is being made by parallel and series combinations of correlator channels and prefilters, as well as with the use of FFT algorithms. Another method is the use of pulse compression techniques but processed only after the SAR processor. This will reduce K_a which will reduce BM. The hardware improvements are in CCD memories and LSI at much lower costs.

As it was said before, with today's digital techniques various mapping modes are possible as well as motion compensation.

Figure 51 shows the four types of mapping used today. The Squint mode (Fig. 51 B) is only a variation in angle of the side-looking SAR. The doppler beam sharpened mapping is a PPI representation with an equivalent antenna of very high azimuth resolution. The spotlight is a mapping where a high resolution snapshot map is generated. Motion Compensation includes various functions: clutter tracking, focusing acceleration compensation and real antenna stabilization. Fig. 52 is a block diagram of a general SAR processor. The blocks are basically the same as those of Fig. 49 except for the motion compensation blocks which are now included.

To achieve lower data rates, various types of algorithms are presently used. Lower rates will be achieved at the expense of more complex hardware. The general concept that applies to all of them is the reduction of rates by the increase in the number of doppler filters.

Figure 53 is a block diagram of the multi-channel prefilter processor approach [19] where m is the number of channels. The prefilter rate becomes

$$R_p = m\, N_R\, f_r$$

and since the number of filters N_F is reduced by1/m, the total arithmetic rate (TAR) is

$$TAR = R_C + R_p = \alpha_1 m + \frac{\alpha_2}{m}$$

$$\alpha_1 = N_R\, f_r$$

$$\alpha_2 = K_{os}\, K_s\, N_F^2\, N_R/\Delta T$$

$$\text{and } \frac{d\ TAR}{dm} = \alpha_1 - \frac{\alpha_2}{m} = 0$$

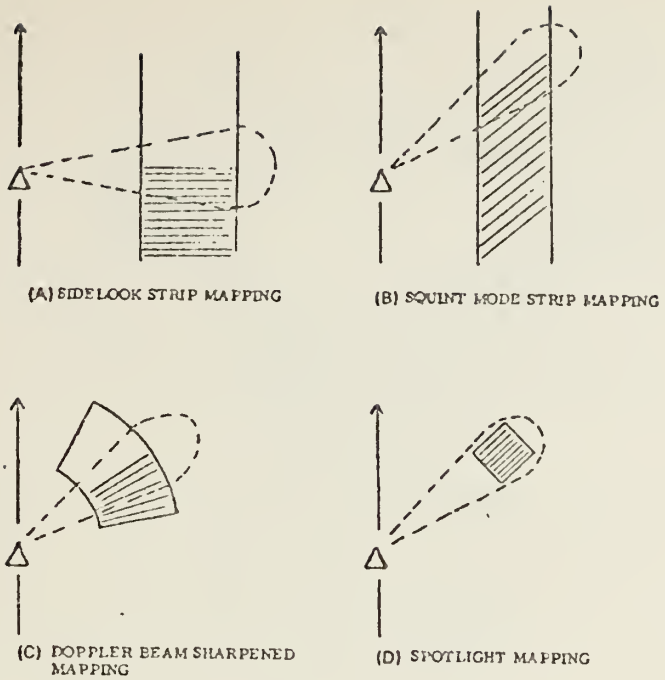
(A) SIDELOOK STRIP MAPPING
(B) SQUINT MODE STRIP MAPPING
(C) DOPPLER BEAM SHARPENED MAPPING
(D) SPOTLIGHT MAPPING

Fig. 51

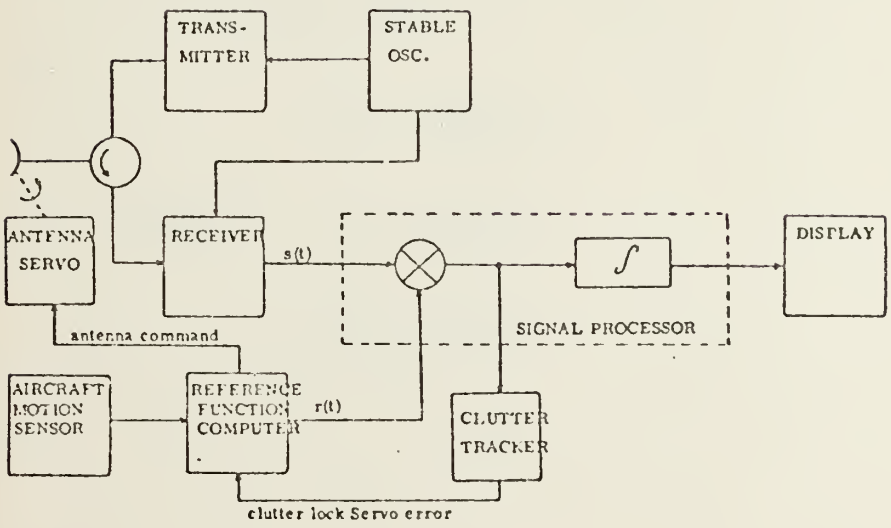
TRANS-MITTER
STABLE OSC.
ANTENNA SERVO
RECEIVER
s(t)
DISPLAY
SIGNAL PROCESSOR
antenna command
AIRCRAFT MOTION SENSOR
REFERENCE FUNCTION COMPUTER
r(t)
CLUTTER TRACKER
clutter lock Servo error

Fig. 52

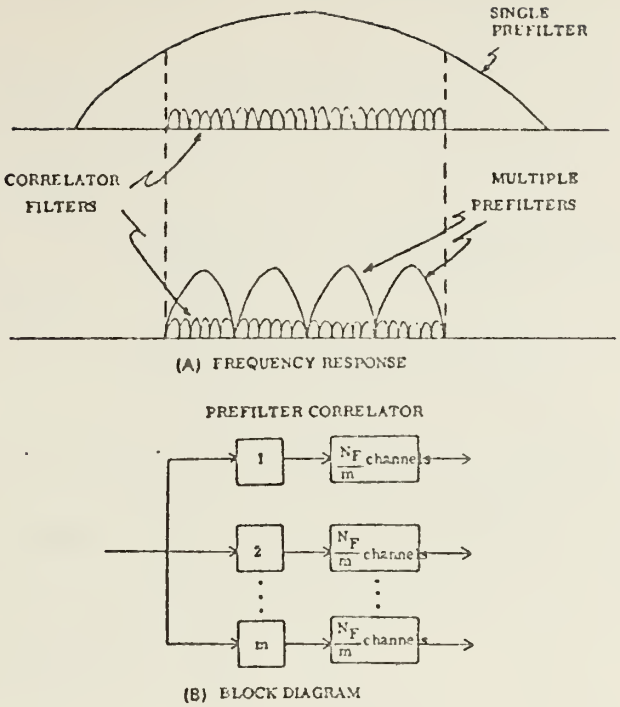
SINGLE
PREFILTER
CORRELATOR
FILTERS
MULTIPLE
PREFILTERS
(A) FREQUENCY RESPONSE
PREFILTER CORRELATOR
1
2
m
$\frac{N_F}{m}$ channels
(B) BLOCK DIAGRAM

Fig. 53

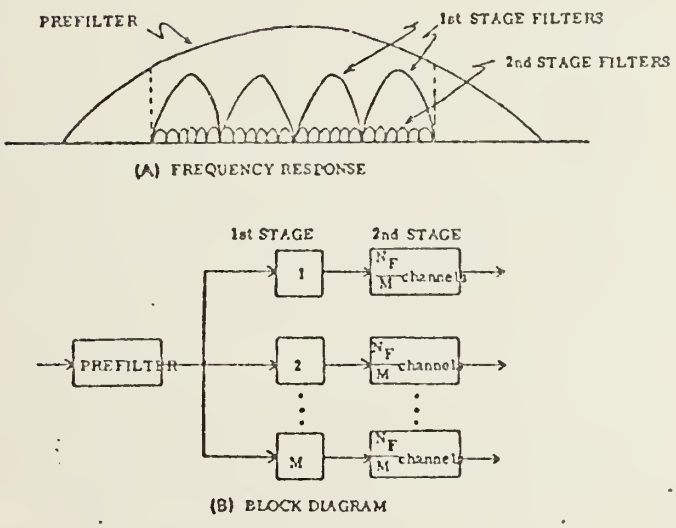
PREFILTER
1st STAGE FILTERS
2nd STAGE FILTERS
(A) FREQUENCY RESPONSE
1st STAGE
2nd STAGE
PREFILTER
1
2
M
$\frac{N_F}{M}$ channels
(B) BLOCK DIAGRAM

Fig. 54

implies that the value of m that minimizes TAR is

$$m = \left[\frac{\alpha_2}{\alpha_1}\right]^{1/2} = \left[K_{os}\ K_s\ N_F^2/f_r\Delta T\right]^{1/2}$$

and the minimum TAR is

$$TAR_{min} = \alpha_1 \left(\frac{\alpha_2}{\alpha_1}\right)^{1/2} + \alpha_2 \left(\frac{\alpha_1}{\alpha_2}\right)^{1/2} = 2(\alpha_1\alpha_2)^{1/2}$$

$$= 2(K_{os}\ K_s\ f_r/\Delta T)^{1/2}\ N_F\ N_R$$

The two-stage correlator (Fig. 54) is another algorithm [19]. The idea is again frequency domain division but only with one prefilter. The equivalent correlator rate will be the sum of the two correlator rates. So

$$TAR = (K_{os}\ K_s\ N_R\ N_F/\Delta T)\ M + K_{os}\ K_s\ N_R\ N_F/M\Delta T$$

where M is the number of first-stage correlation channels. As in the previous case, there is a value of $M = (N_F)^{1/2}$ that minimizes TAR. With the FFT algorithm, it is possible to reduce even more the total rates. Table V is a summary of the calculated values [19] of bulk memory as well as total arithmetic rates for the SAR signal processing algorithms.

Another approach, completely different from those already presented to solve the problem of high data rates on the correlator (Fig. 49) of the SAR processor, is through the use of parallel processing using associative memory [20]. Fig. 55 represents a block diagram of the associative memory and the related input/output registers. In the associative memory,

Algorithm	Bulk Memory	Total Arithmetic Rate
Correlator	$2k_a N_F N_R$	$N_F N_R f_r$
Prefilter plus correlator	$2k_a N_F N_R$	$N_F f_r + (K_{OS} K_S N_F^2 N_R / \Delta T)$
Multiple prefilters plus correlator	$2k_a N_F N_R$	$2(K_{OS} K_S f_r / \Delta T)^{1/2} N_F N_R$
Prefilter plus two-stage correlator	$2k_a K_{OS} K_S N_R [M + (M+3) N_F / 2M]$	$N_R f_r + (2K_{OS} K_S N_R N_F^{N2} / \Delta T)$
Prefilter plus FFT	$2k_a K_{OS} K_S N_F N_R$	$N_R f_r + (K_{OS} K_S N_F N_R \log_2 K_{OS} K_S N / 2\Delta T)$

Note: The number of amplitude bits k_a, will vary slightly among the algorithms and, also, depending upon whether the storage is precorrelator or in the integrator. The first three algorithms are for integrator storage nad the last two are for precorrelator storage.

Table V

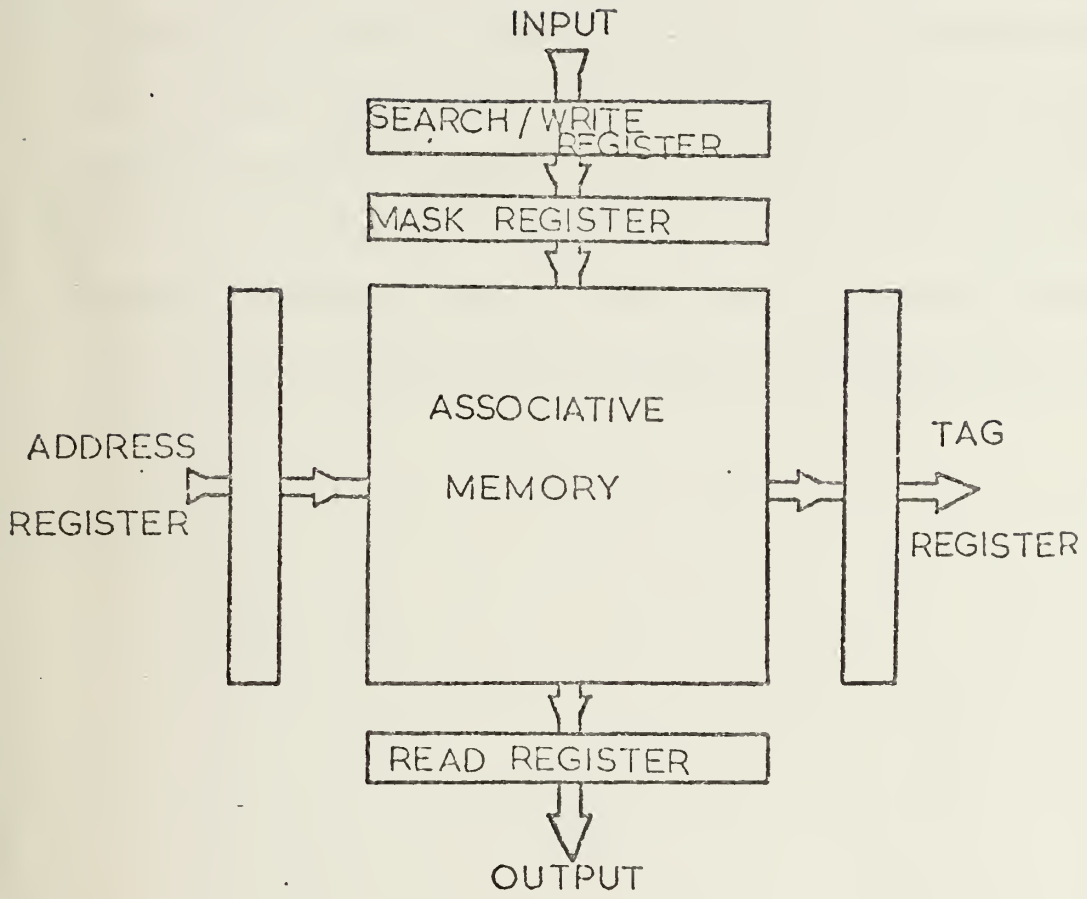
INPUT
SEARCH / WRITE REGISTER
MASK REGISTER
ASSOCIATIVE MEMORY
ADDRESS REGISTER
TAG REGISTER
READ REGISTER
OUTPUT

Fig. 55

multi addressing, multi read/write, multi logical and arithmetic operations are performed. The search/write and the mask registers are used to generate proper codes for multi accessing. The operations are done in a bit serial basis but on all words in parallel at the same time. Ellis [20] showed that for an X band radar with range and azimuth resolutions of 10 meters, 1000 range cells, maximum range of 150 km and maximum aircraft velocity of 200 m/sec, a 50 msec correlation time is necessary: this implies a 40 nsec multiplication time. Using associative memory, it is possible [20] to perform the operations of a correlation period in 31.48 msec. The advantages of hardware parallel operations are thus obvious over the conventional process when speed is an important factor.

VI. CONCLUSIONS. TRENDS

It was shown that due to improvements in integrated circuitry, better microprocessors, faster DFT/FFT algorithms and lower cost of digital logic, most analog processors are being replaced by digital processors. Very high data rates continue to be the major problem of digital processors, but with today's techniques of parallel processing, general purpose digital radar signal processors are already in use. Despite the quantization noise inherent to digital processors, good reliability, extreme flexibility and low cost of digital processors still give them a tremendous advantage over the former analog processors.

The future demand for more reliable and sophisticated radar systems will be a function of cost and military necessities. If the cost of digital logic trends lower as is its present trend, and military demands continues high, digital processors will play an increasingly important role in modern radar system's implementation.

BIBLIOGRAPHY

1. Skolnik, Introduction to Radar Systems, Chapter 12, McGraw-Hill, 1962.

2. Shrader, Skolnik and others, Radar Handbook, pp. 17-18, McGraw-Hill, 1970.

3. Oppenheim and Shafer, Digital Signal Processing, Prentice-Hall, 1975.

4. Rabiner, Gold, Theory and Applications of Digital Signal Processing, Prentice-Hall, 1975

5. Berkowitz, Modern Radar, pp. 202-203, Wiley, 1965. TK6575.B45

6. Berkowitz, Modern Radar, p. 213, Wiley, 1965.

7. Berkowitz, Modern Radar, pp. 218-220, Wiley, 1965.

8. Nathason, Radar Design Principles, p. 522, McGraw-Hill, 1969. .N2

9. Nathason, Radar Design Principles, p. 329, McGraw-Hill, 1969.

10. Oppenheim and Shafer, Digital Signal Processing, Chapter 2, Prentice-Hall, 1975.

11. Oppenheim and Shafer, Digital Signal Processing, p. 206, Prentice-Hall, 1975.

12. Brigham, E., The Fast Fourier Transform, Prentice-Hall, 1974.

13. Cutrona, Skolnik and others, Radar Handbook, pp. 23-9 to 23-15, McGraw-Hill, 1970.

14. Nathason, Radar Design Principles, pp. 564-565, McGraw-Hill, 1969.

15. McAulay, IEEE Trans AES-9, No. 4, July 1973, p. 615.

16. Prinsen, IEEE Trans AES-9, No. 5, September 1973, p. 714.

17. Urkowitz, IEEE 1975 International Radar Conference, p. 91.

18. Ewell, IEEE Trans AES-11, No. 5, September 1975, p. 326.

19. Kirk, John, IEEE Trans AES-11, No. 3, May 1975, p. 326.

20. Ellis, IEEE Radar Present and Future Conf. No. 105, pp. 311-317.

21. Gold and Rader, Digital Signal Processing, McGraw-Hill, 1969.

INITIAL DISTRIBUTION LIST

		No. Copies
1.	Defense Documentation Center Cameron Station Alexandria, Virginia 22314	2
2.	Library, Code 0212 Naval Postgraduate School Monterey, California 93940	2
3.	Department Chairman, Code 52 Department of Electrical Engineering Naval Postgraduate School Monterey, California 93940	2
4.	Associate Professor John Bouldry Department of Electrical Engineering Naval Postgraduate School Monterey, California 93940	2
5.	Lt. Joao P. Barcia Calcada de S. Amaro, 27 Lisbon, Portugal	3
6.	Curricular Officer Electronics and Communications Programs Naval Postgraduate School Monterey, California 93940	1